Development of capacitive deionisation electrodes: optimization of fabrication methods and composition

By

Shonny Nkuna

A thesis submitted in fulfilment of the requirements for the degree of Magister Scientiae in the Department of Chemistry, South African Institute for Advanced Material Chemistry, University of Western Cape.

Supervisor: Prof Bernard Bladergroen

Co-Supervisor: Mr Bongibethu Hlabano-Moyo

November 2017

Declaration

I declare that *Development of capacitive deionisation electrodes: optimization of fabrication methods and composition* is my own work, that it has not been submitted for any degree or examination in any other university, and that all sources I have used or quoted have been indicated and acknowledged by means of complete references.

Shonny Nkuna November 2017

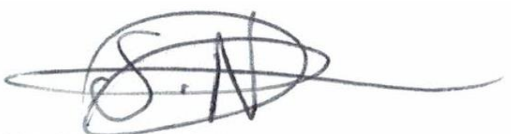

Signed……..

Acknowledgements

My sincere and utmost gratitude goes to the almighty God for his grace, the strength and wisdom that he has granted me.

To my Supervisors Prof Bernard Bladergroen and Mr Bongibethu Hlabano-Moyo thank you very much for the opportunity you gave me and the excellent supervision, support and encouragement during the course of this work.

To all the staff members and postgraduate students at South African Institute for Advanced Material Chemistry (SAIAMC) thank you for all the support, assistance and guidance.

My greatest gratitude to the National Research Foundation (NRF) and Water Research Commission (WRC) for funding my studies.

Thank you to Mr Earl McDonald for Electron Microscope Unit (EMU) University of the Western Cape for assistance with Scanning Electron Microscope (SEM).

To Ms Hanlie Botha from Stellenbosch University chemical engineering department for all her assistance with BET analysis.

To my mother Ms Johannah Mayimele thank you for all your love, support and the encouragement that kept me going.

To the rest of my family and friends thank you so much for the support, love, encouragement and prayers throughout my studies.

Keywords

Membrane Capacitive Deionisation

Desalination

Reverse Osmosis

Nanofiltration

Electrodialysis

Multi-Effect Distillation

Ion Exchange

Activated Carbon

Conductivity

Electrode

Binder

Maximum Salt Adsorption

Capacitance

Scanning Electron Microscope

Cyclic Voltammetry

Brunauer-Emmett-Teller

Porosity

Surface Area

Adsorption

Desorption

Abbreviations

AEM	Anion Exchange Material
ASAR	Average Salt Adsorption Rate
BET	Brunauer Emmet Teller
BM	Batch Mode
CB	Carbon Black
CC	Constant Current
CDI	Capacitive Deionisation
CEM	Cation Exchange Material
CNTs	Carbon Nanotubes
CV	Cyclic Voltammetry
N,N-DMAC	N,N-Dimethylacetamide
ED	Electrodialysis
EDLC	Electric Double Layer Capacitor
HDPE	High Density Polyethylene
IEM	Ion Exchange Material
IEX	Ion Exchange
MCDI	Membrane Capacitive Deionisation
MED	Multi-Effect Distillation
mSAC	Maximum Salt Adsorption Capacity
NF	Nanofiltration
PVDF	Polyvinylidene Fluoride
RO	Reverse Osmosis
SSA	Specific Surface Area
SAIAMC	South African Institute of Advanced Material Chemistry
SAC	Salt Adsorption Capacity
SEM	Scanning Electron Microscope
SP	Single Pass
TDS	Total Dissolved Solids

Abstract

The objective of this research was to optimize the fabrication methods for and compositions of electrodes for the Membrane Capacitive Deionisation (MCDI) system. Two electrode fabrication methods were developed, namely a spray coating- and a casting method. The compositions of the electrodes were varied yielding a total of 14 different electrode in an attempt to optimize the fabrication methods and compositions of the electrodes. Three activated carbons were utilized in this study, TOB, YP50F and YP80F, these activated carbons have different surface areas and porosity therefore were affected different by the materials added in the ink. Carbon black and carbon nanotubes were used as conductivity additives to enhance the conductivity of the electrodes. Lastly a polymer binder was added to increase the mechanical integrity of the electrode, this polymer was typically PVDF. For some electrodes, PVDF was replaced with ion exchange polymers in an attempt to provide ion conductive properties to the electrodes.

To establish the charge capacity of the electrodes Cyclic Voltammetry was used, BET analysis evaluated the surface area and porosity of the raw materials and fabricated electrodes. Scanning Electron Microscopy was used to verify surface morphology and uniformity. Ion adsorption capacity measurements were performed using a specially designed MCDI cell.

The objectives of this study were achieved, the fabrication methods were optimized with the casting method producing superior electrodes. Apart from fulfilling the research objectives, the current research work generated significant scientific value by revealing how the production method impacts the electrode's surface area and electrode adsorption capacity.

Table of Contents

List of figures

List of Tables

Chapter 1 Introduction

This chapter gives a brief introduction on desalination technologies and the potential of Capacitive Deionization.

70% of the earth's surface is covered with water, however 97.5% is salt water and only 2.5% is classified as fresh water [1]. From the available fresh water sources only 0.3% is readily drinkable [1]. According to the World Health Organisation (WHO) 1 in 10 worldwide people has no access to clean safe water. Moreover 85% of the world's population lives in dry areas, and water availability is expected to decrease by 2050 [1]. Therefore, there is an essential need for technologies that use salt water resources as feedstock for production of drinking water. The various technologies currently available are discussed in the section below, their advantages and drawbacks are highlighted.

1.1 Desalination Technologies

One of the key scientific, civil, and economical obstacles of mankind is the accessibility of inexpensive pure water [2]. While the global population continues to grow, recently exceeding 7 billion, it has become more difficult to supply drinking water with defined natural resources [1]. Desalination is an essential technology that can help improve both the amount and quality of water supply [1].

Desalination is the removal of dissolved minerals from brackish water, seawater, ground water or treated wastewater [3]. Desalination technologies can be divided into two types, thermal and membrane-based techniques [3]. Membrane-based techniques are less energy exhaustive than thermal methods, moreover, energy utilization directly influences the cost-effectiveness and viability of using desalination technologies [3]. These universally utilized desalination techniques will be discussed briefly in the following order: Reverse osmosis, Nanofiltration, Electrodialysis, Multi-effect distillation and Ion Exchange. A brief overview of capacitive deionization (CDI) as a relatively new desalination technology is given in section 1.1.6, a more detailed description of CDI is provided in chapter 2.

1.1.1 Reverse Osmosis

Reverse osmosis is a technique which is used global to produce fresh water, by applying high pressure in a feed channel with a semi-permeable membrane fresh water is produces [4]. Moreover, the pressure applied has to be greater than the osmotic pressure of the solution being decontaminated [4]. Figure 1.1 illustrates the process of reverse osmosis. Reverse osmosis has

developed worldwide to a production capacity of 6.4 billion litres of water per day from a few drops per hour in the initial experiments conducted in the 1950's [6].

The pressure applied is the driving force of the reverse osmosis technique moreover, the energy required for the separation is interdependent on the salinity of the solution [6]. The freshwater production rate is dependent on the salt concentration in the feed water and on membrane properties such as the selectivity and the permeability [4]. One of the main challenges of RO is the trade-off effect among water permeability and selectivity of salt [7]. The success of RO is largely attributed to the technique's relative low energy (1-4kWh/m^3) cost as a result of a series of breakthroughs in membrane and module making technology over the last several decades [7].

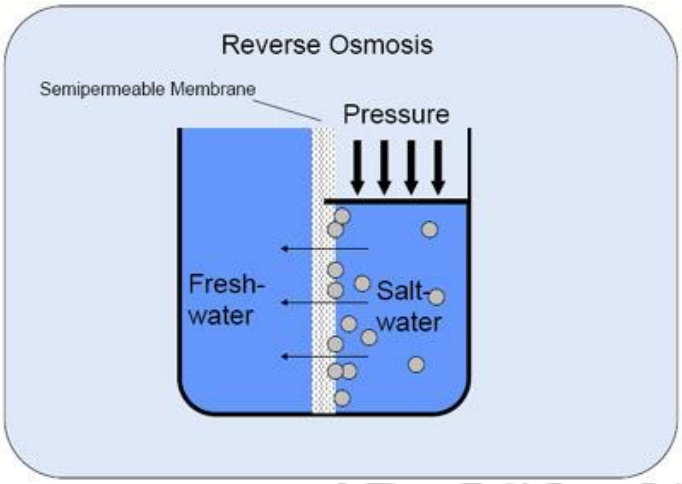

Figure 1.1 Diagram to show the desalination process of reverse osmosis [8].

1.1.2 Nanofiltration

Nanofiltration (NF) is also a pressure driven separation process [9]. The membranes used in NF reject mainly divalent ions and multivalent ions while monovalent ions pass through [10]. The desalination process of NF is illustrated in diagram 1.2 below. NF is a low to moderately high pressure process which consumes less energy and has high flux rates in comparison to reverse osmosis [9, 10]. NF has evolved into a feasible method throughout the years which has resulted in a remarkable growth in its utilization in various industries such as treatment of pulp bleaching effluents from the textile industry, removal of pharmaceutical molecules from fermentation broths, demineralization in the dairy industry, and recovery of metal from wastewater and virus removal [9].

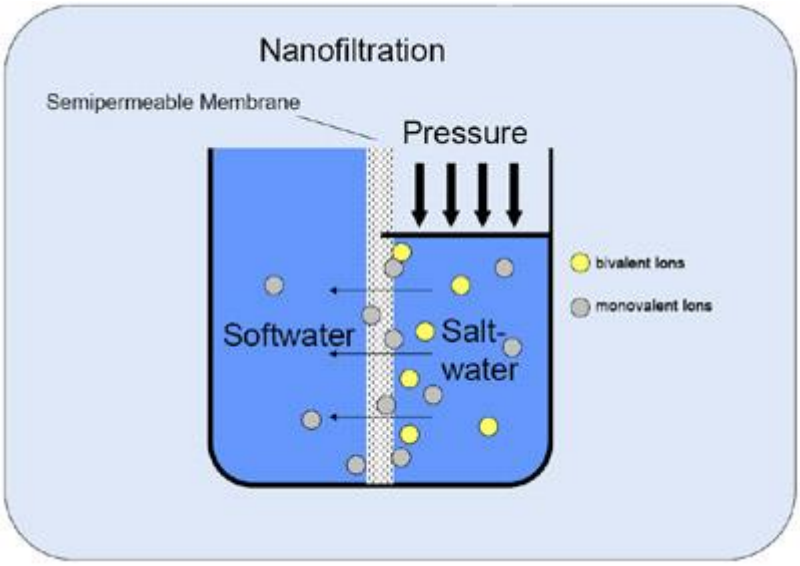

Figure 1.2 Diagram to show the desalination process of nanofiltration [8].

NF membranes demonstrate properties of both ultrafiltration and reverse osmosis therefore, charge and size of particle play a critical part in NF separation, multi-valent salts and low molecular weight organic molecules will be rejected to a much greater degree [9, 10]. Physical sieving is the dominant exclusion mechanism for the colloids and large molecules, while for the monovalent ions and low molecular weight substances, charge effect of membrane and solution diffusion mechanism play a significant part in separation process [9]. The exclusion of uncharged molecules is dictated by size exclusion, while both size exclusion and electrostatic interactions have a significant impact on the exclusion of ionic species [9]. Electrostatic properties of nanofiltration membranes play a critical part in exclusion of anions [9].

1.1.3 Electrodialysis

The electrochemical process of separating ions through charged membranes using a potential difference as a driving force is known as electrodialysis (ED) [3]. ED has been mostly utilized for the production of fresh water from brackish water and seawater, treatment of industrial pollutants, recovery of valuable materials from waste/polluted water and salt production [3]. ED selectively removes dissolved solids, based on their electrical charge, by transferring the brackish water ions through a semi permeable ion exchange membrane charged with an electrical potential [11]. Figure 1.3 below shows an ED cell [3].

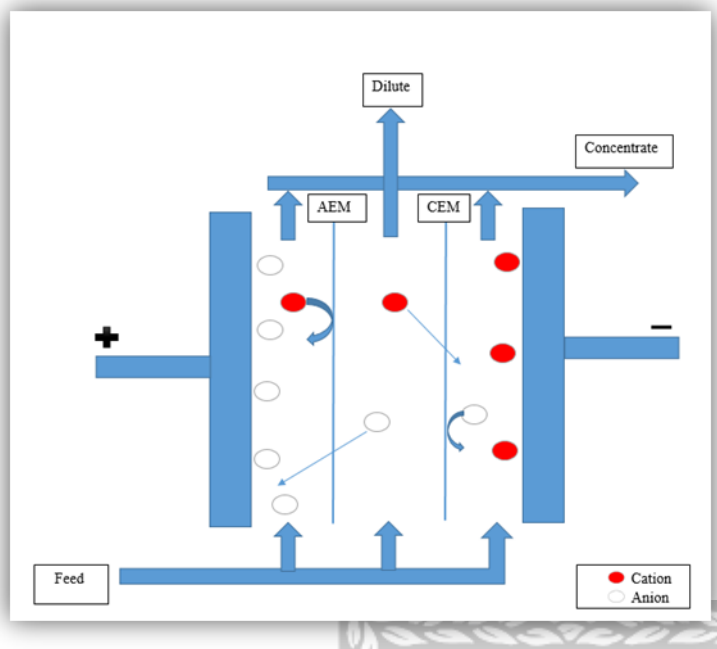

Figure 1.3 Schematic diagram of an electrodialysis cell.

Even though ED has been in operation for a long period since the 1950s, in recent years it has been replaced by RO and NF in desalination of brackish water and waste water treatment [11]. The decrease in use of ED in potable water production is due to the process cost being economical inefficient [11]. The concentration of salt of the feed water strongly determines the energy cost of the process [11]. The advantages of ED in comparison to RO and NF are: high recovery rates of water with high sulphate content, long life expectancy of membranes, larger window of allowable operational temperatures, lower water pre-treatment requirements, high level of chlorine and pH tolerance and less membrane fouling upon process reversal [11]. The major challenge of ED is generation of chlorine gas at the anode which can result in corrosion in the plant environment if venting is insufficient [11].

1.1.4 Multi-Effect Distillation

Multiple-effect distillation (MED) is a thermal technique to acquire pure water, which recovers the vapour of boiling sea water in a sequence of vessels (also known as effects), each maintained at a lower temperature than the last [12]. The basis for development of MED was to save consumed energy cost, hence, MED is more energy efficient than the other evaporation techniques including multi-stage flash [13]. An image showing the process of MED is shown in figure 1.4.

The boiling point of water is interdependent on the pressure therefore, as the pressure decreases, the boiling point of water also decreases [12]. Furthermore, the vapour boiled off in one vessel is used to heat the next vessel, the only vessel that needs an external heat source is the one at the highest pressure [12, 13].

Under ambient conditions a significant amount of energy input is required as distillation occurs on the basis of phase change of water [13]. Steam condensing inside the tubes influences evaporation to occur on the external surface of the tube, then the vapour from one stage flows into the tubes of the next stage and it evaporates more water at a lower pressure and temperature [13].

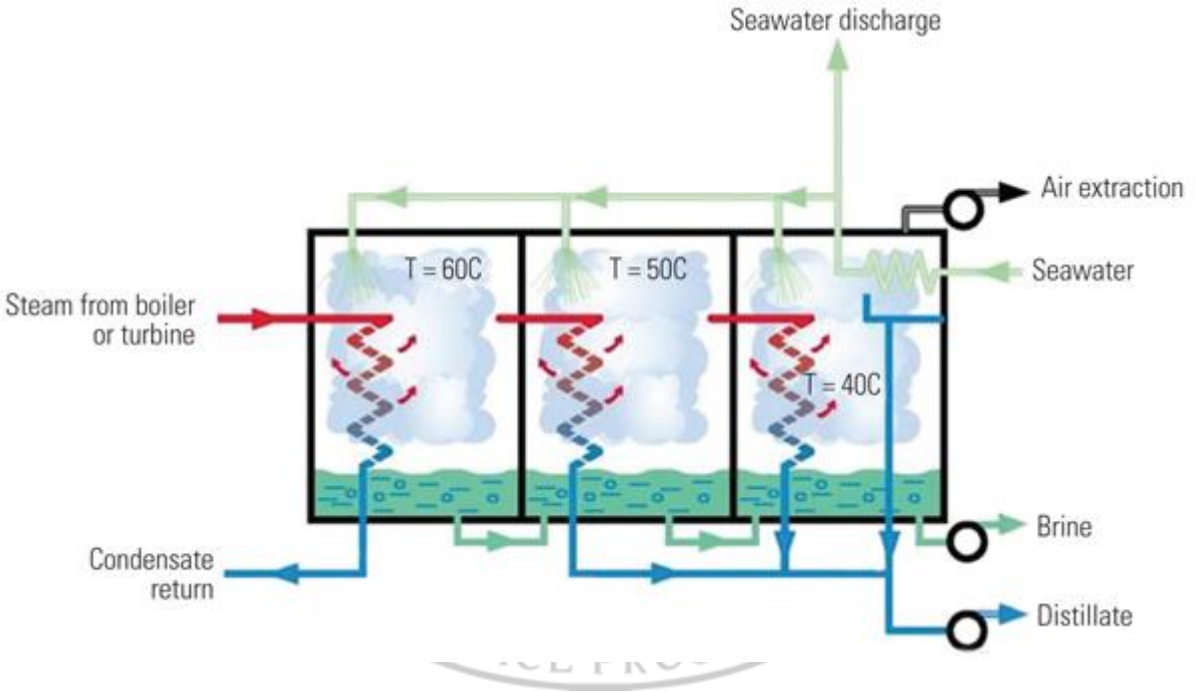

Figure 1.4 Image to illustrate the Multi-Effect Distillation [13].

1.1.5 Ion Exchange

Ion exchange is an adsorption technique which moves target ions in the aqueous phase to a solid phase, the solid phase is predominantly synthetic resins and exchanged with a like-charged presaturant ion that diffuses into solution [15]. Ion exchange is used to eliminate numerous charged water and wastewater contaminants which include various heavy metals and anionic contaminants [15]. The technique is called ion exchange due to the simultaneous confinement and release of ions [16]. Ion exchange was first discovered in 1845 but was only applied in water softening by substituting calcium and magnesium ions by sodium in 1905 [17]. The first anion resin for ion exchange was developed in 1934 and in 1937 the first demineralization plant was first installed in Britain [16].

An ion exchange resin can be defined as an insoluble matrix of 1-2 mm diameter in the form of microbeads produced from organic polymers [16]. There are 4 types of ion exchange resins generally which vary in functional groups, they are: strongly acid with sulphonic acid groups, weakly acidic with carboxylic acid groups, strongly basic with trimethylammonium groups and weakly basic with amino groups [16]. Strong resins have tremendous affinity for all ionized constituents in water and can eliminate the weakly ionized constituents as well whereas, the weak resins are inefficient at eliminating weakly ionized constituents although they can regenerate more efficiently and have two times higher exchange capabilities than strong resins [16]. A photographic image of an ion exchange column is shown in figure 1.5.

Figure 1.5 An image of two Ion Exchange columns [15].

The effluent to be decontaminated is passed through an ion exchange resin fixed bed during the ion exchange process [15, 16]. For ion exchange to be cost efficient it is crucial to ensure that the ion exchange resins can be effectively regenerated, the ion exchange cycles have to be stopped occasionally to regenerate the resins [15]. In the regeneration step the resin goes back to its initial state and the ions that had been substituted on the resin return into the solution [15]. Moreover, an acid solution is used to regenerate cationic resins and a base solution is used for anionic resins thereby resulting in large chemical waste [15]. The cost of ion exchange is mostly linked to cost of acids and bases used for regeneration and not the cost of electricity [15].

1.1.6 Capacitive Deionization

Capacitive deionization (CDI) is a relatively new water desalination technique in which a potential difference is exerted across porous carbon electrodes to remove ions from water [1, 2]. CDI uses porous carbon electrodes for the adsorption of ions and the main factors currently hindering it from competing with established desalination technologies such as reverse osmosis and nanofiltration are scale-up potential, salinity and electrode efficiency [17].

Figure 1.6 shows the energy consumption of reverse osmosis (circles) of various case studies, MCDI for feed water with 0.5 g/L TDS (triangles) and 1 g/L TDS (diamonds). The figure shows that the energy consumption for reverse osmosis is generally below 3 kWh/m^3 and only mildly influenced by the TDS level in the feed water. The triangular and diamond shaped data points were generated by the Centre of Excellence for Sustainable Water Technology in the Netherlands [18]. It is clear that for MCDI the relation between energy consumption and salt concentration in the feed water is much stronger than for RO, the MCDI energy consumption decreases with the decreasing salt concentration.

It should be noted that the upper limit for palatable water is 0.5 g/L whereas the upper limit for drinking water is 1 g/L. The main message from Figure 1.5 is that the energy consumption to treat feed water with TDS below 1.5g/L (palatable) to palatable water with 0.5g/L using MCDI is less than 0.5kWh per m^3 fresh water produced and therefore more energy efficient than RO. Figure 1.5 also shows that the energy consumption for MCDI rapidly increases with increasing influent salt concentration. TDS of the feed water increase above 2g/L, RO becomes the more energy cost effective treatment technology.

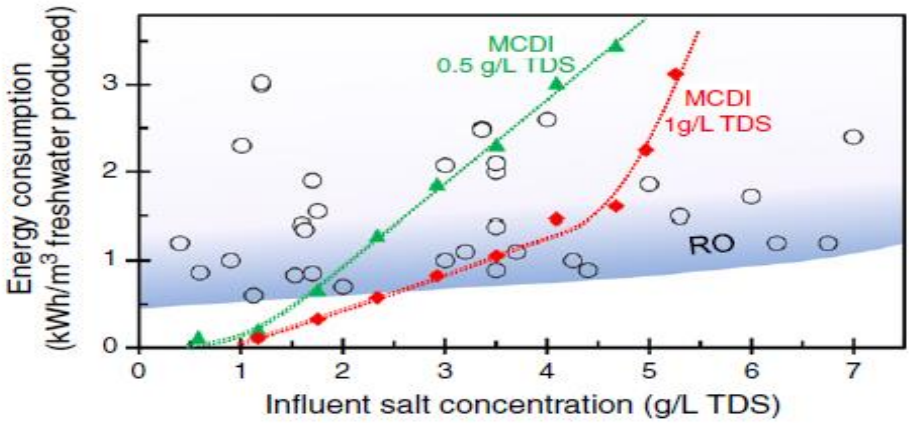

Figure 1.6 Energy consumption between MCDI with product water TDS of 0.5g/l (▲) and product water TDS of 1.0g/l TDS (♦) compared to energy consumption using reverse osmosis (o) [18].

MCDI is closely related to ion exchange technique, both technologies can remove low concentrated ions in water and regenerate the electrodes/resins for use in next cycle. The vast difference between MCDI and ion exchange is the cost and chemical waste as pointed out by a study from the Flemish Institute for Technological Research in Belgium [19]. MCDI currently shows high capital cost (150 €/m^2 cell, 10-20 k€ per pump and 10 k€ per power supply) but very low operating cost (2.5 kW h/m^3 desalination energy and 0.120 €/kW h pump energy) whereas ion exchange has low capital cost (10 k€/m^3 resins, 20 k€ per cation exchange column, 60 k€ per anion exchange column and 15-25 k€ per pump) but very high operating cost (0.120 €/kW h pump energy 78 €/m^3 of 22% hydrochloric acid and 470 €/ton of 100% sodium hydroxide) [19]. The capital cost for both MCDI and ion exchange includes cell or resins and installed equipment supply, conductivity meter and water pump. The operating cost includes cell or resin replacement, water consumption, energy consumption and maintenance [19]. Ion exchange produces a chemical waste stream that is obtained during resin regeneration whereas MCDI generates comparatively a low volumes of concentrated waste.

1.2 Research Purpose Statement

With energy consumption below 0.5kWh/m^3 for a specific range of influent salt concentration, MCDI may develop into an economically viable technology. However, the current capital investment cost related to MCDI technology are relatively high [18] and a reduction of the electrode cost is desired. This study aims to optimize the fabrication method and composition of the electrodes thereby increasing the salt adsorption capacity of the electrode. This will decrease the required number of electrodes in the MCDI cell and thus decrease the overall water production cost.

1.3 Aims and Objectives

The aim of the study is to develop electrodes, optimize the fabrication methods and composition for capacitive deionization of 0.5-2.0 g/l NaCl solutions.

Objectives and their subtask:

(i) To optimize the fabrication method:

- Produce sprayed electrode which includes establishment of electrode ink formulations and operational parameters.
- Produce casted electrodes which includes establishment of electrode ink formulations and electrode drying procedure.

- Evaluation of fabricated electrodes using SEM for surface morphology and uniformity, dimensional analysis and electrode thickness.
- Evaluation of fabricated electrodes for salt adsorption capacity, charge efficiency, average salt adsorption rate and maximum salt adsorption.
- Evaluation of the surface area and porosity of the carbonaceous materials using BET.

(ii) To optimize the electrode composition:

- Evaluation of electrode material using cyclic voltammetry for electrochemical stability and capacitance.
- Fabrication of electrodes using various sources of carbonaceous materials.
- Evaluation of the surface area and porosity of the synthesized electrode using BET analysis.

1.4 Conceptual Diagram

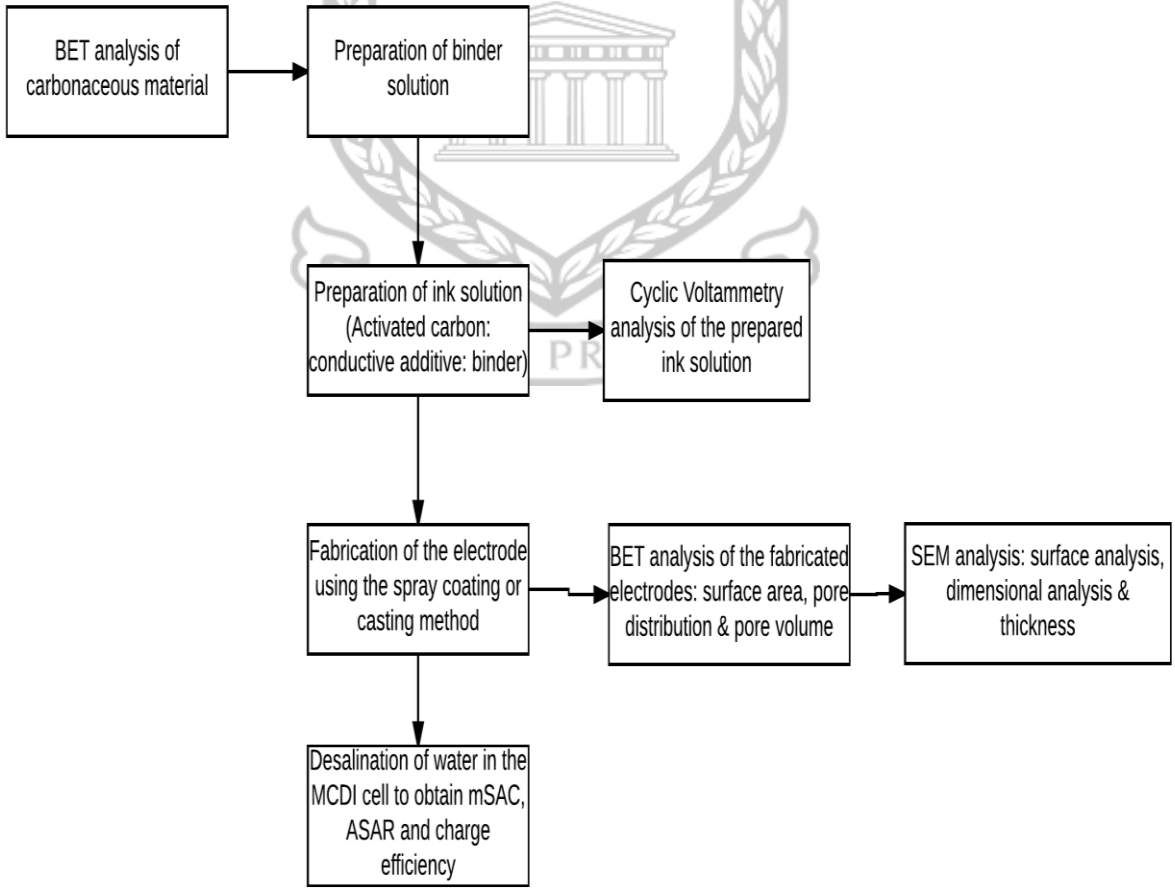

1.5 Thesis Outline

The thesis is divided into 6 chapters

- Chapter 1 provides the background of the study, introduces various desalination technologies and give details of how the technologies work. The aims and objectives of the study are also discussed.
- Chapter 2 consists of the literature review of CDI, the details of the operational conditions CDI and fundamentals and the various materials used for electrode development are also discussed. Comprehensive details of what distinguishes CDI from other desalination technologies are also given.
- Chapter 3 presents methods used for fabrication of electrodes and the instruments used for characterisation of electrodes.
- Chapter 4 provides the results accumulated in the study and the interpretation of the results acquired from CV, BET, SEM and desalination.
- Chapter 5 draws conclusion of the study on the objectives achieved for the development of CDI electrodes. Recommendations and possible future works are also discussed.

Chapter 2 Literature Review

This chapter gives the literature review capacitive deionization of water and the materials used for electrode production.

2.1 Capacitive Deionization

Figure 2.1 shows the process of CDI desalination, upon application of an electric potential between a set of electrodes, ions are adsorbed onto the surface of the porous electrodes, where cations are attracted to the negative electrode and anions are attracted to the positive electrode [2]. CDI requires no additional chemicals for regeneration of electrosorbent whereas other ion exchange processes do [2]. Electrode regeneration occurs when the electric field is reversed which also allows ions to desorb from the surface of the electrodes [1, 2]. In theory, the principle of desalination in CDI process is similar to that of capacitive energy storage in the electric double layer capacitor (EDLC), they are both based on the electrosorption of the ions or the storage of capacitive energy at the formed diffuse double-layer of the charged electrode [17].

When ion-exchange membranes are introduced to capacitive deionization the process is called membrane capacitive deionization (MCDI). MCDI is an ion-removal process based on applying an electrical potential difference across an aqueous solution which flows in between oppositely placed porous electrodes, the ion-exchange are placed in front of the porous electrodes [20, 21, 22, 23]. Furthermore, the ion-exchange membranes are separated by a spacer which water can flow through [20, 21, 22, 23]. MCDI is based on the same operational principles of CDI, in addition the inhibition of co-ions from leaving the electrode region enhances the availability of the interparticle porosity as a reservoir to store salt thereby, increasing the total storage capacity of the porous electrode [20, 21, 22, 23]. In MCDI electrode regeneration can also be performed by reversed voltage to release the ions, this is not possible in CDI because the ions that are released would be adsorbed on the other electrode [20, 21, 22, 23].

Over the years CDI has emerged as a cost effective, energy efficient and robust technology for water desalination with low to moderate salt concentration (below 10 g/L) [1]. In CDI salt ions are removed from the solution instead of water which results in the high energy efficiency of CDI [1]. In order to recover energy, the energy released in electrode regeneration can be used to charge a neighbouring cell operating in the ion electrosorption step [1]. Various configurations and carbon electrode materials can be used to enhance the performance of the CDI system [2]. The type of operational mode is an important operating condition as it is directly related to electrical energy consumption or charge efficiency of CDI process, CDI operational

modes generally consist of constant voltage (CV) and constant current (CC) modes [17]. Compared to CC mode studies, CV mode studies are more common in the academic field due to difficulty in controlling voltage levels in CC mode [24].

CDI has the potential of being the most economic desalination technology based on its high efficiency and low energy requirement for adsorption/desorption.

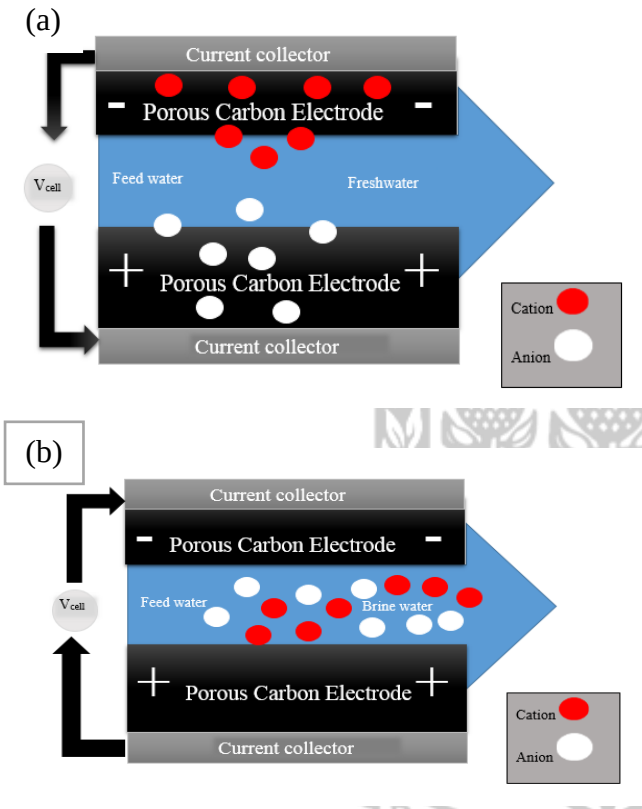

Figure 2.1 Diagram to show (a) CDI cell water desalination when potential difference is applied and (b) CDI cell electrode regeneration when cell voltage is reversed [1].

2.1.1 Historical Perspective and Timeline of CDI

Blair, Murphy and co-workers initiated the idea of water desalination called ‘‘electrochemical demineralization of water’’ in the early 1960s and it went on until the late 1960s [1]. Classification of electrodes was done according to their ‘‘ion-representatives’’ during that period as it was presumed that the ions could only be detached from water when certain functional groups on the surface could undergo redox reactions which resulted in an ionic bond between the ion in solution and the ionized group on the carbon surface [1].

The study on the extent of ion adsorption in the absence of an external voltage difference began after the study of ‘‘electrochemical demineralization’’ conducted by Evans and Hamilton [1].

The crucial mechanism of removal of ions in CDI was explained by Evans and Hamilton [1]. Reid *et al.*[1] proved the commercial relevance and long term operation of a demineralization unit without substantial loss of salt adsorption capability over time in 1968 [1].

In the early 1990's carbon aerogel materials were developed by Farmer *et al*., since then most researchers have been focusing on developing effective electrode carbon materials for water desalination [1, 2, 25].

CDI was identified as a potential mass desalination technology in laboratory conditions by Lawrence Livermore National Laboratories (LLNL), the object of their research was to convert a laboratory scale CDI system into a commercial or industrial system [25]. In 1996 Capacitive Deionization Technology Systems Incorporated was the first company to attempt commercialization of the CDI system based on the work done Lawrence Livermore National Laboratories (LLNL) but later filed for bankruptcy in 2008 [26]. Several other companies including Materials Method, Sanabelle Water, and WL Gore & Associates were also once active in the CDI field research and made a decision to abandon the market, which may be due to lack of initial market identification, technical challenges or both [26].

Figure 2.2 shows a brief timeline of CDI development from 1960 to 2012. The development took place in different areas namely theoretical, electrode production material and engineering-based-development.

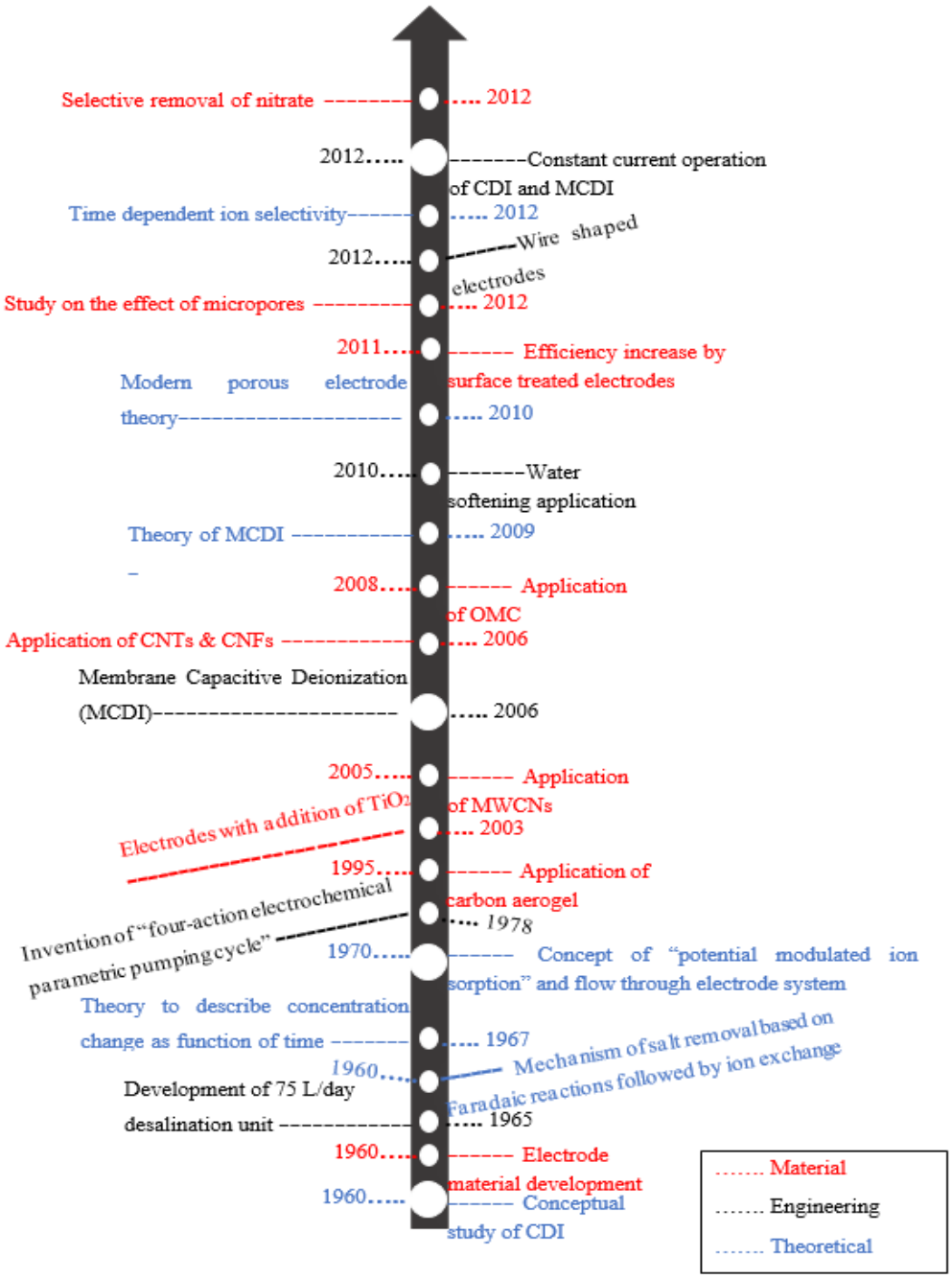

Figure 2.2 Timeline to show scientific development of CDI indicating various milestones [1].

2.1.2 Commercial Applications of CDI

Capacitive deionization was first developed by Lawrence Livermore National Laboratories (LLNL) scientists and has not been widely adopted for commercial use since because it had high capital cost and required high amount of energy (4.2-8.5 kWh/m^3) [25]. Capacitive deionization technology studies escalated in the mid-1960s however in 1998 it was still in the lab and had not scaled up to mass use [25].

Commercial applications of CDI have since been developed in the industry by different companies which include: AquaEWP, Voltea and Pionetics Linx [27, 28]. AquaEWP is currently selling to the consumer market, selling about 500-1000 units per year [27, 28]. For numerous industrial applications the AquaEWP CDI system is substituting reverse osmosis because of the simple and low operations cost, low maintenance and 80-95% water recovery plus reduction of TDS (Total Dissolved Solids) [27, 28].

Pionetics Linx partnered with Culligan international for distribution and sales of their CDI technology [28]. The Voltea CDI system in the Netherlands is the most developed CDI system in the market, the technology is able to treat water ranging from residential consumer appliances to large industrial plants [29]. The Voltea CDI system allows adjustable TDS reduction from 25%-95% [29]. Furthermore, the system can recover up to 95% of the water it treats and does not require chemicals. The technology is cost effective and has a low environmental impact [29].

The current CDI technology systems still require research to improve quality of cell design and manufacture to withstand internal pressure for higher TDS applications and further scaling up [28]. Electrode upscaling is a huge issue encountered in the CDI process, when the system is scaled up for commercial use electrode fouling is encountered [26]. Companies such as AquaEWP use citric acid to clean the CDI units to help reduce the electrode fouling however, there is not enough information on how effective it is [26].

2.1.3 Fundamentals of CDI: The Electric Double Layer Theory

Molecules in polar solvents generally develop surface charges due to either dissociation of functional groups on the surface or to chemical binding or physical adsorption of ions from the electrolyte, this surface charge is balanced by an equal opposite net charge of ions in the electrolyte [30]. Moreover, these counter-ions are attracted to the oppositely charged surface however, due to the entropy they remain dispersed in the solvent in the domain of the surface [30].This charge separation is known as Electric Double-Layer Capacitor (EDLC).

The EDLC affects the properties of individual molecules and also the interactions between them [30]. Normally two similarly charged particles in a solvent will repel each other however the repulsion is not given simply by Coulomb's law due to the presence of counter-ions in the double layer [30].At large separations there is no interaction because the `bare' charge on the particles is screened by the neutralising counter-ions that surround them; at small separations

their diffuse double layers begin to overlap and the ions in them must rearrange, which gives rise to a force [30].

EDLCs store electrical energy by physisorption of ionic species at the surface of porous electrodes or the formation of closely spaced layers of charge at the electrode-electrolyte interfaces moreover, they have fast charging kinetics, high power densities and long life cycling span [31]. The performance of EDLCs strongly corresponds to the non-redox ionic behaviour found inside the electrodes [30, 31, 32]. The minuscule separation distance between the ions and the charged electrode together with the large surface area of highly porous activated carbon electrodes, enables EDLCs to have a significantly higher capacitance than traditional capacitors [32]. Moreover, physical storage of charge instead of chemical storage, prevents the degradation of the electrochemical cells over nearly unlimited charge/discharge cycles [30, 32].

2.2 Detailed Outline of CDI

2.2.1 CDI Flow Modes

CDI consists of four most relevant flow modes also known as cell geometries which are: flow-by mode, flow-through mode, electrostatic ion pumping mode and desalination with wires mode [2, 33]. The electrodes for flow-by mode can be constructed as either as freestanding thin films or can be coated directly to a current collector [2]. Furthermore, each electrode is the same as the other in a cell pair as they need to have similar characteristics [2]. A schematic representation of these mode variations is shown in Figure 2.3 below.

In the flow-by mode (Figure 2.3 a), there is a spacer in between the electrodes arranged in a stack which allows water to flow [2, 33]. Furthermore, flow –by mode is the most frequently used mode for CDI applications [2, 33].

In the flow-through mode (Figure 2.3 b), water flows right through the interparticle pores of the porous carbon electrodes [33]. The benefit of the flow-through approach is that the ions directly migrates through the pores of the electrodes, hence reducing the transport restrictions encountered in the flow-by mode [33].

Electrostatic ion pumping mode or flow-electrode mode (Figure 2.3 c) is comparable to flow-by mode with inclusion of membranes in front of both electrodes, however, instead of having solid electrodes a carbon suspension (slurry) flows between the membranes and the current collector [33]. Moreover, its design is similar to that of the flow-by mode with the addition of membranes in forepart of both electrodes [33]. For water to be desalinated a potential difference has to be applied between both channels of flowing carbon slurries [33]. Since the electrodes do

not saturate due to the carbon suspension flow for this cell design it can be utilized for desalination of water with high salt concentration with approximately 30 g/L concentration of salt [33]. After the carbon suspension is removed from the cell it can be separated from the concentrated salt water stream therefore, a discharging step is not required [33]. Electrostatic ion pumping produces fresh water and waste at the same time, unlike in CDI, where the two streams are produced subsequently [2].

In desalination with wires (figure 2.3 d), the freshwater stream flows consecutively in an amended configuration where the anode and cathode electrode pairs are not fixed in space, but cyclically from one stream, in which the cell voltage is applied and salt is adsorbed, to another stream, where the cell voltage is reduced and salt is released [33].

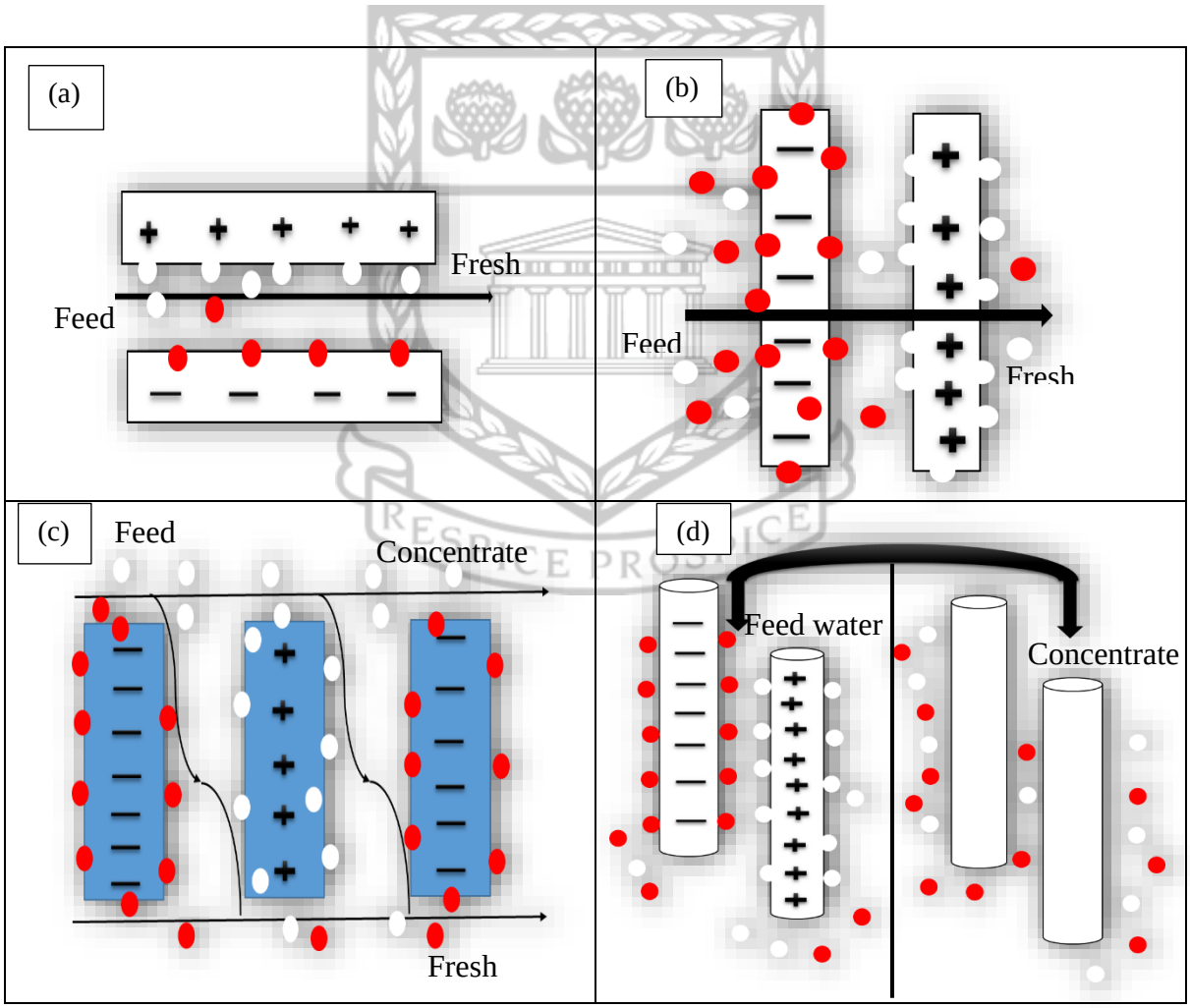

Figure 2.3 Overview of CDI flow modes. (a) Flow-by mode, (b) Flow-through mode, (c) Electrostatic ion pumping and (d) Desalination with wires.

2.2.2 CDI Configurations

The change in concentration of ions in water have to be measured over time for all the CDI system designs to know the actual water desalination [1, 34]. This can be achieved by analysing the ion composition of water samples taken at various time intervals [1, 34]. For most real water sources or complex artificial mixtures this is also the required procedure [1, 34].

If only a single salt solution is used such as sodium chloride or potassium chloride, simple on-line measurement of the water conductivity adequate [1, 34]. Two methods are possible for the layout of a CDI experiment, specifically the location of the conductivity probe, the layout methods are: single-pass method (Fig. 2.4 a) and batch-mode method (Fig. 2.4 b) [1, 34].

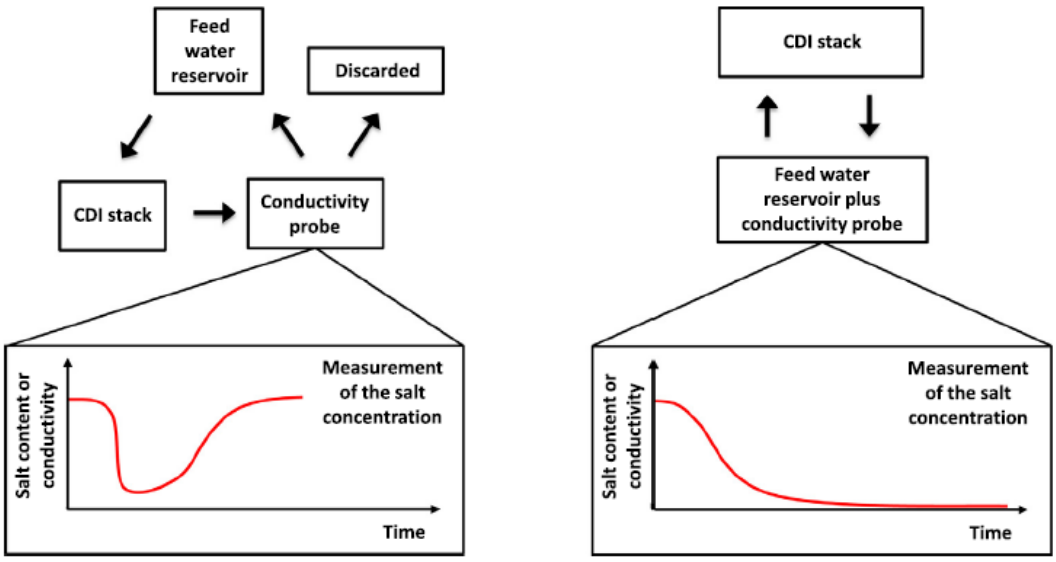

Figure 2.4 Schematic diagram of CDI configurations (a) Single-pass method and (b) Batch-mode method [1].

Single-Pass Method

In single-pass (SP) method the water feed from a storage vessel and the salinity or conductivity of the water exiting the cell is measured directly as it leaves the cell [1, 34].When cell voltage is applied in the single-pass method, the effluent salinity drops [1, 34]. Moreover, the effluent salinity increases again when the electrodes reach their maximum adsorption capacity [1, 34]. The effluent water can be either discarded or recycled to a reservoir container [1, 34]. The reservoir has to be large to ensure that the concentration changes very slightly within the adsorption cycle, so that the influent concentration remains essentially constant during the cycle [1, 34].The benefit of single-pass method is more similar to a real CDI application with water to be treated only passing through the device once, instead of being recycled many times which is less efficient [1, 34].

Batch-Mode Method

In the batch-mode (BM) method (Fig. 2.4 b), the water conductivity is measured in the recycling reservoir [1, 2]. The volume of the recycling reservoir for BM has to be smaller compared to SP so that the change in salinity can be maintained and allow for accurate conductivity measurement [1, 2]. In batch-mode method, the measured salinity drops evenly until it levels off at a minimum value [1, 2].The total amount of ions removed from water, is calculated by taking the difference between the initial and final values of salinity then multiplied by the total volume of the system [1, 2].

The measurement of salt concentration or conductivity by the batch-mode method is simpler than by the single-pass method [1, 2]. However, the main challenge in the batch-mode method is that the equilibrium salt adsorption is measured for a different reservoir concentration in each experiment which is unknown a priori [1, 2]. Hence, it is inappropriate to compare results for equilibrium adsorption at the same salt concentration of various feeds in the batch-mode method, for example, for a range of cell voltages [1, 2]. The reason is that with increasing cell voltage, desalination increases and thus decreasing the salt concentration in the system [1, 2]. Furthermore, for this experimental design it is more difficult to make a parametric relation between theory and experiment due to all the challenges mentioned above whereas with the single-pass method as all properties are measured at well-defined values of the salinity of the feed stream [1, 2].

2.2.3 Materials for Electrode Development and Design

Electrodes play an important role in the CDI process as that is where ions are stored [2]. Theoretically electrodes can be manufactured from all conductive and porous materials [2]. There are six major requirements for electrode materials used in a CDI cell, they are: good polarizability, low electrical resistance, high surface area and capacitance, electrochemical stability at applied voltage, high porosity and conductivity [34, 35]. High conductivity in electrode material ensures that the entire electrode surface of all particles is charged without large voltage gradients within the carbon [2]. A binder solution has to be utilised to maintain uniformity in the electrode to maximize the electrode capacity by maintaining the pore distribution evenly [2, 36].

For CDI and MCDI research most focus is on the development and synthesis of various electrode material [36-48]. Several researchers have investigated the performance of various electrode materials mostly carbon based materials. Moreover, the material used for electrodes

is the most critical for the success of CDI [35].The materials that have been analysed in literature include activated carbons [39, 43, 45, 46, 47, 48], alumina and silica nanocomposites [41, 43], carbide derived carbons (CDCs) [42], carbon aerogel [43, 46], carbon nanotubes (CNTs) [38] and carbon nanofibers (CNFs) [38, 40, 44], graphene and mesoporous carbons [41, 46].

Highly porous material synthesized through the pyrolysis of carbon rich material is known as activated carbon [36]. Activated carbon has hydrophobic properties by nature and mostly poly(vinylidene fluoride) is used as a binder for the activated carbon to maintain uniformity in the material structure [36]. Furthermore, the hydrophobicity of the electrode is undesirable as the electrode will tend to repel the water solution reducing the degree of contact for sorption to occur [36]. Ion exchange resins can be used to make the electrode to be more hydrophilic furthermore, the hydrophilicity ensures that the entire pore volume participates in the CDI process [2, 36].

Carbon aerogel electrodes has been an electrode of choice for many CDI applications, it exhibits superior electrical properties (10-100 S/cm electrical conductivity), low electrical resistivity, high specific surface area (400 -1100 m^2/g) and controllable pore size distribution (<50 nm) [17, 49]. Mesoporous carbon based electrodes have showed superior salt sorption capacity in comparison with carbon aerogel based electrodes with a performance difference by a factor of three [36]. CNTs, CNFs and graphene electrodes are new materials acquiring recent recognition in the CDI field [36]. The specific surface area of graphene is approximately 2630 m^2/g which is exceptionally higher than that of activated carbons (1000-2000 m^2/g) [36]. Furthermore, graphene and CNTs have high theoretical conductivity exceeding 7200 S/m [36]. CNTs and Single Walled Nanotubes (SWNTs) exhibit the highest electrosorption capacity in comparison to graphene with values of 7.87, 9.35 and 12.79 μmol/g for graphene, CNTs and SWNTs respectively [36].

In CDI the pore size, pore distribution and specific surface of the electrode influence the performance of the CDI system. Recent work has shown that micropores, are the most effective for salt adsorption in CDI [33].

2.3 State of the Art CDI

2.3.1 Significance of CDI

The accessibility of inexpensive clean water is one of the biggest challenges of the 21st century [1]. Over the years CDI has emerged as an energy efficient, robust and cost effective desalination technology [1]. Unlike other desalination technologies the main ion removal mechanism of CDI is electrostatic adsorption by direct contact of electrodes with the solution [36]. The key benefits of CDI are simple structure, easy operation and high energy efficiency [56]. CDI consumes less energy than reverse osmosis, specifically at a low salt concentration (<60 mM) of the feed solution [2, 50].

Compared to other desalination techniques CDI uses a low cell voltage of 1.2 V to operate and is simple to operate which results in relatively low energy consumption [50]. Moreover, during desorption of ions from electrodes energy stored in the CDI cell can be recovered by directly connecting two cells together using a super capacitor or using a direct current-to-direct current converter [1, 50].

CDI electrodes are not susceptible to irreversible fouling seen in ion exchange membranes thus the CDI system can be designed to be low maintenance [51]. Furthermore the electrical working principles of CDI show that it is able to treat any ionic pollutant which can be a salt or dangerous arsenic; CDI is an adaptable method [51].

2.3.2 Shortcomings of CDI

A general goal for ongoing research is to develop CDI into a more energy efficient and cost effective technology, both for the deionization of seawater and brackish water [1]. Electrodes play an important role in water desalination, thus, more research focus aims to produce better electrodes with high surface area, conductivity, efficiency and low cost as discussed above (section 2.2.4.3) [1].

It has been established by Dykstra *et al* [52] that for inflow salt concentrations up to 20 mM the resistance is mainly located in the spacer channel and the external electrical circuit, not in the electrodes therefore an increase in electrode thickness doesn't significantly increase energy consumption per mol of salt removed.

Positive electrode corrosion is one of the challenges encountered in CDI processes. In flow-through CDI cells, *Cohen et al* [53] observed an interesting phenomenon which was referred to as the inversion effect. The inversion effect was demonstrated by a rise in conductivity or

desorption of ions while the cell was being polarized and charged [53]. Upon the discharging of the cell, a decrease in conductivity was observed [53, 57].

The continuous corrosion of the positively polarized electrodes during charging is attributed to the inversion effect [53]. Upon cycling cells consisting of identical pairs of activated carbon electrodes which are initially symmetric lose their symmetry [53]. Pores of the positive electrodes are damaged as the electrodes are gradually oxidized, as a result the potential applied to the cell is not split equally therefore accelerating the oxidation of water and decrease in pH upon the charging steps [53]. To avoid corrosion of positive electrode, Cohen *et al* [53] applied a low enough potential so that the positive electrode never reaches the oxidation stage. However, applied low potential resulted in low desalination capacity therefore, more research still needed to be done to eliminate the corrosion of the electrodes [53].

Díaz *et al* [54] recognized the necessity to revisit the methods used for evaluating the desalination efficiency. The most widely used method to estimate ion retention capability is based on ionic conductivity (σ) measurements of the treated water, which allows the progress of the CDI experiment to be continuously controlled [54]. A linear relationship between the ionic conductivity measured and the salty ions concentration in the corresponding solution is assumed, and the desalination efficiency (Λ) is calculated from the difference between ionic conductivity before and after the polarization step [54]. However, the ionic conductivity values and consequently, the desalination performance evaluation can be influenced by variations in the pH of the solution, which are commonly observed during the polarization/depolarization steps [54]. Díaz *et al* [54] suggested as a more reliable alternative for evaluating the desalination performance based on the determination of the chloride ion concentration by means of a chloride selective electrode (CSE). It was clearly demonstrated that the use of a chloride selective electrode to determine the salt concentration in CDI was not only precise in a wide range of concentrations but was also independent of pH [54]. Furthermore, it appeared to be a simple and reliable alternative for monitoring the CDI process efficiency [54].

During the regeneration step in CDI desorption and adsorption occurs simultaneously which results in incomplete regeneration of electrode leading to depletion in the adsorption capacity of the electrodes, longer regeneration times and causes residual ion accumulation blocking the way for other ions in the next purification step [36]. To solve this problem ion exchange membranes can be introduced, this is known as membrane capacitive deionization (MCDI) [36]. Ion exchange membranes prevent adsorption during the regeneration step [36].

2.3.3 CDI Research Summary

Electrode synthesis and design has been the main objective for most researchers as electrodes play an important role in CDI [1, 2, 36]. New materials and design strategies for novel and improved electrodes continue to arise, the choice of electrode material largely depends on required performance, system requirements, and cost considerations [1]. System performance is rated using desalting capacity and final salt concentration, while system requirements are determined by flow rate and stack configuration, cost is calculated based on efficiency of the system and material, material cost and the lifetime of the system and material [1].

Various researchers have discovered that the establishment of high capacitance and low cost of electrode materials is a crucial factor for a successful and economic commercial application of CDI. Identification of electronic and ionic resistances in the CDI cell is crucial in enhancing the performance of CDI [52].

For CDI with carbon aerogel electrodes the major research findings include: greater sorption capacity for monovalent ions than divalent ions, only 10% of the electrode surface area is used for sorption, preliminary tests have shown that organic matter pollutes the electrodes thus, limiting the inorganic solute removal efficiency [57]. Furthermore, the electrosorption efficiency of the electrode material can be enhanced by controlling the pore size distribution [1].

In CDI, salt removal occurs through the storage of ions in electric double layer (EDL), therefore, physics of EDL can give an inside understanding of how much salt can be removed during a CDI cycle [58]. Mutha H.K. [58] studied the physics of double-layer charging in order to optimize CDI electrode materials, vertically aligned carbon nanotubes were used for the study with pore diameter of 1-10 nm and tunable heights between 1-1000 µm. The study showed that the time scale for charging varies linearly with height and decreases with solution concentration [58].

Demirer O.N. [51] performed two experimental approaches for CDI, performance optimization and flow visualization. For performance optimization, the effects of inlet stream salinity and CDI system size were characterized to assess the feasibility of a commercial CDI system operating at brackish water salinity level [51]. For flow visualisation, laser induced fluorescence (LIF) visualisation was used to study physical phenomena occurring inside of the CDI microstructure [51]. It was found that thermodynamic efficiency of CDI system can be maximized by switching from desalination to regeneration and vice versa [51]. Moreover, it was found that inlet solution concentration is directly proportional to the energy recovery ratio [51].

For flow visualization, simultaneous concentration measurements for both anions and cations were performed by dual fluorophore LIF and effects of ion mobility on transport were illustrated [51]. It was observed that fluorophores of similar size and mobility should be chosen in order to observe comparable electrosorption of both anions and cations [51].

2.4 General Review of CDI

Further development of CDI into a mature technology for application in water desalination is of utmost importance. From all the information gathered in literature it is clear that the basic concept of CDI is either to capture and harvest valuable ions from a solution, or to remove undesired ions which may be harmful or poisonous. Further research is needed to determine the most appropriate pore size and pore distribution of electrode material. Also cost must be taken into consideration to make CDI a viable technology and available to the mass market.

Chapter 3 Methodology

The method used for fabrication of electrodes and instruments used for characterisation are discussed in detail in this chapter.

3.1 Membrane Capacitive Deionization Cell Design and Description

3.1.1 Cell Design

The MCDI cell shown in figure 3.1 was designed at SAIAMC using various materials listed in table 3.1.

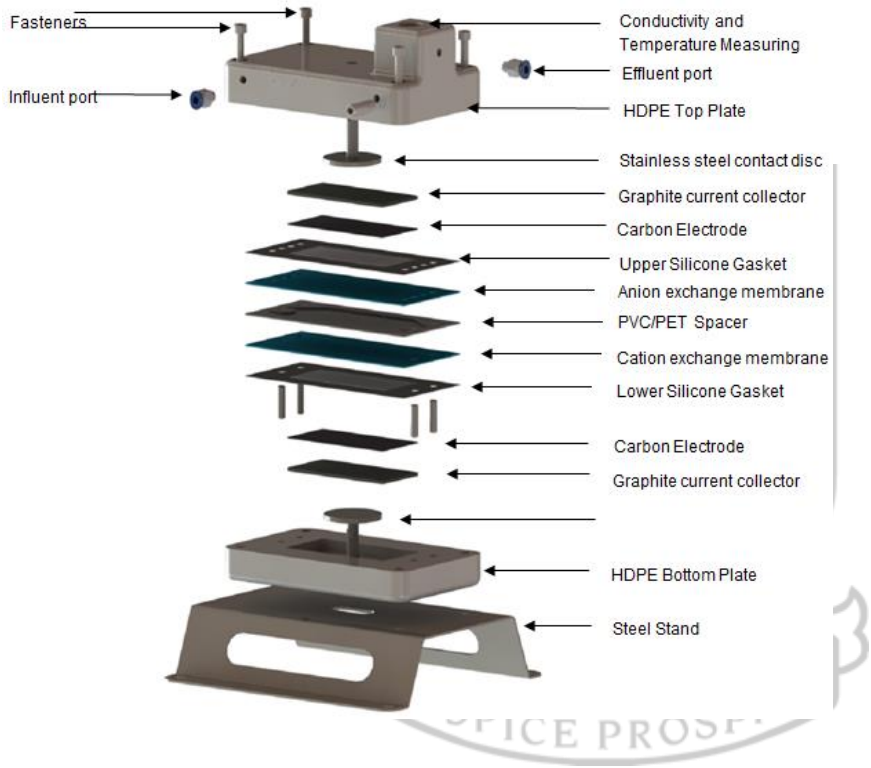

Figure 3.1 An exploded overview of the Membrane Capacitive Deionisation cell

The cell consists of a single electrode pair and the outer plate of the cell was fabricated with high density polyethylene (HDPE) which is resistant to corrosion. The stainless steel contact were coated with gold to prevent corrosion, these plates serve as the electrical point of contact. The PVC/PET spacer in between the carbon electrode enhanced a turbulent flow pattern of the feed volume with limited pressure drop. The cation and anion exchange membranes adjacent the spacer allowed the transport of negatively and positively charged ions respectively. The carbon electrodes in the cell serve to adsorb/desorb the negatively and positively charged ions. The graphite current collectors were responsible to transport the current from inside the cell to the outside through the gold coated stainless steel plates. The two silicone gaskets in between

the membranes were employed to prevent water leakage in the cell. The bolts and nuts kept the cell components intact as the effluent and influent ports introduced and discharged the feed water to and from the cell. The feed water flows into the cell through the influent port on the left side of the cell, the water then flow through the porous carbon electrodes for adsorption/desorption, the water then exits the cell through the effluent port.

Table 3.1. List of the cell components used for the MCDI cell design

Material/Component	**Specifications**	**Supplier**
Bolt & nuts	M5 Bolts and M5 nuts 5 mm inner diameter 53 mm bolt length	Parow bolt and tool, South Africa
Influent/effluent port	Festo Pneumatic straight threaded-to-tube adapter M6 male push in 6 mm	Festo Fittings, South Africa
HDPE top plate	150 × 90 × 25 mm (L × W × H)	Maizey plastics Pty Ltd, South Africa
HDPE bottom plate	150 × 90 × 20 mm (L × W × H)	Maizey plastics Pty Ltd, South Africa
Conductivity meter port (mounted on HDPE top plate)	40 × 40 × 45 (L × W × H) 15.3 inner diameter	SAIAMC, South Africa
Gold coated stainless steel plates	Stainless steel 304/316 38 mm disc diameter 10 mm threaded shaft	Goldfinger Electroplating, South Africa
Graphite	79 × 39 × 2 mm (L × W × H)	SAIAMC, South Africa
Carbon electrode	79 × 39 mm (L × W)	JNT
Silicone gasket	130 × 60 × 1 mm (L×W×H)	Cape Town Rubber, South Africa
Anion exchange membranes	Fumasep FAA-3-PE-30 94-96 % selectivity 0.2-0.7 Ωcm^2 specific area resistance	Fumatech, Germany
Cation exchange membranes	Fumasep E-620-PE 98-99 % selectivity 0.3-0.9 Ωcm^2 specific area resistance	Fumatech, Germany
PVC/PET spacer	130 × 60 mm Thickness: 0.30 mm and 0.50 mm	Fumatech, Germany
Stainless steel stand	155 × 95 × 40 mm (L×W×H)	WAKE engineering, South Africa
Torque Wrench	2882 Torque Vario-S 0.1-0.6 N.m	Wiha Werkzeuge GmbH, Germany

3.1.2 Cell Assembly Procedure

To assembly the MCDI cell the graphite current collector was placed on the fold coated stainless steel plate in the HDPE bottom plate and the silicone gasket was placed on the HDPE bottom plate. Thereafter electrode was placed on top of the graphite and the cation exchange

membrane was placed on the silicone gasket carefully removing any bubbles and not tear the membrane. The PVC/PET spacer was then placed on the cation exchange membrane watchful of blocking the influent and effluent holes. At this point the anion exchange membrane was placed on the surface of the PVC/PET spacer followed by the anode electrode active side facing the lower HDPE plate. The graphite current collector was then placed on the electrode and the silicone gasket was position cautiously without blocking the influent and effluent holes. Thereafter the HDPE top plate was put on the HDPE bottom plate and the cell was fastened using the bolts and nuts cautious not to place too much pressure on the cell and break cell components. The torque of the cell set to 0.3 N.m using. The cell was placed on the stainless steel stand, the influent feed tube was connected together with the effluent tube. The conductivity meter was inserted into the conductivity and temperature port of the cell, lastly the terminals of the power source were connected through the stainless steel contact plates using Hirchmann crocodile clips.

3.1.3 Salt Removal Capacity

3.1.3.1 Experimental Desalination Setup

The complete desalination experimental setup is shown in figure 3.2 below. A Watson-Marlow Sci-Q 300 Series peristaltic pump was used to transfer the feed solution from the feed reservoir into the MCDI cell.

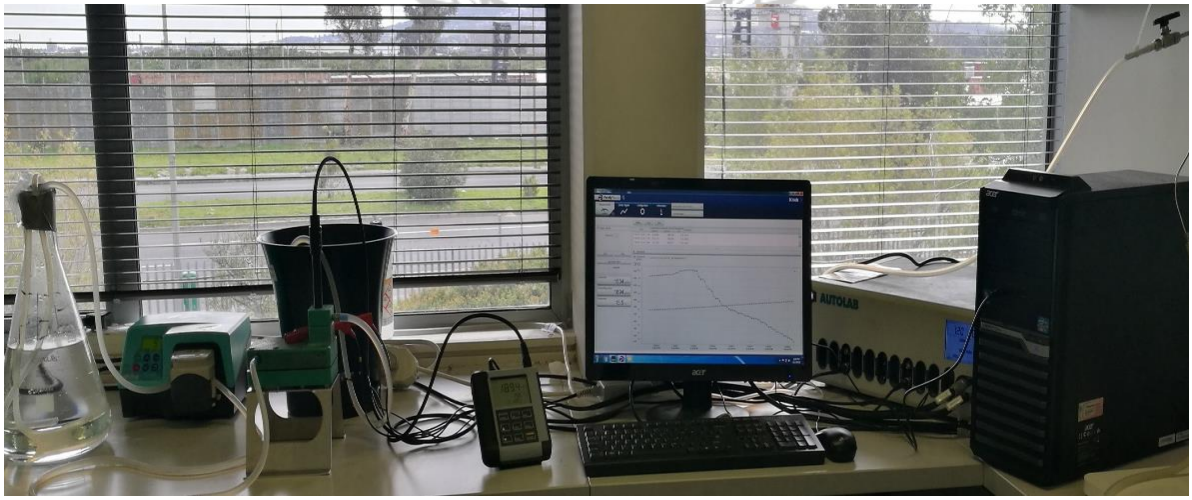

Figure 3.2 Photographic image to show the MCDI cell set-up for desalination of water.

With the aid of a software package Nova 1.9, the Autolab PGSTAT320N was programmed to supply a fixed voltage to the MCDI cell for a set period of time, while the resulting current was logged. Concurrently, the conductivity and temperature were measured using a Knick SE

204 4-electrode sensor and data was collected using Paraly SW112 software. The treated water from the MCDI cell was pumped out into a treated water reservoir.

3.1.3.2 Determination of mSAC, Capacitance and Charge Efficiency

Maximum salt adsorption capacity (mSAC) is a measure of the amount of salt adsorbed in mg per gram of electrode used in the MCDI cell. The mSAC was calculated by integrating the reduction of salt concentration multiplied by the flowrate as a function of time multiplied by the molecular weight of NaCl divided by the mass of both electrodes using equation 1 below.

$$mSAC\left({}^{mg}/_{g_{electrode}}\right) = \frac{Mw \times \int (C_i - C_o)\phi dt}{m_e} \quad (1)$$

Where:

Mw is the molecular weight of NaCl 58.443 mg/mmol

C_i and C_o are the influent and effluent concentrations (mM) respectively

ϕ is the flowrate (mL/min)

dt is the period of time during which charging occurred (min)

m_e is the mass of both electrodes (g)

Capacitance is the ability of a system to store an electric charge, it is the ratio of the electric charge in a system corresponding to the change in its electric potential. Capacitance (F/g) was calculated using equation 2 where C_{esorp} (F) is charge divided by applied voltage (Q/V) and m being the mass of the electrodes.

$$C = \frac{C_{esorp}}{m} \quad (2)$$

Charge efficiency ($\wedge$) is the ratio of the removed amount of ions multiplied by the Faraday's constant to the total charge to the MCDI cell. Charge efficiency was calculated according to equation 3 below where: C_{esorp} is the electrosorption capacity of the electrodes, Q_{total} is the total amount of charge applied during adsorption, M_{mass} is the molar mass of NaCl and F is the faraday constant (F= 94, 485,3365 C/mol).

$$Charge\ efficiency(\wedge) = \frac{F \times C_{esorp}}{M_{mass}} / Q_{total} \quad (3)$$

3.1.3.3 Pre-Conditioning and Test Procedure

The electrodes were pre-treated by wetting before any adsorption/desorption measurements were performed. A feed solution of NaCl (1 g/L) was prepared at the beginning of each desalination test, the solution is prepared by weighing out appropriate amount of NaCl into an Erlenmeyer flask with 3 L of milli-Q® ultrapure water. The feed solution is flushed with nitrogen gas for 15 minutes to remove any dissolved oxygen that may oxidize the electrodes during the adsorption-desorption. The MCDI cell assembled using the cell assembly procedure discussed in section 3.1.2 above, the electrodes to be tested as anode and cathode would be used for the MCDI cell assembly. A constant voltage of 1.2 V was used for the adsorption/desorption measurements. The feed flow rate was set at 13 mL/minute which relates to 9 rpm of the Watson-Marlow Sci-Q 300 peristaltic pump. All tests were conducted in a single-pass method.

For each electrode pair to be evaluated accurately 6 adsorption/desorption cycles were performed to pre-condition the MCDI system. This pre-conditioning is required to create a constant flow path for the water across the electrode surface. One pre-conditioning cycle runs for 600 seconds with 300 seconds adsorption (1.2V between anode and cathode) and 300 seconds desorption (-1.2V between anode and cathode).

The mSAC, capacitance and charge efficiency were determined by evaluation of the conductivity, temperature, time and current data obtained from the measurement that followed the pre-conditioning procedure. The test consisted of 900 seconds desorption and 900 seconds adsorption, the time was increased from 300 to 900 seconds to allow sufficient time for the electrodes to be completely saturated during adsorption and regenerated during desorption.

3.2 Electrode Production

The electrodes for the MCDI cell were fabricated using the casting method and spray coating method using various activated carbons. The electrodes were characterised using cyclic voltammetry for electrochemical stability, specific capacitance and electrosorption performance, scanning electron microscope for morphology, surface uniformity and electrode thickness, and Brunauer-Emmett-Teller for specific surface area, pore distribution and pore volume. The fabricated electrodes were utilized for desalination in the MCDI cell.

The materials and reagents used in this study are shown in table 3.2 as well as their purpose and supplier whereas the equipment used, purpose of the equipment and supplier of the equipment is shown in table 3.3.

Table 3.2. Various materials and reagents used for this research study

Chemical/Material	**Specifications**	**Purpose**	**Supplier**
YP50F	Activated carbon 1500-1800 m^2/g	Electrode ingredient that increases surface area	Kuraray Co. Ltd., Japan
YP80F	Activated carbon 2000-2500 m^2/g	Electrode ingredient that increases surface area	Kuraray Co. Ltd., Japan
PVDF	Polyvinylidene difluoride	Acts as a binder Provide uniformity in the electrode	Sigma Aldrich Pty. Ltd., South Africa
N,N-DMAC	N,N-Dimethylacetamide, 99.8% purity	Dissolve the binder	Sigma Aldrich Pty. Ltd., South Africa
1-Propanol	1 normal Propanol 99.7% purity	Dissolve the ion exchange materials	Sigma Aldrich Pty. Ltd., South Africa
Super-p CB	Carbon Black	Additive to increase electroconductivity of the electrode	Alfa Aesar, Germany
CNT	Multi walled carbon nano tubes	Additive to increase electroconductivity of the electrode	Carbon Nano-material Technology Co. Ltd., Korea
NaCl	Sodium Chloride 99.5% purity	To prepare feed solution for desalination experiments	Sigma Aldrich Pty. Ltd., South Africa
GDL	Gas diffusion layer	MCDI cell benchmarking	JNTG Co. Ltd., Korea
JNT45	Carbon substrate, 80 g/m^2 area weight	Electroconductive backbone of the electrode	JNTG Co. Ltd., Korea
N_2	Nitrogen gas, 99.999% ultra high purity	To create an inert environment	Afrox Ltd., South Africa
Fumion E-550	Cation exchange polymer	Ion exchange polymer to be used as binder	Fumatech, Germany
Fumion FAA-3-ionomer film	Anion exchange polymer film	Ion exchange polymer to be used as binder	Fumatech, Germany
Fumasep FAA-3-PE-30	Anion exchange membrane	To prevent contamination of the anode during the discharge cycle	Fumatech, Germany
Fumasep E-620-PE	Cation exchange membrane	To prevent contamination of the cathode during the discharge cycle	Fumatech, Germany

Table 3.3. List of the equipment used in this study

Equipment	Specifications	Purpose	Supplier
Autolab	Autolab PGSTAT 8256 potentiostat/galvanostat 100 mA to 10 nA current range +/-10 V potential range	Electrode composition: Cyclic Voltammetry	Metrohm Autolab BV, The Netherlands
BET	1.3 $\times 10^{-9}$ to 1.0 P/P_o analysis range 3 micropore ports Standard measurable surface area of 0.01 m^2/g	Electrode development: Surface area & Porosity	Micromeritics, United States
Conductivity meter	Portavo 904 X Knick SE 204 4-electrode sensor measuring range: 0.05 to 500 mS/cm	Electrode performance	Mecosa Pty Ltd, South Africa
MCDI cell	MCDI cell produced in-house 39 mm x 79 mm area Flow-by mode	Electrode performance	SAIAMC, South Africa
Milli-Q Integral water	Resistivity 18.2 MΩ.cm Flowrate 2 mL/min TOC[2] ≤5 ppb	Electrode performance: ultrapure water for electrolyte preparation	Merck KGaA, Germany
Casting roller	Roller casting tool produced in-house 210 x 50 mm area	Electrode development: ink casting	SAIAMC, South Africa
SEM	Auriga Field Emission Scanning Electron Microscope 30 kV Hi resolution	Uniformity & thickness	Carl Zeiss Microscopy GmbH, Germany
Ultrasonic bath	Bandelin Sonorex RK 514 BH 325 x 300 x 200 (tank dimensions)	Electrode development: Ultra sonication of electrode ink	Monitoring & Control Laboratories Pty Ltd, South Africa
Spray coating machine	USI Prism ultracoat300 500 mm/sec head speed +/- 0.05 mm positioning accuracy	Electrode development: Electrode ink spraying	Ultrasonic systems inc., United States of America
Peristaltic pump	Watson-Marlow Sci-Q 300	To pump the feed solution through the CDI cell	Dune Engineering, South Africa
Graphtec Cutting pro	FCX2000(VC) 36”×24” 920 mm × 610 mm Maximum cutting force-Tool 1: 500 gf and Tool 2: 1000 gf	To cut electrodes into required area	Graphtec America Inc., United States

3.2.1 Ink Preparation

For the preparation of the ink required to produce electrodes, activated carbon, conductivity additive and binder were used. The ink is prepared according to the process described below in section 3.2.1.1 and 3.2.1.2 and the amounts used for each constituents are given in table 3.4 below. The amounts used for the electrode ink was based on the length, width and height of the required electrode. The excel sheet used for calculations of the electrode ink amounts was shown in Appendix B using the equations discussed in section 3.1.3.2 above.

3.2.1.1 Binder Solution Preparation

For the production of a 5% binder solution, 23.68 mL of solvent, N,N-Dimethylacetamide, was added into a mixing bottle and heated to 100-120^{o}C. Binder powder (1.18g) was added to the solvent and was vigorously stirred to ensure that the powder dissolved completely. The binder solution was stored in a closed container at room temperature.

3.2.1.2 Ink Solution Preparation

Table 3.4 below shows the various inks produced, their compositions and amounts of each material used. The activated carbon and conductive additive were weighed into a clean mixing bottle, and the solvent was added with vigorous stirring to dissolve the powder materials. The required amount of binder solution was then added into the activated carbon/additive mixture and the solution was ultra-sonicated at 25^{o}C for 1 hour using the Bandelin Sonorex RK 514 BH ultrasonic bath. The composition consists of activated carbon: additive: binder, the solvent was not included in the composition of the electrode as it evaporated during the drying and did not add to the weight of the electrode.

Table 3.4. The ink compositions and amounts of all material used for each sample produced in this study

Ink no.	**Activated carbon**		**Additive**		**Binder**		**Solvent**		**Composition (%)**
	Type	Mass (g)	Type	Mass (g)	Type	Mass (g)	Type	Mass (g)	
I10	TOB	2.94	CB	0.365	PVDF	7.411	DMAC	89.95	80:10:10
I11	YP50F	7.412	CB	0.928	PVDF	18.57	DMAC	225.1	80:10:10
I12	YP50F	0.722	CB	0.091	PVDF	1.912	DMAC	2.00	80:10:10
I13	YP80F	0.726	CB	0.093	PVDF	1.812	DMAC	2.00	80:10:10
I14	YP80F	1.492	CB	0.188	PVDF	3.945	DMAC	29.74	80:10:10
I15	YP80F	0.679	CB	0.045	PVDF	2.728	DMAC	1.25	75:10:15
I16	YP50F	1.369	CB	0.091	PVDF	5.413	DMAC	2.00	75:10:15
I17	YP50F	0.724	CNT	0.092	PVDF	1.822	DMAC	2.00	80:10:10
I18	YP80F	0.725	CNT	0.091	PVDF	1.812	DMAC	2.00	80:10:10
I19	YP50F	0.725	CB	0.091	AEM	1.813	DMAC	2.00	80:10:10
I20	YP50F	0.724	CB	0.091	CEM	1.812	1-Propanol	2.00	80:10:10
I21	YP80F	0.723	CB	0.093	AEM	1.816	DMAC	2.00	80:10:10
I22	YP80F	0.724	CB	0.094	CEM	1.812	1-Propanol	2.00	80:10:10
I23	YP50F	0.636	CNT	0.181	PVDF	1.812	DMAC	2.00	70:20:10
I24	YP50F	0.543	CNT	0.364	PVDF	1.812	DMAC	2.00	60:30:10

3.2.2 Ink Deposition

Two methods were used for the production of electrodes in this study namely spray coating method and casting method, both methods are explained in detail below.

3.2.2.1 Spray Coating Method

The USI prism ultra-coat 300 was used for electrode spraying, an image of the machine is shown in figure 3.3 below. USI prism ultra-coat's main switch was turned on and the USI prism interface software was opened and the home button was utilized to reset the position accuracy of the spray head.

Figure 3.3 USI spray coating machine used for CDI electrode production.

For each spray coating session, a procedure was created with the USI coating settings. After a series of spray optimization trials the continuous coat fill was selected as the spraying option, and the coating direction (X and Y) of the head were selected to be 90^{o} and 0^{o} respectively, the spray width was set to 5 mm and the area of the electrode was set varying according to the various electrode areas. The spray area dimensions were set to (X1, Y1, X2, Y2), the spray head height at 30 mm, spray pitch 5 mm, flow rate 0.5 ml/min, air pressure 25 psi and temperature to 120 ± 10˚C to evaporate the solvent. For the spray coating 120 commands were programmed into the software, the ink was loaded onto the syringe (120 mL) and spray coating was commenced onto the JNT carbon substrate. When the electrode spraying was completed it was allowed to cool to room temperature and then cut to required dimensions.

The desalination of water in the MCDI cell was conducted. To characterise the electrodes BET analysis for surface area, pore size and pore volume was performed. The surface images and electrode thickness were obtained from SEM analysis.

3.2.2.2 Casting Method

The ink slurry was casted on the carbon substrate using the casting roller, this casting tool was designed and manufactured in-house (SAIAMC) and is shown in figure 3.4 below. Its design enhances an optimal distribution of ink and assists with the electrode drying process at room temperature while avoiding cracking of the ink slurry. The initial casts were conducted with an ink identical to the spray coating experiments. Later, the solvent proportion in the inks used for casting was reduced to roughly 13%, details are provided in Table 3.4. The electrodes produced were used for desalination of water in an MCDI cell and also analysed with BET for surface area, pore size and pore volume, and SEM for surface image and electrode thickness.

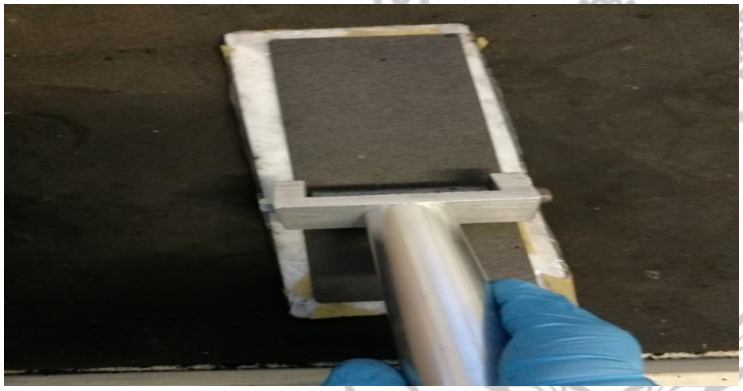

Figure 3.4 Casting roller tool used for CDI electrode production.

3.3 Characterisation of Electrodes

3.3.1 Cyclic Voltammetry

Cyclic voltammetry is one of the most widely used electroanalytical techniques, it is an efficient technique to analyse new materials for electric double-layer capacitors [64]. Cyclic voltammetry is based on scanning the potential of the stationary working electrode in a triangular waveform and measuring the resulting current [65]. The resulting plot of current versus potential is known as a cyclic voltammogram and it is a function of various physical and chemical parameters [64, 65]. The cyclic voltammogram is time dependent moreover, the time required for a particular scan depends on the scan rate and potential window used [65].

The electrochemical cell used consists of three electrodes and an electrolyte solution; working electrode, counter electrode and reference electrode. The working electrode is the electrode

where the process of interest is taking place, in this study it consisted of active carbon material of 80:10:10 YP50F:CB:PVDF composition ink (ink 11 on table 3.4 of the ink compositions). The counter electrode is the electrode which provides the current path in an electrochemical cell, platinum wire was utilized for this study [66]. A reference electrode is the electrode against which the potential of the working electrode is measured it is a stable electrochemical half-cell, for this study silver/silver chloride (Ag/AgCl) was utilized. An electrolyte is a conductive solution in which flow of current is followed by adsorption/desorption of ions, for this study 3 concentrations of sodium chloride (NaCl) were used which are 1 g/L, 2 g/L and 3 g/L [64, 65].

A PGSTAT320N Autolab potentiostat was used to supply voltage of -0.6 to 0.3 volts, and nitrogen gas was flushed through the electrochemical cell to create an inert environment. The ink casted on the working electrode was dried using a Philips HP 3616 infrared lamp. To maintain a constant temperature (25 ^{o}C) during the experiments the electrochemical cell was connected to a water bath. Activation of the working electrode was performed by running 100 cycles at a scan rate of 5 mV/s for each experiment.

Cyclic voltammetry was used to determine the electrochemical performance of the electrodes, the electrosorption performance, specific capacitance of fabricated electrodes and electrochemical stability [67, 68, 69]. Cyclic voltammetry was adapted as a technique to predict the performance of the fabricated electrodes prior to desalination experiments and reproducibility of the ink preparation method. Three samples of ink 11 were prepared and the CV analysis was performed at a scan rate of 25 mV/s to analyse the reproducibility of the preparation method. To determine the specific capacitance, ink performance and electrochemical stability of ink 11 (80:10:10 YP50F:CB:PVDF) an analysis was performed at 3 scan rates 5 mV/s, 10 mV/s and 25 mV/s furthermore, equation 4 was used to calculate the specific capacitance.

$$C_s = \frac{dQ}{dV} = \frac{1}{mv\Delta V}\int_{V_1}^{V_2} I\,(V)dV \qquad (4)$$

3.3.2 Scanning Electron Microscope

Electron microscopes are instruments that use a beam of highly energetic electrons to analyse objects on a very fine scale, they can be used to analyse the morphology (shape and size of the particles making up the sample material), topography (surface features of a sample), composition (the elements and compounds that the sample is made up of and the relative amounts of them) and the crystallographic information (how the atoms are arranged in the

sample) [70, 71]. Electron microscope delivers a higher resolution than optical microscopy due to the difference in wavelength between visible light beams and electron beams.

The scanning electron microscope is used for examination of specimen surfaces. To examine the specimen it is irradiated with an electron beam known as electron probe to emit secondary electrons from the specimen surface, topography of the surface can be observed by two-dimensional scanning of the electron probe over the surface and an image can be acquired from the detected secondary electrons [71]. Secondary electrons are the electrons that escape from the specimen with energies below 50 eV moreover, secondary electrons give topographic images. Backscattered electrons crystal images of the specimen, they are electrons closer to the nucleus and have higher energy than secondary electrons [71].

The quality and resolution of SEM images are a function of three major parameters which are: instrument performance, selection of imaging parameters and nature of the specimen [70, 71]. SEM can achieve high magnification of up to 1000000X and a resolution as low as 1 nm [71].

The morphology, uniformity and thickness of fabricated electrodes was studied using a Zeiss Leo 1450 Scanning Electron Microscope. Sample preparation entailed immersion of electrode sample in liquid nitrogen and physically fracturing the electrode to obtain a clear cross-section distinctly showing the electrode and substrate layers, the samples were then sputter coated with a 50 – 100 nm gold-palladium layer to enhance their conductivity and thus enhance ultimate image visibility. Sample cross-sections were placed perpendicular to the electron beam for cross-sectional images and the same applied for surface images.

3.3.3 Brunauer-Emmett-Teller

The Brunauer-Emmett-Teller (BET) theory was developed by Stephen Brunauer, Paul Emmett and Edward Teller in 1938, as an extension of the Langmuir theory developed by Irving Langmuir [73]. The Langmuir theory relates the monolayer adsorption of gas molecules (also called adsorbates) onto a solid surface to the gas pressure of a medium above the solid surface at a fixed temperature [73]. Adsorption is defined as the adhesion of atoms or molecules of gas to a solid surface. The quantity of gas adsorbed depends on the exposed surface area of the solid, temperature, gas pressure and the strength of interaction between the gas and solid [73]. In BET analysis nitrogen gas is usually used due to its availability, high purity and its strong interaction with most solids [73, 74].

BET equation: $$\frac{1}{X\left[\left(P_{0/P}\right)-1\right]} = \frac{1}{X_m C} + \frac{C-1}{X_m C}\left(\frac{P}{P_0}\right) \quad (5)$$

The BET equation uses information from the isotherms to determine the surface area of the sample, where X is the weight of nitrogen adsorbed at a given relative pressure (P/P_0), X_m is a monolayer capacity which is the volume adsorbed at a standard temperature pressure (STP) and C is the BET constant. When BET equation is plotted the graph should be linear graph with a positive plot however, if such a graph is not obtained then the BET method used was insufficient in obtaining the surface area [73, 74, 75]. The monolayer capacity X_m can be calculated using equation 6, the total surface area can be calculated using equation (7) where, N is the Avogadro's number, A_m is the cross sectional area of the adsorbate and equals to 0.162 nm^2 for an adsorbed nitrogen molecule, and M_v is the molar volume and equals 22414 mL.

$$X_m = \frac{1}{s+i} = \frac{C-1}{C_s} \tag{6}$$

$$S_s = \frac{X_m N A_m}{M_v} \tag{7}$$

The data obtained from BET is in the form of isotherms, which plots the amount of gas adsorbed as a function of relative pressure, there are six types of isotherms showed in Fig. 3.5 below. According to the International Union of Pure and Applied Chemistry (IUPAC) pores are classified by their internal pore width: micropore has ≤2 nm pore width, mesopore has a pore width of between ≥2 nm and 50 nm, and macropore has an internal width of greater than 50 nm [74].

Type I isotherm is a reversible concave which is obtained when P/P_o is less than 1 and BET constant is greater than 1 in the BET equation [73, 74, 75]. Type I isotherms are obtained when the adsorption is limited to only a few molecular layers, moreover, this isotherm represents microporous materials, micropore filling and high uptakes are detected at low pressures due to the narrow pore width and high adsorption potential [73, 74, 75]. The limited uptake is mainly due to the available pore volume rather than specific surface area [73, 74, 75].

Type II isotherm are typically obtained for non-porous or macroporous material where unlimited monolayer-multilayer adsorption can occur, type II isotherm is obtained when the BET constant is greater than 1 [73, 74, 75]. At the inflection point labelled B monolayer adsorption occurs and then multilayer adsorption occurs at medium pressures, at high pressures capillary condensation occurs [73, 74, 75].

The reversible convex type III isotherm is obtained when the BET constant is less than 1 and shows formation of a multilayer [73, 74, 75]. This isotherm has no asymptote therefore no

monolayer is formed, the adsorbate-adsorbent interactions are very weak and this isotherm is very rare [73, 74, 75].

Type IV isotherms are typical for mesoporous material, with the hysteresis loop being the most characteristic detail of the isotherm [73, 74, 75]. The hysteresis loop is related to the occurrence of pore condensation which occurs at pressures below the saturation pressure of the gas [73, 74, 75]. At lower pressures monolayer-multilayer adsorption occurs similarly to type II isotherm.

Type V isotherm show a hysteresis and pore condensation, this isotherm is related to isotherm III, indicating relatively weak interactions between the adsorbent and adsorbate [73, 74, 75]. This type of isotherm is not applicable to BET.

Type VI isotherm shows stepwise multilayer adsorption on a uniform non-porous surface, the sharpness of the steps depends on the homogeneity of the adsorbent surface, the adsorptive and the temperature [73].

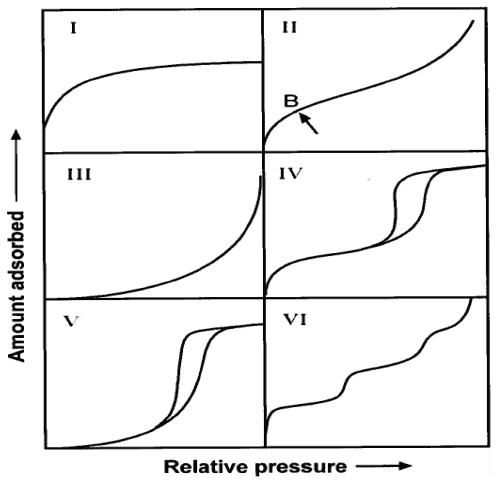

Figure 3.5 Isotherm plots of gas adsorbed as a function of pressure on a solid surface [73].

For this study multipoint BET analysis was employed to determine the specific surface areas and pore distribution in the carbonaceous materials in use. Carbon samples were weighed into test tubes, placed in oven apertures of a Micromeritics Flow prep 060 sample degas system and degassed using a low nitrogen gas flux at 110 °C for a minimum of 12 hours so as to release contaminants and moisture trapped within the porous structure and thus facilitate accurate specific surface area determination. After degassing the sample loaded test tubes were mounted on a Micromeritics 3Flex surface area and porosity analyser for surface area measurements conducted at -196˚C. Liquid nitrogen was used as the coolant.

The surface area of the electrodes obtained was normalized to that of the activated carbon as it is the main material in the electrode and the surface area of the electrodes is mainly based on the surface area of activated carbon. The data was normalized in order to relate the surface area of the electrode to that of the activated carbon moreover, it was established how the surface area of the electrodes is affected the fabrication method, the composition of the electrodes, the conductivity additive and the enhanced amount of binder.

3.4 Optimization of the Electrode

To optimize the electrode fabrication, 3 electrodes E10, E11 and E14 were fabricated using the spray coating method using 3 different activated carbon (TOB, YP50F, and YP80F), the fabricated electrodes had the same composition 80:10:10, the amounts used for each electrode are given in Table 3.4. These 3 electrodes were produced using different activated carbons with different surface area and porosity to be able to determine a suitable activated carbon for the production of electrodes for the MCDI cell. The electrodes were named using the following code, E- for electrode, followed by electrode number: I- for ink, followed by ink number: activated carbon used: substrate used.

Two methods of production were used for the production of the electrodes namely the casting method and spray coating method, these two methods allowed for the optimization of the fabrication process. In the casting method the ink was deposited using the casting tool in which pressure was applied on the surface of the substrate and the electrodes were dried at room temperature. In the spray coating method the ink was simply dropped on the surface of the substrate and dried at a high temperature (120^{o}C). The electrodes fabricated to optimize the method of fabrication for spray coating were E11 (80:10:10 YP50F: CB: PVDF) and E14 (80:10:10 YP80F: CB: PVDF) and for casting method were E12 (80:10:10 YP50F: CB: PVDF) and E13 (80:10:10 YP80F: CB: PVDF). E11 and E12 were fabricated using YP50F as an activated carbon whereas E13 and E14 were fabricated using YP80F as an activated electrode.

To achieve the objectives of the study the composition of the electrodes were further investigated by variation of the conductivity additive, variation of binder amount to determine the optimum amount of binder required for the electrodes and introduction of ion exchange material (IEX).

Carbon black (CB) and Carbon Nanotubes (CNT) were used as conductive additives to enhance the conductivity of the electrodes, E12 (80:10:10 YP50F: CB: PVDF), E17 (80:10:10 YP50F: CNT: PVDF), E13 (80:10:10 YP80F: CB: PVDF) and E18 (80:10:10 YP80F: CNT: PVDF)

were fabricated using the casting method to study the effect of the two additives. To optimize the amount of CNT in the electrodes, the amount of the CNT was increased in electrodes E23 (70:20:10 YP50F: CNT: PVDF) and E24 (60:30:10 YP50F: CNT: PVDF).

For the optimization of the binder electrodes E12 (80:10:10 YP50F: CB: PVDF), E15 (75:10:15 YP80F: CB: PVDF), E13 (80:10:10 YP80F: CB: PVDF) and E16 (75:10:15 YP50F: CB: PVDF) were fabricated, the amounts used for the fabrication of each electrode was given in Table 3.4.

IEX was introduced into the electrode fabrication material to optimize the electrode performance, E19 (YP50F: CB: CEM) was fabricated using YP50F as an activated carbon it had cation exchange material (CEM) and E20 (YP50F: CB: AEM) was fabricated using YP50F as an activated carbon it had anion exchange material (AEM). Electrode E21 (YP80F: CB: CEM) was fabricated using YP80F as an activated carbon and it consisted of CEM and electrode E22 (YP80F: CB: AEM) was fabricated using YP50F as an activated carbon and it consisted of AEM. Table 3.5 below shows all the electrodes that were fabricated in this study.

Table 3.5. List of all the electrodes fabricated from this study.

Electrode Name	**Composition**	**Electrode Materials**	**Electrode Weight (g)**	**No. of electrode pairs**
E10-I10-TOB-JNT30	80:10:10	TOB: CB: PVDF	1.266	1
E11-I11-YP50F-JNT45	80:10:10	YP50F: CB: PVDF	1.192	3
E12-I12-YP50F-JNT45	80:10:10	YP50F: CB: PVDF	1.269	1
E13-I13-YP80F-JNT45	80:10:10	YP80F: CB: PVDF	1.164	1
E14-I14-YP80F-JNT45	80:10:10	YP80F: CB: PVDF	1.118	1
E15-I15-YP50F-JNT45	75:10:15	YP50F: CB: PVDF	1.492	1
E16-I16-YP80F-JNT45	75:10:15	YP80F: CB: PVDF	1.138	1
E17-I17-YP50F-JNT45	80:10:10	YP50F: CNT: PVDF	0.981	1
E18-I18-YP80F-JNT45	80:10:10	YP80F: CNT: PVDF	1.083	1
E19-I19-YP50F-JNT45	80:10:10	YP50F: CB: CEM	0.805	½
E20-I20-YP50F-JNT45	80:10:10	YP50F: CB: AEM	0.591	½
E21-I21-YP80F-JNT45	80:10:10	YP80F: CB: CEM	0.981	½
E22-I22-YP80F-JNT45	80:10:10	YP80F: CB: AEM	0.584	½
E23-I23-YP50F-JNT45	70:20:20	YP50F: CNT: PVDF	0.995	1
E24-I24-YP50F-JNT45	60:30:10	YP50F: CNT: PVDF	0.962	1

Chapter 4 Results and Discussions

This chapter discusses in detail the results with the fabricated electrodes and the interpretation of the data from all the characterisation techniques utilized.

4.1 MCDI System Benchmark

Gas Diffusion Layer (GDL) electrodes were purchased from JNTG Co. Ltd. in Korea and used as a benchmark for the MCDI system. These GDL electrodes have a similar structure as a CDI electrode, consisting of fibrous carbon support material coated with a layer of fine carbon particles. The thickness of both layers are highly consistent and therefor suitable for the initial experimental work. The GDL electrodes used had a total mass of 1.5853 g and dimensions of 79 × 39 mm. The GDL electrode was used as a benchmark to probe the accuracy of the MCDI cell and eliminate errors in the cell assembly and performance. The Scanning Electron Microscope was used to capture the surface images of the electrodes as shown in figure 4.1 to analyse the uniformity of the electrodes, the electrodes are uniform therefore the carbon materials used in the production is the same throughout the electrode. The average thickness of the electrodes was found to be 395.20 µm, the thickness was only measured on the carbon material excluding the substrate. It can be deduced from the uniformity and thickness of the electrode that the adsorption of ions is roughly the same throughout the electrode.

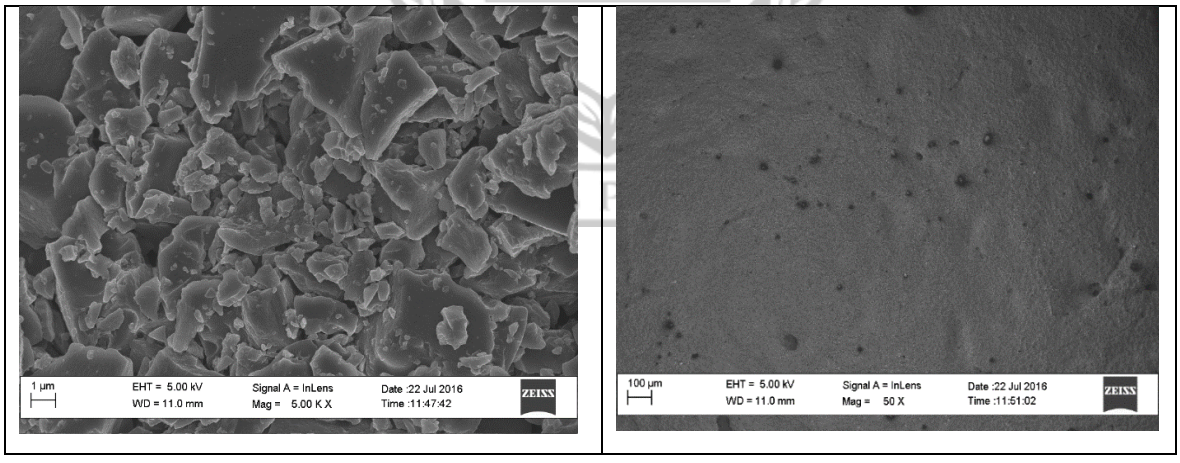

Figure 4.1 SEM surface images of GDL electrodes at different magnifications.

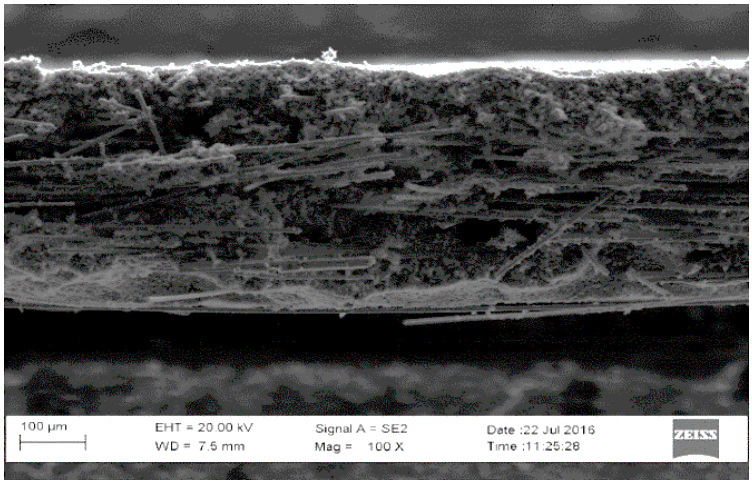

Figure 4.2 SEM cross-sectional image of GDL electrodes.

GDL electrodes were used for desalination of water in the MCDI cell, the adsorption-desorption graph is shown in figure 4.8 below and table 4.1 shows a summary of the mSAC, capacitance and charge efficiency.

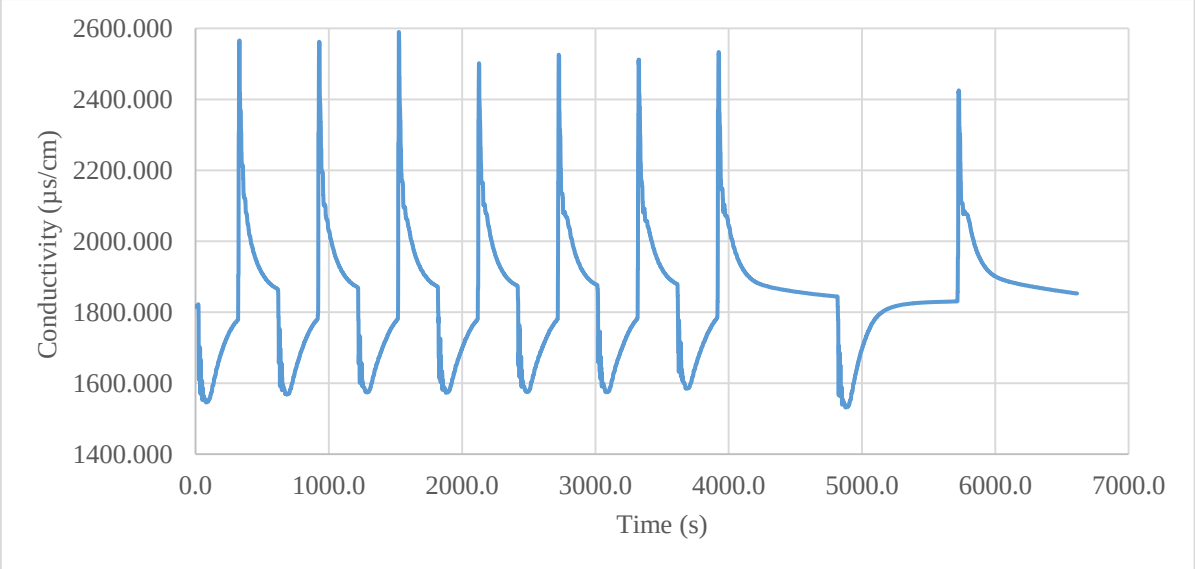

Figure 4.3 Adsorption-desorption measurement of the commercial GDL electrodes.

The graph shown in figure 4.3 represents conductivity of the water exiting the MCDI cell as a function of time, values of each mSAC, capacitance and charge efficiency calculated are presented in table 10 below. An average mSAC of 7.146 mg/g was obtained at a charge efficiency of 100% at a feed flowrate of 13 mL/min. The mSAC obtained is significantly lower compared to what has been published in literature by other researchers with the lowest mSAC being 10 mg/g. The commercial GDL electrodes served their purpose in the establishment of reproducible salt adsorption- desorption measurements. However, these commercial GDL

electrodes cannot be recommended for use in MCDI systems due to their low salt adsorption capacity.

Table 4.1. mSAC, capacitance and charge efficiency of the commercial GDL electrodes

Electrode name	Electrode mass (g)	Feed flowrate (mL/min)	mSAC (mg/g)	Capacitance (F/g)	Charge efficiency (%)
GDL	1.1231	13	7.048	9.675	100
GDL	1.1231	13	7.111	9.771	100
GDL	1.1231	13	7.278	9.962	100

4.1.1 Resistance of the MCDI cell

To determine the electrical resistance of the electrically conductive cell as function of the torque applied during cell assembly, the DC current was measured at numerous charge voltages (0.2 V, 0.4 V, 0.6 V, 0.8 V, 1 V and 1.2 V) for both sprayed and casted electrodes. Components such as the ion exchange membranes and the spacer were removed during this exercise as they are electrically insulating. The different torques applied were 0.1 N·m, 0.2 N·m, 0.3 N·m, 0.4 N·m and 0.5 N·m. The resistance was calculated by dividing the charge voltage applied by current obtained. The current versus voltage graphs were plotted and also the resistance against various torque. Figure 4.4 (a) and (b) below showed the current versus voltage and the resistance against torque for a sprayed electrode whereas figure 4.5 (a) and (b) showed current versus voltage and the resistance against torque for a casted electrode.

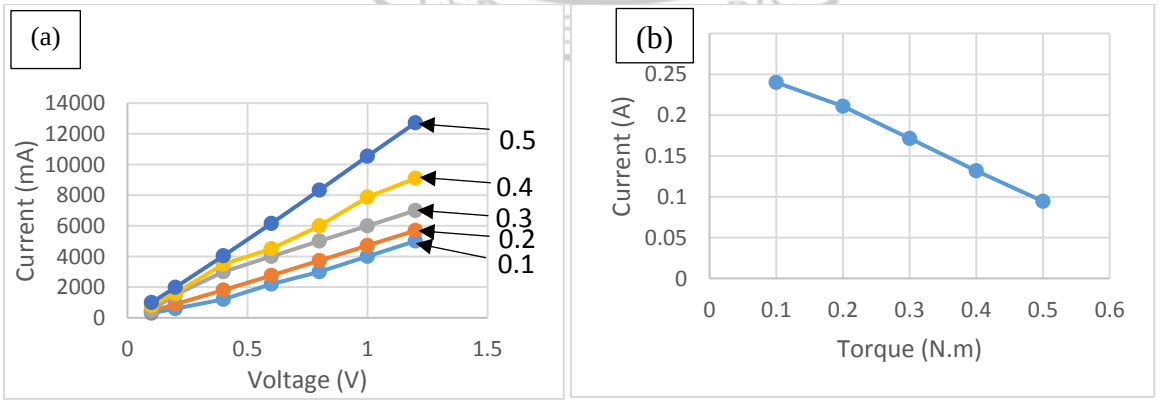

Figure 4.4 (a) The charge voltage applied versus current at different torque values (0.1-0.5) for a sprayed electrode pair and (b) the resistance versus torque plot values for a sprayed electrode pair at 1.2 V.

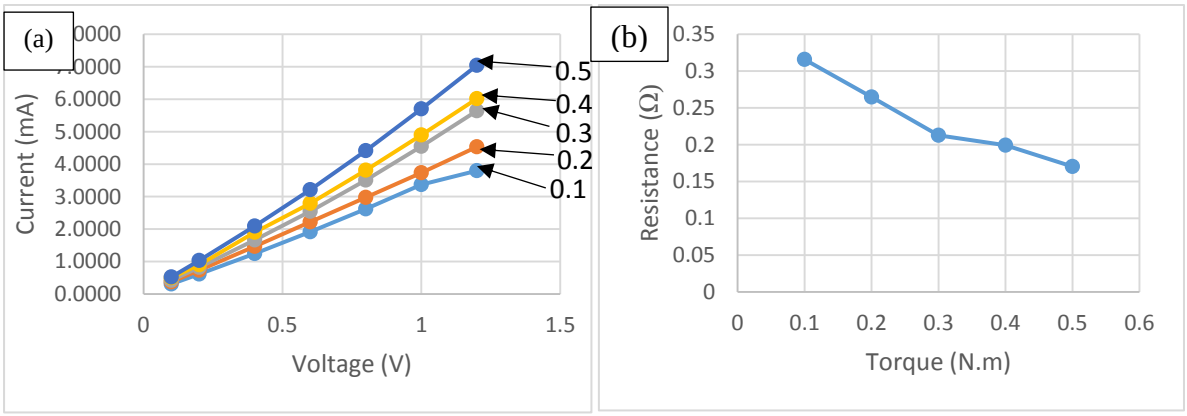

Figure 4.5 (a) The charge voltage applied versus current at different torque values (0.1-0.5) for a casted electrode pair and (b) the resistance versus torque plot values for a casted electrode pair at 1.2 V.

When the voltage was increased the current also increased following Ohms law (electrical current is proportional to the voltage and inversely proportional to the resistance). When the torque was increased the resistance of the layered system decreased, likely due to a reduced contact resistance between the various layers. The electrode preparation method seems to affect the resistance of the system. Firstly, the resistance of sprayed electrodes is significantly lower (40-50% lower) than the casted electrodes. Secondly, the sprayed electrode pair showed a steady decrease in the resistance as the torque was increased. The casted electrode pair showed a decrease in resistance from torque of 0.1-0.3 N·m but appears to be less pronounced above 0.3 N·m. In fear of breaking the graphite electrodes at excessive torque, all MCDI experiments were performed at a torque of 0.3 N·m. The Ohmic resistance incurred during an adsorption desorption experiment is likely to be around 200mV at the onset of any cycle and tails off below 20mV several seconds after the onset.

4.2 Optimization of Spray Coating Process

4.2.1 Electrode Morphology

Parameters inclusive of spray head height, platen temperature and ink flow rate aided the optimisation of the spray coating process discussed in Section 3.2.2.1. This optimization of the spray coating process was done by adjusting the spray coating parameters whilst observing the surface of the electrodes visually.

The spray head height was set at three different heights (10 mm, 20 mm and 30 mm), which showed an improvement in the spray coated electrode uniformity with increased height. When the spray head height was set at 10 mm above the substrate surface, it was very close to the substrate which led to narrowing of the spray path. This resulted in the formation of an uneven spray coat, that is, heavily sprayed and unsprayed sections of the electrode. Increasing the spray

head height to 20 mm did not offer a significant change. However, increasing the spray head height to 30 mm, widened the spray path resulting in the formation of an even spray on the substrate, thus forming an even and uniform electrode.

Both the platen temperature of the spray coating process and ink flow rate which is the volume of the ink that passed through the spray head per unit time measured in mL/min played an important role in electrode production as the fabricated electrodes needed to be dried without cracking and without ink seeping through and out of the electrode. With a solvent boiling point of 165 ^{o}C the platen temperature was initially set at 150 ^{o}C, the ink hardened on the tip of the spray head as the solvent evaporated at a higher rate. Lowering the temperature to 120 ^{o}C to stop ink hardening and with an ink flow rate of 2 mL/min, electrode ink seeped through the substrate and spilt onto the platen as the drying rate was slow since the solvent used has a boiling point of 165 ^{o}C. Lowering the ink flow rate further to 1.0 mL/min improved the spilling off of ink, which was then eliminated when the ink flow rate was lowered further to 0.5 mL/min, and thus resulted in a finely sprayed electrode. As such, when the temperature was set at 120 ^{o} C with an ink flow rate of 0.5mL/min an optimum drying temperature was achieved which allowed for ideal evaporation of solvent without spilling and cracking.

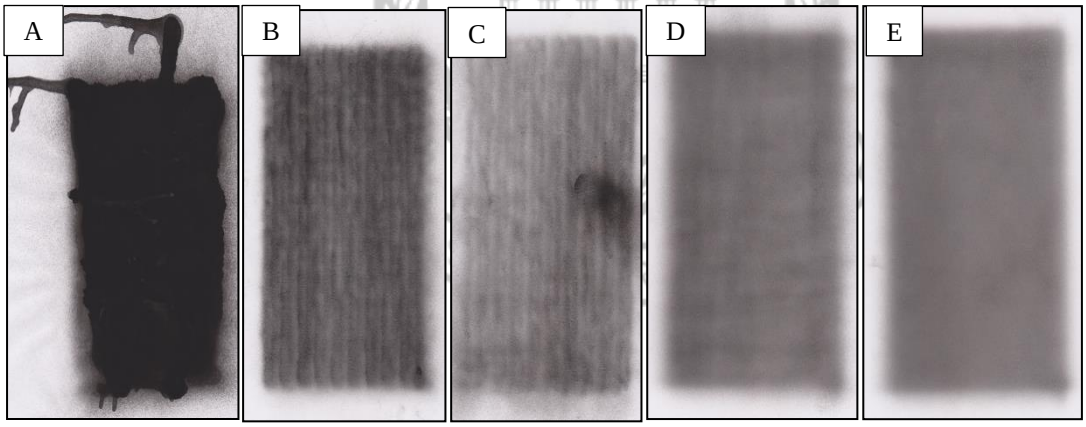

Figure 4.6 Photographs captured while adjusting the spray coating parameters.

Figure 4.7 Photograph of a spray coated electrode.

Figure 4.6 showed the images captured while adjusting the spray coating parameters, on 4.6 A the spray head height was too close to the substrate which resulted in the ink spilling. The spray head height and platen temperature was adjusted until optimum spray coating parameters were achieved and uniform sprayed was observed on figure 4.6 E. A spray coated electrode was shown in figure 4.7, the electrode showed surface uniformity and no cracks were observed.

The substrate used for spraying was cut to be 20 mm more than the required amount of surface for the MCDI electrodes so that samples were left for characterisation using BET and SEM analysis.

4.2.2 Electrode Uniformity

As was presented in Section 3.2.2 evaluation of the dimensional and surface uniformity of the fabricated electrodes was conducted through SEM analysis. The sample preparation in SEM analysis played a significant role in the images obtained both the surface and cross-sectional images. The images obtained from nitrogen freeze fractured electrode samples are shown in figure 4.8.

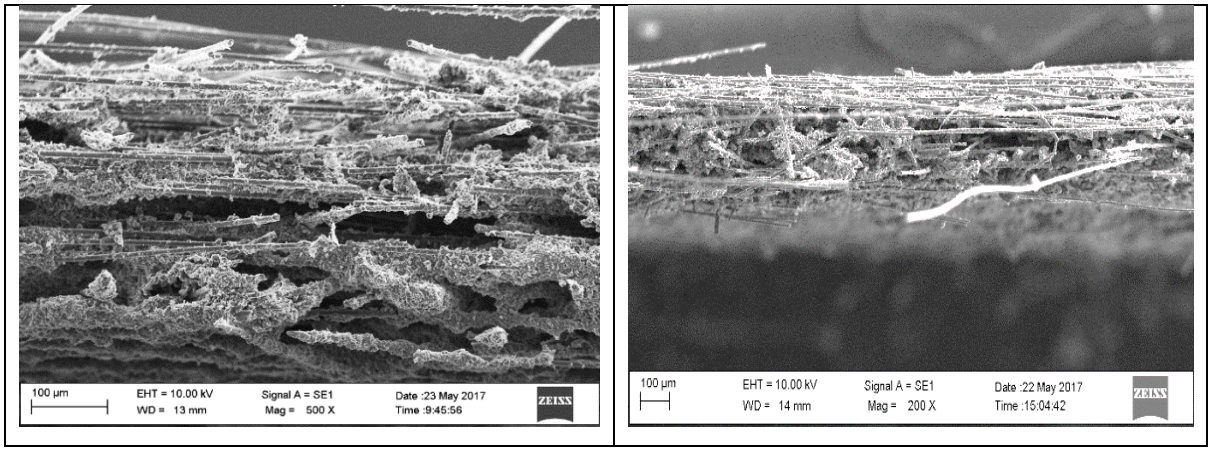

Figure 4.8 SEM images of electrode 11 prepared using liquid nitrogen fractured manually.

Figure 4.8 shows substrate fibres obstructing the view of the actual electrode, neither would a blade be used for a better cut as it would compress the electrode/substrate layers which would result in inaccurate thickness measurements. The use of a Graphtec cutting pro cutter facilitated the production of clear images shown in figure 4.9.

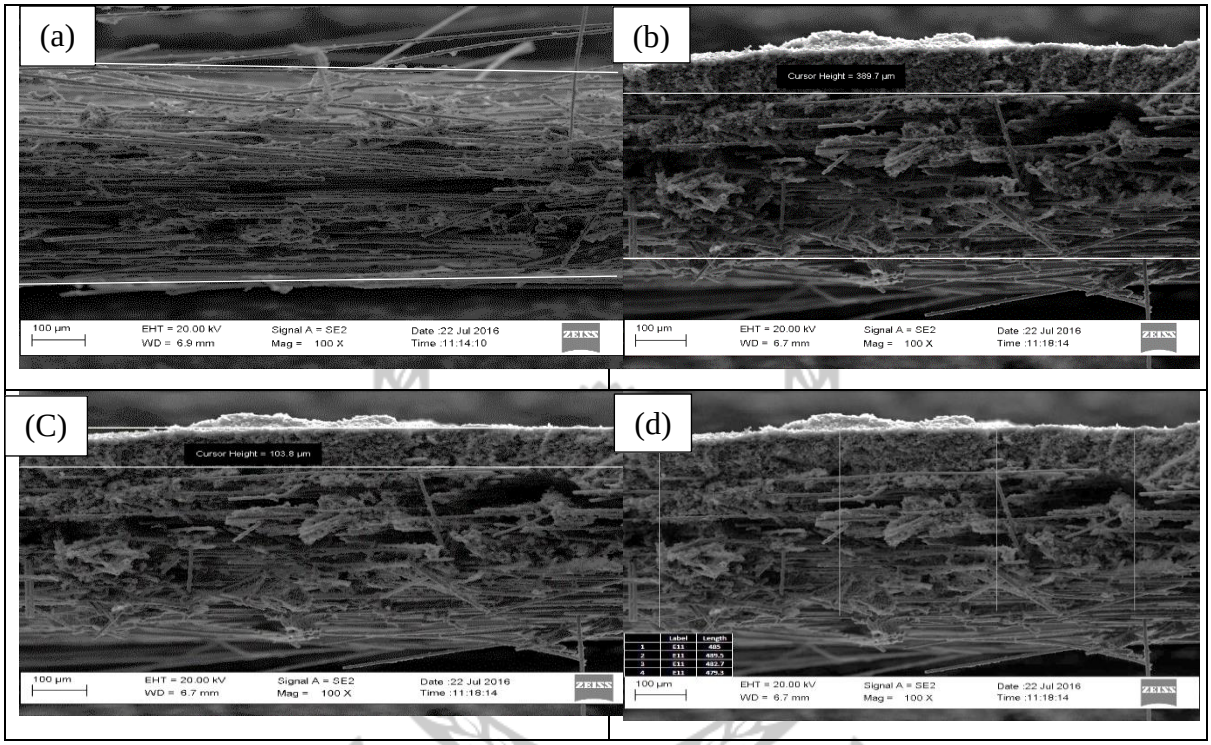

Figure 4.9 (a) SEM cross-sectional image of uncoated substrate JNT45, (b), (c) and (d) marked SEM cross-sectional image of electrode E11 prepared with the Graphtec cutting pro.

Figure 4.9 (a) showed the image of uncoated substrate JNT45 which allowed for a comparison between the sprayed electrode. The marked point in the images showed the points where the thickness was measured. A clear thick layer was observed on top of the substrate on the SEM image which was formed by the sprayed ink, the ink did not penetrate the surface of the substrate. Image of Fig. 4.9 (b) was marked from where the fibres of the substrate begin and end. Figure 4.9 (c) was marked to show the ink layer on the fibres of the substrate. JNT45 was found to have a thickness of between 389-400 µm. A total thickness of 480-485 µm of the entire electrode including the substrate was measured on the marked points of the image in Fig. 4.9 (d), an even distribution of ink throughout the substrate was observed. From the surface image a uniform distribution of the ink was observed the images are shown in appendix C.

4.3 Optimization of the Casting Method

4.3.1 Electrode Morphology

For the casting method of electrode production various factors had to be taken into consideration, these including the viscosity of produced slurry application of pressure on the substrate upon casting, drying temperature and time.

The ink prepared for casting had to be much more viscous than the ink used for spray coating hence the term "slurry" as such less solvent had to be used. Addition of 10 mL of solvent per gram of solid ingredients (activated, conductive additive and binder) resulted in a non-stable low viscosity slurry that could not be cast onto the substrate as it seeped through the substrate. Decreasing solvent amount to 7.5mL and then 5 mL of ink/gram of solid ingredients yielded a slurry of optimum viscosity that was castable onto the substrate.

Initially, the substrate was placed directly on the casting tool, however upon removal of the substrate with the dried casted ink slurry it would break rendering it unfit for adsorption-desorption measurements in the MCDI cell. Breakage of the electrode could be prevented when the casting tool was covered with a plastic wrap prior to the casting of the ink slurry.

The first pair of casted electrodes were dried in the oven at 180 ^{o}C for an hour however the electrodes appeared with cracks (shown at figure 4.10 a) and were not used for adsorption-desorption measurements in the MCDI cell. A second pair of electrodes was casted then left to dry at room temperature overnight (shown at figure 4.10 b), these electrodes had no cracks they were smooth and were used for adsorption-desorption measurement in the MCDI cell.

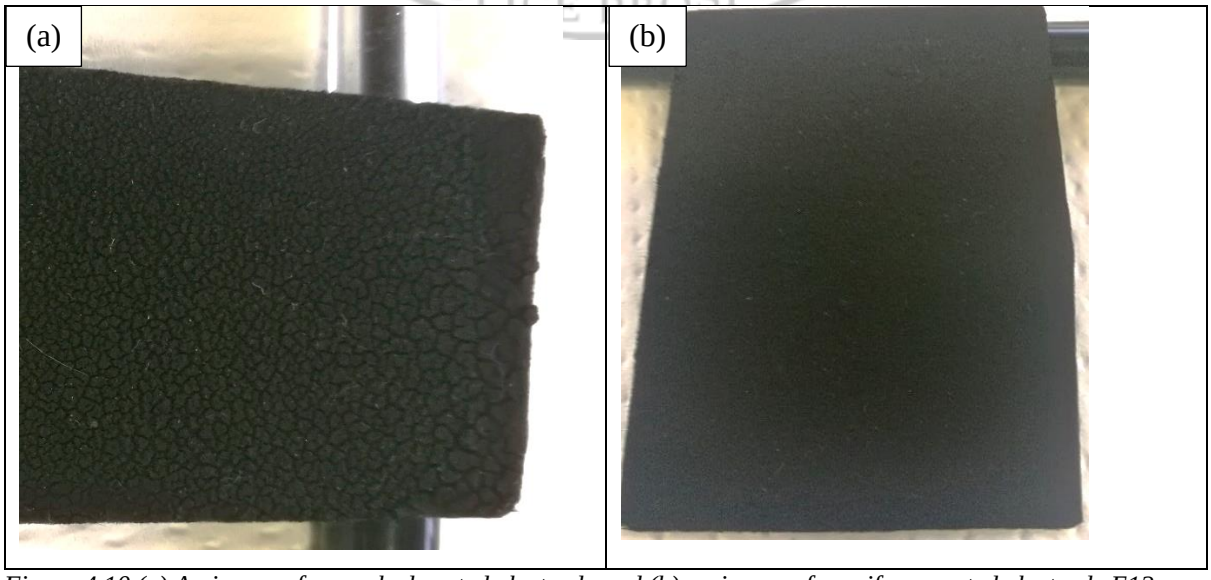

Figure 4.10 (a) An image of a cracked casted electrode and (b) an image of a uniform casted electrode E12.

4.3.2 Electrode Geometry and Uniformity

To evaluate the uniformity of the fabricated electrodes SEM analysis was used, sample preparation was the most important step for this analysis as a clear cut of the edge of the electrode is required to get suitable images from the microscope. The electrode were cut using Graphtec cutting pro cutter and the images obtained from SEM are shown in figure 4.11 below.

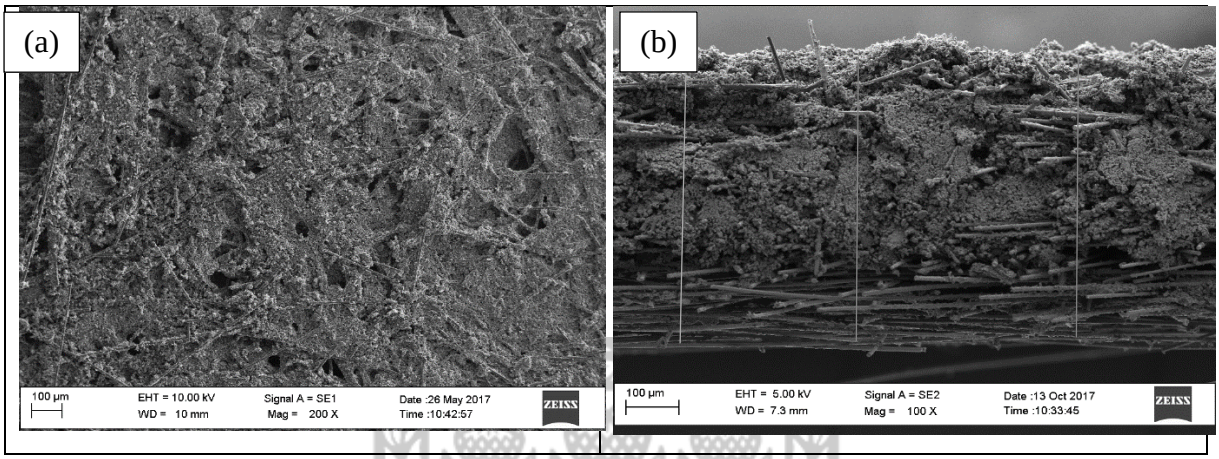

Figure 4.11 (a) Surface images obtained from SEM analysis and (b) Cross-section image obtained from SEM analysis for the casted electrode E12.

Uniformity of the electrodes was observed on the surface of the electrodes, a thickness of between 596-600 µm was obtained from the three marked points in the electrode image. However, on the cross-section image of the electrodes it was observed that the ink slurry penetrated the pored of the substrate and not only form a thick layer on top like the spray coating method.

4.4 Reproducibility of the Fabrication Method and MCDI Cell

4.4.1 Reproducibility of Ink Preparation Method

Cyclic Voltammetry was used as a technique to verify the reproducibility of the ink preparation method, to anticipate the ability of the carbon material to adsorb and desorb NaCl, specific capacitance and electrochemical stability prior to desalination of water.

To examine the reproducibility of the ink fabrication method and electrochemical stability of the carbonaceous materials 3 samples of ink 11 (80:10:10 YP50F: CB: PVDF) were prepared and CV analyses was conducted at 25 mV/s scan rate, the voltammograms obtained are shown in figure 4.12-4.14 below. Each ink was produced using the 80:10:10 composition, the amounts of the raw materials (YP50F, CB and PVDF) were the same in each ink, 3 inks had to be produced to examine the variation in the production method of the ink. The reproducibility was only performed on ink 11 as all the ink compositions were prepared the same way therefore

similar results were expected. It is important to note that the working electrode was prepared using three ink batches that were prepared on different dates.

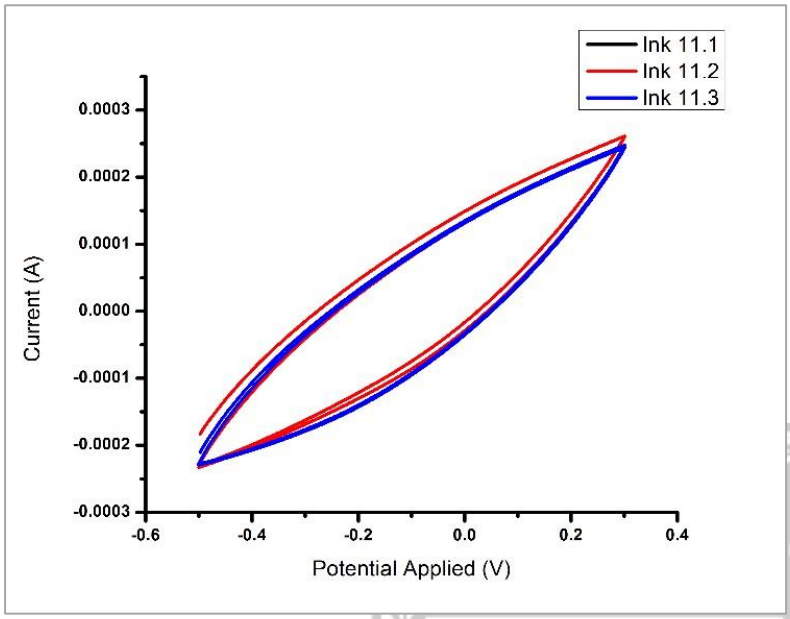

Figure 4.12 The voltammogram of electrode E11 at 0.5 g/L NaCl electrolyte at 25 mV/s scan rate.

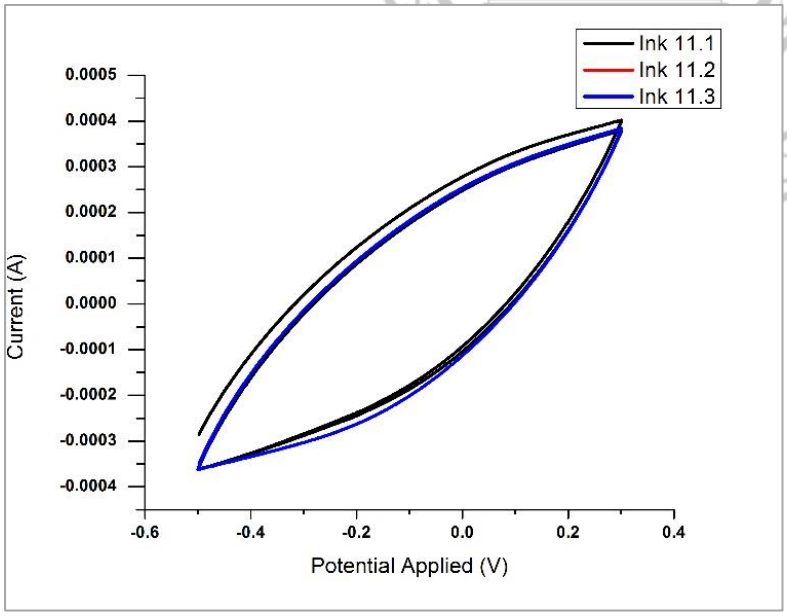

Figure 4.13 The voltammogram of electrode E11 at 1 g/L NaCl electrolyte at 25 mV/s scan rate.

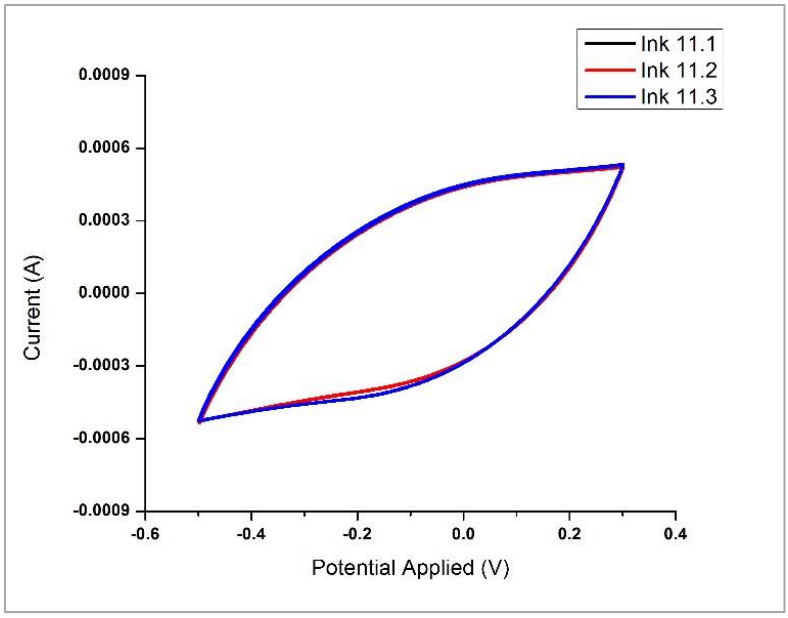

Figure 4.14 The voltammogram of electrode E11 at 2 g/L NaCl electrolyte at 25 mV/s scan rate.

On the voltammograms obtained no faradaic reactions or oxidation/reduction peaks were observed on the chosen potential range, the Na^+ and Cl^- ions were adsorbed onto the ink surface which illustrated the formation of an electrochemical double layer behaviour. The carbonaceous materials seemed electrochemical stable, ions were adsorbed onto the surface and the materials didn't show any oxidation/reduction peaks. Temperature fluctuations during the measurements were kept at a minimum as all measurements were performed in a jacked cell with active temperature control. Based on the good overlap of the voltammograms obtained for ink 11.1, 11.2 and 11.3 the ink fabrication method was deemed to be reproducible, the absence of the noticeably deviation between the cycles the electrode materials is considered electrochemically stable.

Specific capacitance of each ink was calculated and the results are shown in Table 4.2 below. Specific capacitance is the ability of the capacitor to store charge in farads per gram of the capacitor. The energy stored in the electrodes after the adsorption of ions charged species can be used to power-up another cell or system. At an electrolyte concentration of 0.5 g/L the average capacitance for ink 11 was determined to be 2.65 F/g with a standard deviation of 0.055 between the measured values of the 3 samples, at an electrolyte concentration of 1 g/L the average specific capacitance was 5.51 F/g with a standard deviation of 0.04 and at an electrolyte concentration of 2 g/L NaCl the average specific capacitance was 11.49 F/g with a standard deviation of 0.035. As the standard deviation includes analytical errors in both the

preparation of the ink and the working electrode, the obtained standard deviations are acceptable.

Table 4.2. The capacitance obtained for ink 11 at various concentrations of NaCl.

Ink name	Electrolyte Concentration (g/L)	Specific Capacitance (F/g)	Standard Deviation
Ink 11.1	0.5 g/L	2.60	0.055
Ink 11.2	0.5 g/L	2.65	
Ink 11.3	0.5 g/L	2.71	
Ink 11.1	1 g/L	5.47	0.04
Ink 11.2	1 g/L	5.51	
Ink 11.3	1 g/L	5.55	
Ink 11.1	2 g/L	11.45	0.035
Ink 11.2	2 g/L	11.50	
Ink 11.3	2 g/L	11.53	

According to literature carbon material with high surface area have high specific capacitance, the specific capacitance of ink was examined at 3 scan rates (5 mV/s, 10 mV/s and 25 mV/s) in the 3 NaCl concentrations (0.5 g/L, 1 g/L and 2 g/L). The specific capacitance calculated at the various scan rates and electrolyte concentrations are shown in table 4.3 below.

Table 4.3. Capacitance obtained for ink 11 at scan rates 5 mV/s, 10 mV/s and 25 mV/s.

Ink name	Electrolyte Concentration (g/L)	Scan Rate (mV/s)	Specific Capacitance (F/g)
Ink 11.1	0.5 g/L	5 mV/s	17.56
Ink 11.1	0.5 g/L	10 mV/s	7.73
Ink 11.1	0.5 g/L	25 mV/s	2.60
Ink 11.1	1 g/L	5 mV/s	28.42
Ink 11.1	1 g/L	10 mV/s	15.73
Ink 11.1	1 g/L	25 mV/s	5.47
Ink 11.1	2 g/L	5 mV/s	45.89
Ink 11.1	2 g/L	10 mV/s	43.86
Ink 11.1	2 g/L	25 mV/s	11.43

Two trends were observed on the specific capacitance of ink 11; trend 1, when the scan rate increased at the same NaCl concentration, the specific capacitance decreased. Increasing the scan rate decreases the time of adsorption which limits the adsorption. Trend 2, when the

concentration of NaCl was increased at the same scan rate the specific capacitance increased as more ions are available to participate in the adsorption/desorption process.

4.4.2 Reproducibility of the Fabrication Method and MCDI System Performance

To test the repeatability of the system an electrode (E11) of 210 × 150 mm dimensions was fabricated using the spray coating technique. The electrode was cut into 3 pairs of electrodes of 79 × 39 mm dimensions namely electrodes E11.1, E11.2 and E11.3. Each pair of electrode was subjected to 6 MCDI experiments, for each experiment the electrode was subjected to the standard preconditioning cycles as described in section 3.1.3.3. For each electrode pair, the mSAC and capacitance was derived from the 7th cycle and for each electrode pair the mSAC was established with 6 different experiments respectively. To determine the reproducibility of not only the testing procedure but also the cell assembly procedure the cell was completely disassembled and reassembled between each experiment. Figure 4.15 and table 4.4 below shows the mSAC and capacitance results for all the 18 experiments using the 3 electrode pairs that were cut from E11.

Table 4.4. Summary of the mSAC, capacitance and charge efficiency of electrode E11.

Electrode duplicate number	Electrode mass (g)	Feed flowrate (mL/Min)	Experiment number	mSAC (mg/g)	Capacitance (F/g)	Charge efficiency (%)
11.1	1.192	13	1	11.173	13.999	100
			2	11.182	14.222	100
			3	11.196	14.855	100
			4	12.119	15.550	100
			5	12.328	15.895	99
			6	12.484	16.112	100
11.2	1.192	13	1	10.171	13.870	96
			2	10.180	13.378	98
			3	10.190	14.071	99
			4	11.549	14.498	99
			5	11.707	14.887	100
			6	12.202	14.932	100
11.3	1.192	13	1	10.211	12.385	99
			2	10.218	12.941	99
			3	10.410	13.115	100
			4	10.512	13.416	100
			5	10.610	13.856	100
			6	10.759	13.999	99

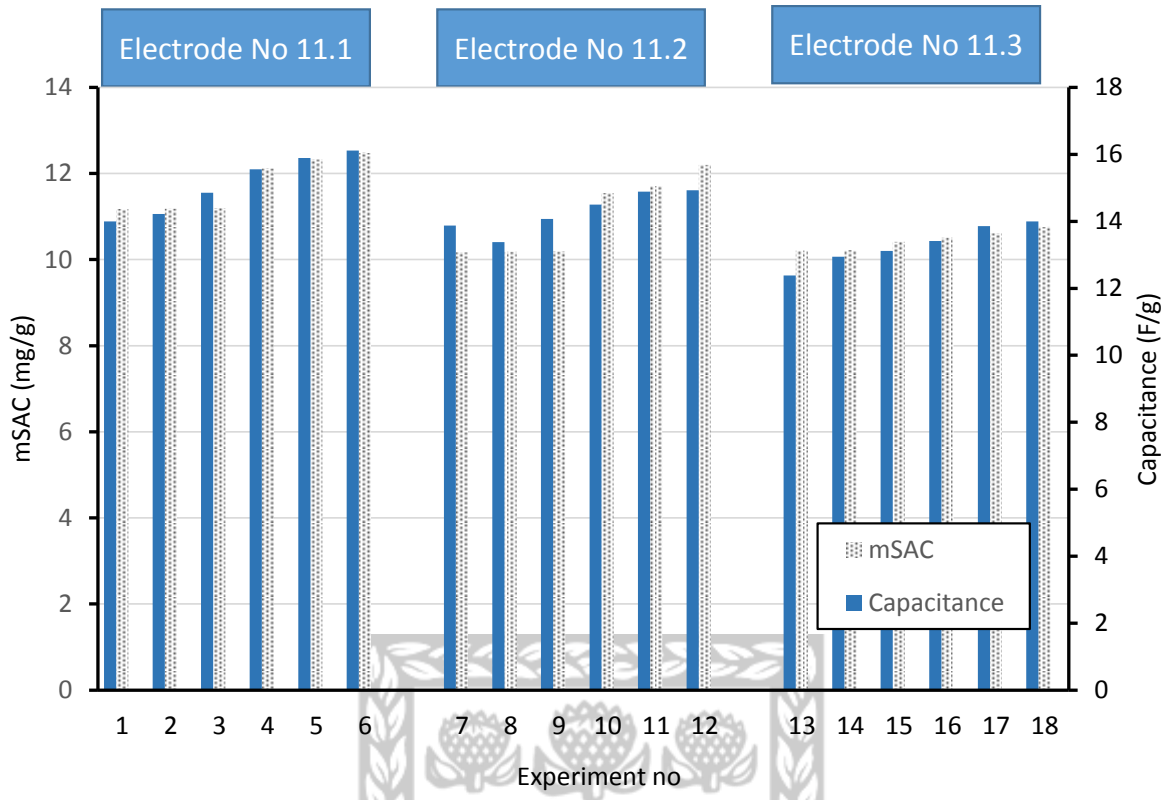

Figure 4.15 The mSAC and capacitance obtained from the 3 electrode pairs of electrode E11.

Table 4.4 illustrates the mSAC, capacitance and charge efficiency of the 3 electrode pairs of E11 whereas figure 4.15 shows a bar graph of mSAC and capacitance obtained from the 3 electrode pairs of E11. It was observed that the mSAC and capacitance consistently increased with each MCDI experiment. The first mSAC value obtained for each electrode is 11.17, 10.17 and 10.21 mg/g for electrode pair 11.1, 11.2 and 11.3 respectively, a mean value of 10.5 mg salt/g active material with a standard deviation of 0.56 mg salt/g active material. This variance was observed in the mSAC values between the electrodes prepared and measured following the same procedure.

As explained in section 3.1.3.2 capacitance is derived from the electrical charge (current) over the duration of the adsorption cycle. The mSAC is derived from the difference in the water conductivity between the feed water and treated water during the adsorption cycle. For each experiment, the capacitance and mSAC values are following the same trends. The charge efficiency being close to 100% confirmed that the nature of the adsorption and desorption is electrostatic and 100% reversible. Figure 4.16 shows the adsorption-desorption plot of the 3 electrode pairs 11.1, 11.2 and 11.3 respectively.

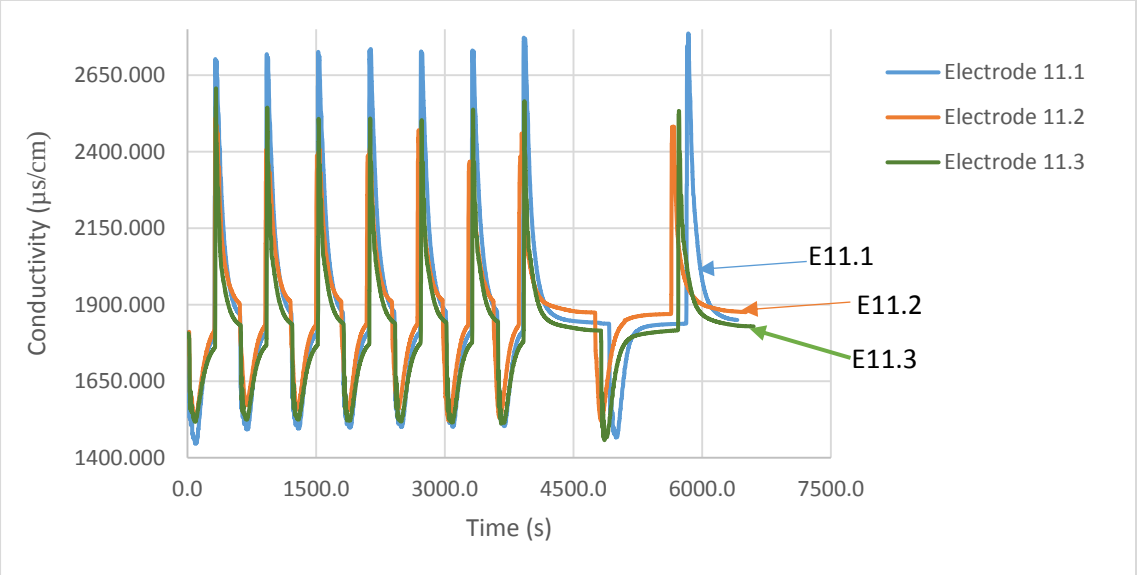

Figure 4.16 Adsorption-desorption measurement of three pairs of electrode E11.

In figure 4.16 the adsorption-desorption curves of the three electrode pairs were superimposed. Apart from a relative small deviation in the conductivity of the feed solution, the conductivity of the treated solution show a close resemblance for each electrode pair. The electrode pairs were adsorbing and desorbing approximately the same amount of ions under the same operational conditions. The variation of conductivity was observed on the adsorption-desorption curves and can be subscribed to the combination of the following parameters:

A. The cell assembly, at this point in time, the torque on the screws that hold the two cell parts together and influence the contact between electrodes, membranes and current collectors was not controlled other than the instruction to make it hand-tight.

B. Analytical errors in the feed solution preparation and conductivity measurement.
C. Fluctuation of the temperature, this variation is not expected to affect the adsorption-desorption greatly neither should it have a significant influence on the conductivity readings as they are temperature compensated.
D. Variation in the electrode assembly, the thickness of each electrode was confirmed by SEM and was found to be between 482 µm and 489µm.

According to the adsorption-desorption cycles of the electrode pairs and thickness measured on the cross-section of the electron pairs, reproducibility of the fabrication method of the electrodes and MCDI measurements was confirmed.

4.5 Optimization of the Electrode Materials and Production Materials

The main aim of this study was to develop electrodes, optimize the fabrication methods and the composition of the electrodes for MCDI. This section discusses the optimization of the materials used for production of electrodes (activated carbon), optimization of the methods of production (spray coating and casting method) and optimization of the electrode composition (various amounts of binder, conductivity additives which are carbon black and carbon nanotubes respectively and introduction of ion exchange material). The BET analysis was performed for all the carbonaceous materials and fabricated electrodes for this study and the results were recorded in table 4.5 and 4.6. In order to make a fair comparison of data, the surface area of the electrodes was normalized using the weight ration of the activated carbon as part of the sample, these normalized values are given in brackets.

Table 4.5. The BET results obtained for the activated carbon YP50F, TOB, Carbon black, Carbon nanotubes and electrodes fabricated using YP50F and TOB.

Sample			**Surface Area (m^2/g)**			**MPV** [c] **(cm^3/g)**	**Pore Size (Å)**
Name	Info [a]	R [b]	Obtained	Micropore	External		
CB (SA: 50-80m^2/g)		0	68	69	0.00	0.00	118
CNT (SA: 150-250m^2/g)		0	216	26	195	0.0098	237
TOB (SA: 2000-2500m^2/g)		1.0	2046	1285	761	0.59	10
E10-I10-TOB-JNT30	C-CB	0.51	876 (1460)[n]	629 (1048)[n]	155 (258)[n]	0.56	10
YP50F (SA: 1500-1800m^2/g)		1.0	1680	1350	330	0.54	20
E11-YP50-I11-JNT45	S-CB	0.49	634 (1294)[n]	503 (1027)[n]	131 (267)[n]	0.20	20
E12-YP50-I12-JNT45	C-CB	0.51	731 (1437)[n]	587 (1154)[n]	144 (283)[n]	0.23	20
E15-YP50-I16-JNT45	C-Binder (15)	0.46	629 (1413)[n]	507 (1139)[n]	122 (274)[n]	0.20	19
E17-YP50-I17-JNT45	C-CNT (10)	0.42	638 (1509)[n]	509 (1204)[n]	129 (305)[n]	0.20	22
E23-YP50-I23-JNT45	C-CNT (20)	0.36	445 (1187)[n]	346 (923)[n]	99 (264)[n]	0.14	27
E24-YP50-I24-JNT45	C-CNT (30)	0.31	322 (1036)[n]	242 (776)[n]	80 (257)[n]	0.097	35
E19-YP50-I19-JNT45-Anode	C-AEM	0.42	652 (1552)[n]	520 (1238)[n]	132 (317)[n]	0.21	19
E20-YP50-I20-JNT45-Cathode	C-CEM	0.41	460 (1121)[n]	358 (873)[n]	102 (249)[n]	0.14	21

[a] S=Sprayed C=Casted, CNT (10)=CNT 10% etc
[b] R; Ratio between sample weight and weight of active material
[c] MPV; Micro Pore Volume
[n] Normalized

Table 4.6 The BET analysis results for activated carbon YP80F and electrodes fabricated using YP80F.

Sample			**Surface Area (m^2/g)**			**MPV** [c] **(cm^3/g)**	**Pore Size (Å)**
Name	Info [a]	R [b]	Obtained	Micropore	External		
YP80F (SA: 2000-2500m^2/g)		1.0	2316	348	1969	0.16	22
E14-YP80-I14-JNT45	S-CB	0.46	524 (1145)[n]	93 (203)[n]	431 (941)[n]	0.039	22
E13-YP80-I13-JNT45	C-CB	0.46	922 (2010)[n]	177 (386)[n]	745 (1624)[n]	0.077	22
E16-YP80-I16-JNT45	C-Binder (15)	0.52	762 (1472)[n]	161 (311)[n]	601 (1161)[n]	0.20	22
E18-YP80-I18-JNT45	C-CNT (10)	0.46	778 (1697)[n]	153 (334)[n]	625 (1363)[n]	0.066	24
E21-YP80-I21-JNT45-Anode	C-AEM	0.42	862 (2052)[n]	164 (390)[n]	697 (1660)[n]	0.071	22
E22-YP80-I22-JNT45-Cathode	C-CEM	0.42	899 (2140)[n]	137 (326)[n]	763 (1817)[n]	0.060	22

[a] S=Sprayed C=Casted, CNT (10)=CNT 10% etc
[b] R; Ratio between sample weight and weight of active material
[c] MPV; Micro Pore Volume
[n] Normalized

4.5.1 Analogy of Three Activated-Carbons

According to literature the ideal electrode materials should have polarizability, low electrical resistance, high surface area and capacitance, electrochemical stability at applied voltage and high porosity [51]. High electrical conductivity of the electrode ensures that the electrode surface particles are charged with low electrical voltage losses whereas the binder maintains the structural stability of the electrode.

Three different activated-carbons were utilized in this study namely TOB, YP50F and YP80F, the following electrodes E10 (80:10:10 TOB: CB: PVDF), E12 (80:10:10 YP50F: CB: PVDF) and E13 (80:10:10 YP80F: CB: PVDF) were fabricated to compare the effect of the activated carbon material on the electrode performance and to select an activated carbon that would produce electrodes with superior adsorption capabilities for MCDI. The fabricated electrodes all have the same composition 80:10:10 which comprises of 80% activated-carbon 10% conductivity additive and 10% binder, the same amount of each ingredient was the same in all these electrodes. The BET results of the activated carbons, carbon black and fabricated electrodes shown in table 4.5 and 4.6.

The activated carbon material TOB had a surface area of 2046 m^2/g and an external surface area of 761 m^2/g. The activated carbon material YP50F had a surface area of 1680 m^2/g with a relative small external surface area of 330 m^2/g. The activated carbon material YP80F showed

the largest surface area of 2316 m^2/g with the most significant part measured as external surface area 1969 m^2/g.

The surface area of electrode E10 was normalized to its TOB contents (1460 m^2/g) which is only 71% of its original surface area. The surface area of electrode E12 normalized to its YP50F content was 1437 m^2/g, which is 86% of its original surface area. The surface area E13 normalized to its YP80 content was 2010 m^2/g, which is 87% of its original surface areas. The observed reduction in the available surface area of the active material in the electrode may be subscribed to the binder material that is blocking a portion of the highly developed surface of the activated carbon.

The activated carbon contributes mostly towards the surface area of the electrodes as the binder has no surface area and the conductivity additive has very low surface area (68 m^2/g). It was observed that YP80F has the highest external surface area of 1969 m^2/g whereas TOB had 761 m^2/g and YP50F 330 m^2/g. Table 4.7 summarises the surface areas of electrode E10, E12 and E13.

Table 4.7 Summary of the surface areas of electrode E10, E12 and E13.

Sample	**Normalized Surface Area (m^2/g)**			
	Total	%	Micropore	External
E10-I10-TOB-JNT30	1460	71	1048	258
E12-YP50-I12-JNT45	1437	86	1154	283
E13-YP80F-I13-JNT45	2010	87	386	1624

To evaluate the adsorption capacity of the electrodes, an adsorption-desorption measurement was performed in the MCDI cell, the time versus conductivity plot is shown in figure 4.17 below. The mSAC calculated from the data obtained from the adsorption-desorption measurement was plotted into a bar graph in figure 4.18.

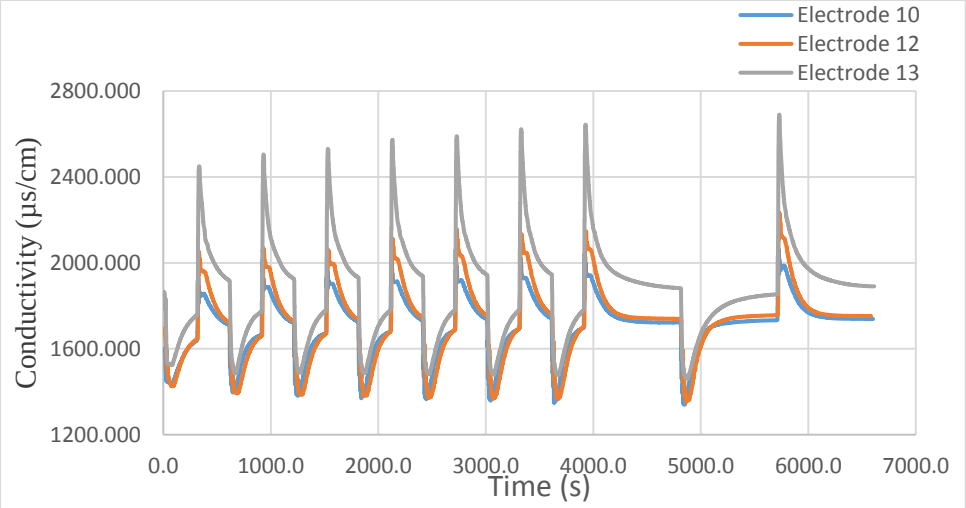

Figure 4.17 The adsorption-Desorption measurement of electrodes E10, E12 and E13.

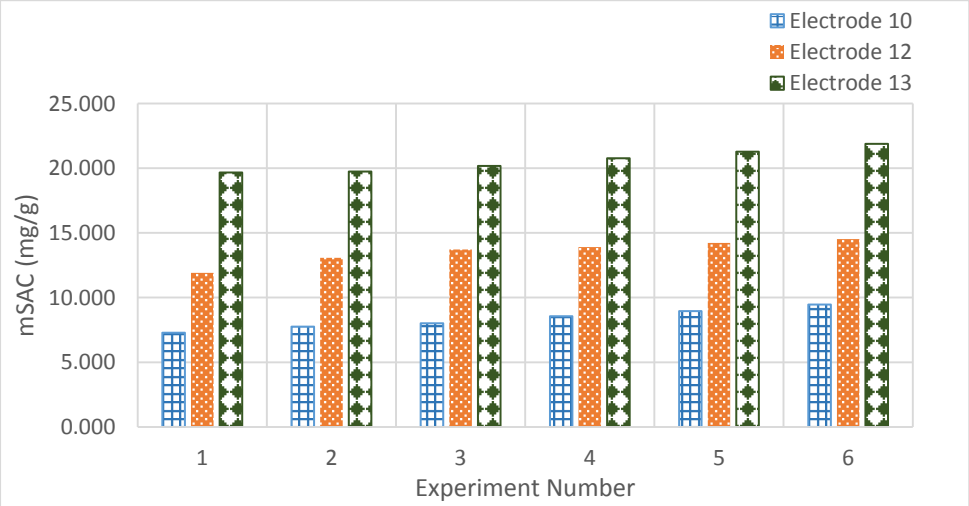

Figure 4.18 The calculated mSAC of electrodes E10, E12 and E13 for each experiment.

A small analytical error of about 0.0001% in feed water preparation may have resulted in a slightly different feed water conductivity but other reasons to explain the rather significant difference should be investigated.

The highest mSAC value obtained for electrode 10 was 9.46 mg/g, for electrode 12 it was 14.52 mg/g and for E13 it was 21.88 mg/g. When the trends with mSAC values are compared with the trends observed with the BET results the following conclusion can be drawn, the electrode showing the largest BET surface area, shows the largest mSAC performance. Secondly, mSAC performance of electrode material is predominantly determined by the external surface area and not by micropores surface area. Activated carbon YP80F with its superior external surface area and less significant microporous area is showing to be the most promising activated carbon for the production of MCDI electrodes.

4.5.2 Effect of the Fabrication Method on Electrode Performance

Highly effective electrodes are a combination of high surface area and conductivity materials however, the dynamics of the adsorption-desorption of ions into to the electrodes is also influenced by the method of fabrication. The spray coating method and casting method were used for electrode production, the methods of fabrication are explained in detail in chapter 3 section 3.2.2. To study the effect of the method of production on the electrode performance, electrodes E13 and E14 were fabricated with the same composition (80:10:10 YP80F: CB: PVDF). E14 was produced using the spray coating method whereas E13 was produced using the casting method. Adsorption-desorption measurement was performed in the MCDI cell, figure 4.19 shows the plot of the time versus conductivity.

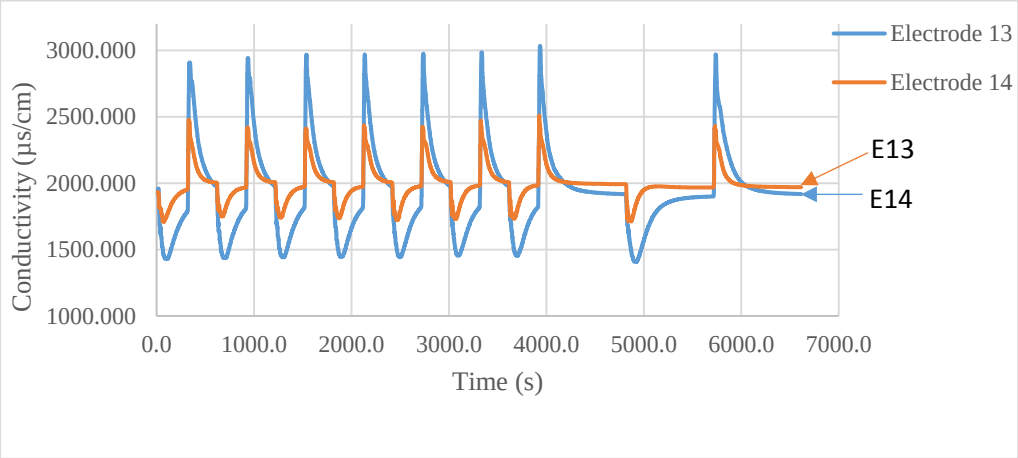

Figure 4.19 The adsorption-Desorption measurement of casted E13 and sprayed E14 electrodes

Despite a minor variance in feed water conductivity between the two experiments, it was evident that electrode E13 showed a significantly higher adsorption capacity than electrode E14. The mSAC values were calculated from the data obtained on the adsorption-desorption measurement results, figure 4.20 shows the mSAC obtained for both electrode E13 and E14.

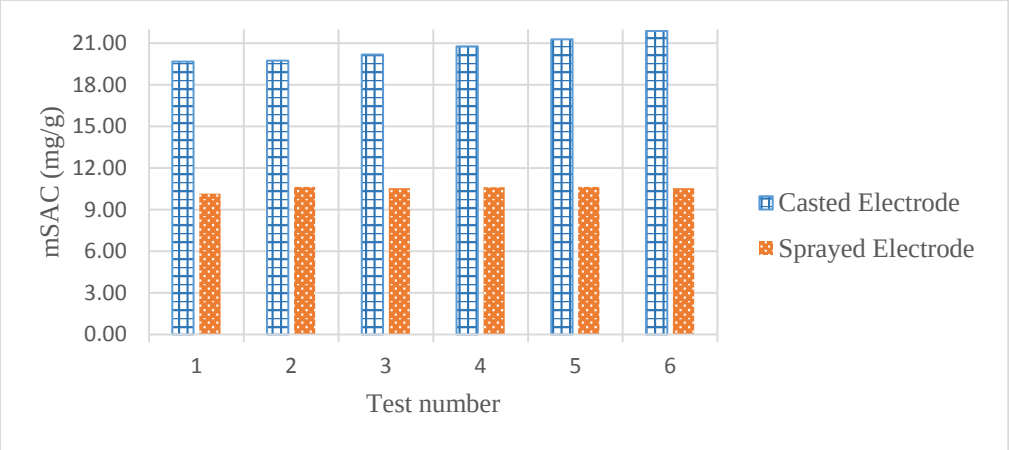

Figure 4.20 The calculated mSAC of the casted and sprayed electrodes for a series of 6 experiments.

Table 4.8 summarizes the surface areas of electrodes E13 and E14, normalized to the weight of YP80F in relation to the electrode. BET results of the unprocessed YP80F powder is also provided.

Table 4.8 Summary of the surface area of electrodes E13 and E14.

Sample	**Normalized Surface Area (m^2/g)**				**MPV (cm^3/g)**
	Total	%	Micropore	External	
YP80F (SA: 2000-2500m^2/g)	2316		348	1969	0.16
E13-YP80F-I13-JNT45 (Casted)	2010	87	386	1624	0.08
E14-YP80F-I14-JNT45 (Sprayed)	1145	49	203	941	0.04

An interesting observation was that the normalized surface area for casted electrodes was much closer to the value of unprocessed YP80F (87%) than the normalized surface area for sprayed electrodes where only 49% was retained. This observation correlates with the mSAC values found for the electrode E13 and E14 (Fig. 4.19). It is important to emphasize that both electrodes are made with the same ingredient and with identical ratios between activated carbon, carbon black and binder. The difference in the performance relates to the difference in the production technique. Since the difference in performance were rather remarkable, this set of experiments was repeated several months after the first set, providing the same conclusion.

As mentioned before, the decrease in the electrode surface area was due to the method of production of the electrode. During the casting method, the ink was dispersed onto the support structure as a liquid but during the spray coating method the ink was dispersed into the support structure as microscopic droplets which when exposed to temperatures between 100-140^oC

loose most of their solvent and become solid particles that stack onto each other when reaching the support structure. Figure 4.18 (a) and (b) below depict the cross-sections of casted electrode E13 and sprayed electrode E14 respectively.

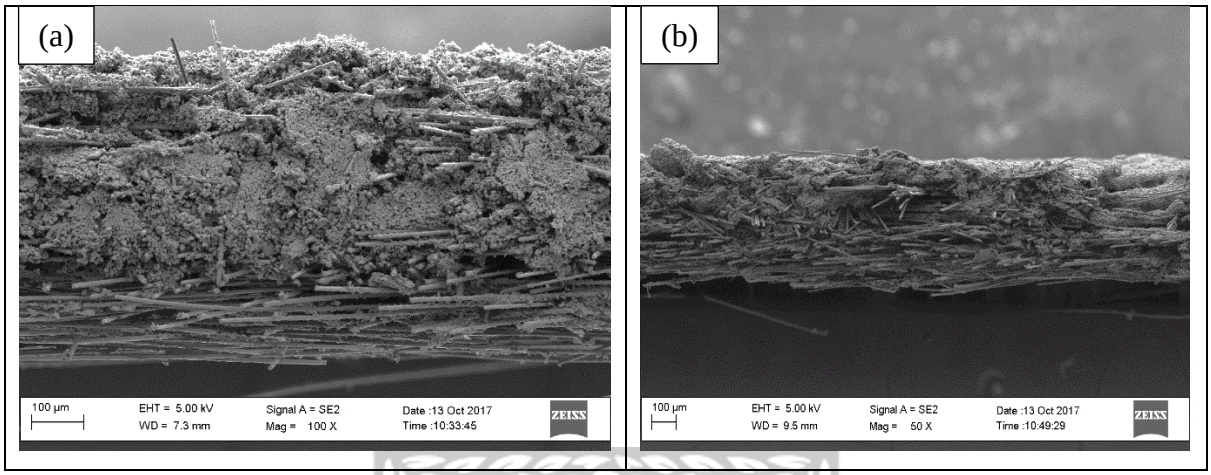

Figure 4.21 SEM cross-sectional images of (a) E13 and (b) E14.

The images confirm that spray coating method yield a coating that does not penetrate the support whereas the casting method shows deposits throughout the support. My hypothesis was that the conditions created during spray coating allow the binder to encapsulate the agglomerates in the ink which leads to the significant loss of external surface area.

The method of electrode production affects the performance of the electrodes significantly. The sprayed electrode yields lower BET surface area, external surface area, micropore area and micropore volume compared to the casted electrode. The casted electrode showed higher adsorption capacity than the sprayed electrode. The casting method is the preferred method of production for MCDI electrodes.

4.5.3 Comparison of Two Different Electrical Conductivity Additives

For all the surface particles in the electrode to remain charged as ions are being adsorbed high electrical conductivity of the electrode is desired. Activated-carbon used for the electrode fabrication has a relatively low electric conductivity therefore a conductivity additive had to be added. Carbon nanotubes and carbon black were used respectively as additives to enhance the conductivity of the electrode.

4.5.3.1 Casted YP50F electrode with CB and CNTs

The performance of electrode E12 (80:10:10 YP50F: CB: PVDF) with carbon black and electrode E17 (80:10:10 YP50F: CNT: PVDF) with carbon nanotubes were analysed. BET

analysis results performed on the activated carbon, carbon black, carbon nanotubes and fabricated electrodes were shown in table 4.9.

Table 4.9 Summary of the BET results of fabricated of electrode E12 and E17 and their raw materials.

Sample	**Normalized Surface Area (m^2/g)**				**MPV (cm^3/g)**
	Total	%	Micropore	External	
YP50F (SA: 1500-1800m^2/g)	1680		1350	330	0.54
CB (SA: 50-80m^2/g)	68		69	0	0
CNT (SA: 150-250m^2/g)	216		26	195	0.001
E12-YP50-I12-JNT45	1437	86	1154	283	0.23
E17-YP50-I17-JNT45	1509	90	1204	305	0.20

The normalised surface areas of electrode E12 and E17 obtained were recorded in table 4.9. Electrode E17 showed a higher surface area of 1509 m^2/g which was 90% of the activated carbon YP50F. Electrode E12 had a surface area of 1437 m^2/g which was 86% of the activated carbon YP50F. CNTs have a weight specific surface area of 216 m^2/g whereas CB has a weight specific surface area of 68 m^2/g. This meant that a larger portion of the binder was interacting with the CNT surface, hence the lower reduction in the normalised surface area for electrode E17 when compared to electrode E12 even though they showed the same ratios between the active carbon and binder, share the same method of production and contain the same amount and type of activated carbon.

An adsorption-desorption measurement was performed in the MCDI cell, figure 4.22 shows the plot of the time versus conductivity. The mSAC values were calculated from the data obtained on the adsorption-desorption measurement results, figure 4.23 shows the mSAC obtained for both electrode E12 and E17.

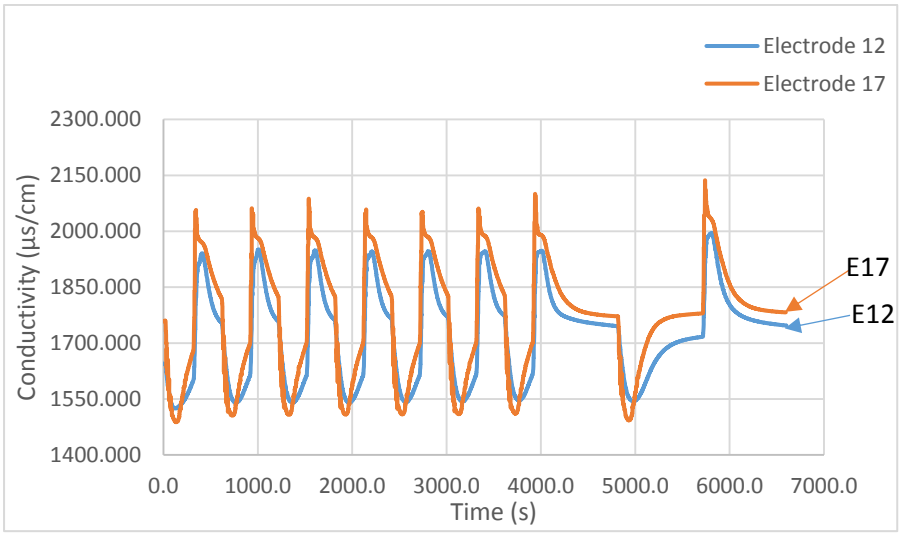

Figure 4.22 Adsorption-desorption measurement for electrode E12 and electrode E17

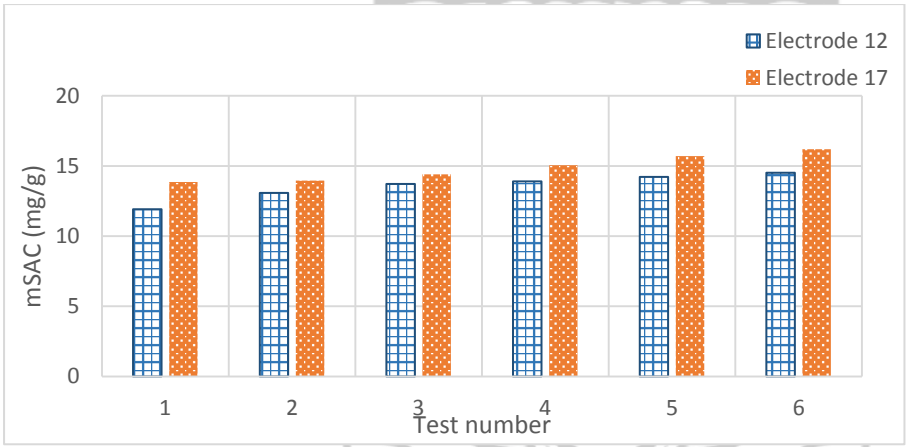

Figure 4.23 The mSAC values calculated of electrode E12 and electrode E17

Electrode E17 showed higher adsorption than electrode E12 on the plot in figure 4.22. From the adsorption-desorption measurement mSAC was calculated for the 6 experiments for both electrode E12 and E17. From the bar graph it was clear that the mSAC of electrode E17 was on average 6% higher than the mSAC of electrode E12. As per prior experiments, an increase of the mSAC was observed for consecutive experiments.

CNTs have a higher BET surface area, micropore area and external surface area than CB. The electrode with CNTs as a conductivity additive had higher BET surface area, micropore area and external surface area than the electrode with CB. Electrode E17 with CNTs performed consistently better to electrode E12. From a technical point of view, CNTs would be the preferred electrical conductivity additive of choice for MCDI electrodes. For large scale electrode production, the cost implications have to be weighed against performance parameters.

4.5.3.2 Casted YP80F electrodes with CB ad CNTs

As mentioned in the section above carbon black and carbon nanotubes were used as electrical conductivity additives and electrode were fabricated with E12 and E13 having CB, E17 and E18 having CNTs. Similar to electrode E17, electrode E18 was produced, also with CNT instead of CB but with YP80F as an activated carbon. Electrode E18 had to be compared to electrode E13.

Due to the difference in the properties of YP50F and YP80F they may be affected differently by the binder and conductivity additives in the ink used for electrode production. The BET analysis results of YP80F, CNT, CB, E13 and E18 obtained are shown in Table 4.6. Table 4.10 showed the summary of the normalised BET results of electrodes E13 and E18 with their raw materials.

Table 4.10 Summary of the BET results of electrode E13 and E18 and their raw materials.

Sample	**Normalized Surface Area (m^2/g)**				**MPV (cm^3/g)**
	Total	%	Micropore	External	
YP80F (SA: 2000-2500m^2/g)	2316		348	1969	0.16
CB (SA: 50-80m^2/g)	68		69	0	0
CNT (SA: 150-250m^2/g)	216		26	195	0.001
E13-YP80-I13-JNT45 (10% CB)	2010	87	386	1624	0.08
E18-YP80-I18-JNT45 (10% CNT)	1697	73	334	1363	0.07

Contrary to the results presented in the previous section, the normalised BET surface area of electrode E13, the one with CB, was significantly higher than that of electrode E18, the one with CNT. The results suggest that YP80F in combination with CB is less prone to the coverage with conductivity additive than YP80F in combination with CNT, at this stage it remains unclear why.

To study the performance of the electrodes, an adsorption-desorption measurement was performed in the MCDI cell. Figure 4.24 showed the adsorption-desorption measurement graph. The adsorption capacity of the electrodes was determined by calculating the mSAC for each experiment, figure 4.25 shows a bar graph of the mSAC obtained for both electrodes E13 and E18.

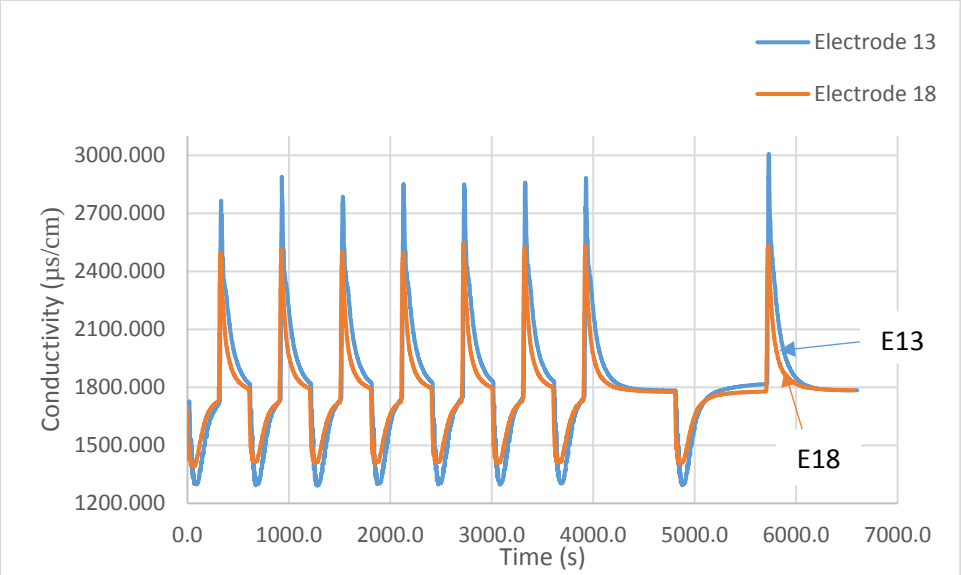

Figure 4.24 Adsorption-desorption measurement of electrode 13 and electrode 18.

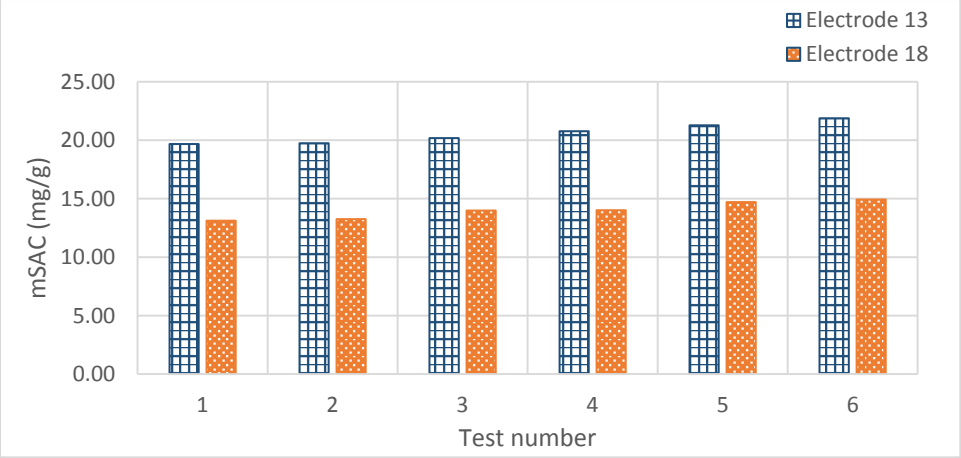

Figure 4.25 mSAC of electrode E13 and electrode E18 for all 6 experiments of each electrode.

On figure 4.24 adsorption-desorption plot, electrode E13 showed higher adsorption than electrode E18. The mSAC calculated from the adsorption-desorption measurement results also showed electrode 13 to have higher adsorption capacity. The mSAC of E13 obtained was 38% higher than that of E18. It appeared that electrode 18 with CNTs as an additive had a 17% lower surface area than that of electrode 13 with CB. CNTs have a higher BET surface area, micropore area, external surface area and micropore volume than CB.

Electrode E18 with CNTs as electrical conductivity additives had lower adsorption capacity than electrode E13 with CB. The CNTs affected the surface area and micropores of YP50F and YP80F electrodes differently, this may be due to the difference in the properties of the virgin activated carbon. For large scale electrode production the cost implications would have to be weighed against performance parameters to pick the preferred electrical conductivity additive.

4.5.4 Effect of Inflated Amount of Binder on Electrode Performance

To maintain the uniformity and mechanical stability of the electrode a binder solution is utilized in the electrode fabrication methods. However, the binder can also block pores thereby affecting the performance of the electrode. Therefore, it is important to optimize the amount of binder utilized in the electrode fabrication.

4.5.4.1 Comparison of YP50F electrodes

Electrode E12 (80:10:10 YP50F: CB: PVDF) and E15 (75:5:15 YP50F: CB: PVDF) were fabricated to determine the optimum amount of binder suitable for electrode production. BET analysis of the electrodes was performed to study whether the amount of binder utilized affected the BET surface area, external surface area, pore size and pore volume of the electrodes, the BET results obtained are shown in table 4.5 above. The summary of the BET results of electrode E12 and E15 as well as the activated carbon YP50F were shown in table 4.11.

Table 4.11 Summary of the BET results of electrodes E12 and E15 and activated carbon YP50F.

Sample	**Normalized Surface Area (m^2/g)**				**MPV (cm^3/g)**
	Total	%	Micropore	External	
YP50F (SA: 1500-1800m^2/g)	1680		1350	330	0.54
E12-YP50-I12-JNT45 (10% Binder)	1437	86	1154	283	0.23
E15-YP50-I15-JNT45 (15% Binder)	1413	84	1139	274	0.20

The normalised surface area of electrode E12 was slightly higher than that of electrode E15 which was 86% of that of virgin YP50F. The normalised surface area of electrode E15 was only lower by 2% from electrode E12, which was 84% that of the virgin YP50F. The increase in the binder amount reduced the external surface area of the electrodes. The external surface area of electrode E12 decreased by 15% whereas the external surface area of electrode E15 decreased by 18%. This decrease in the surface area of the electrodes may be due to the covering by the PVDF binder.

To establish the effect of the amount of binder in the electrode, the performance was examined by the adsorption-desorption of water measurement in the MCDI cell. The conductivity versus time shown in figure 4.26 was obtained from the adsorption-desorption measurements. The mSAC of both electrode 12 and 15 was calculated from the data obtained from the adsorption-desorption measurement, figure 4.27 shows the plot of the mSAC calculated for each experiment of electrode 12 and 15.

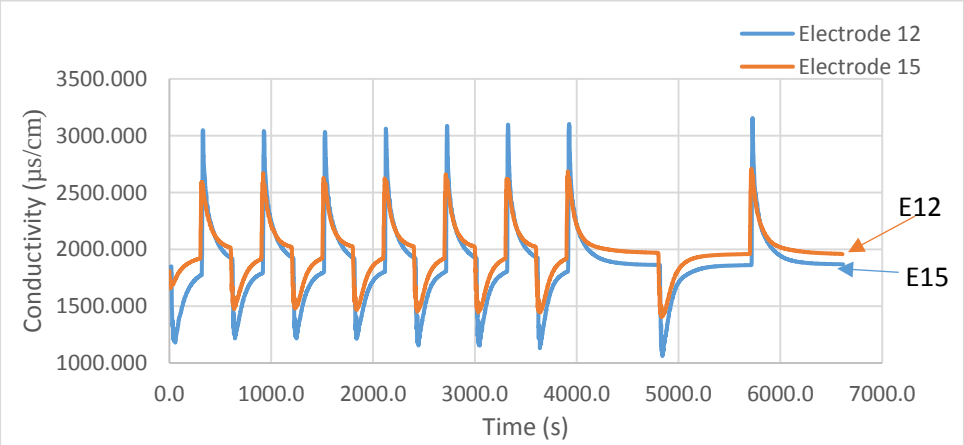

Figure 4.26 Adsorption-desorption measurement of electrodes E12 and E15.

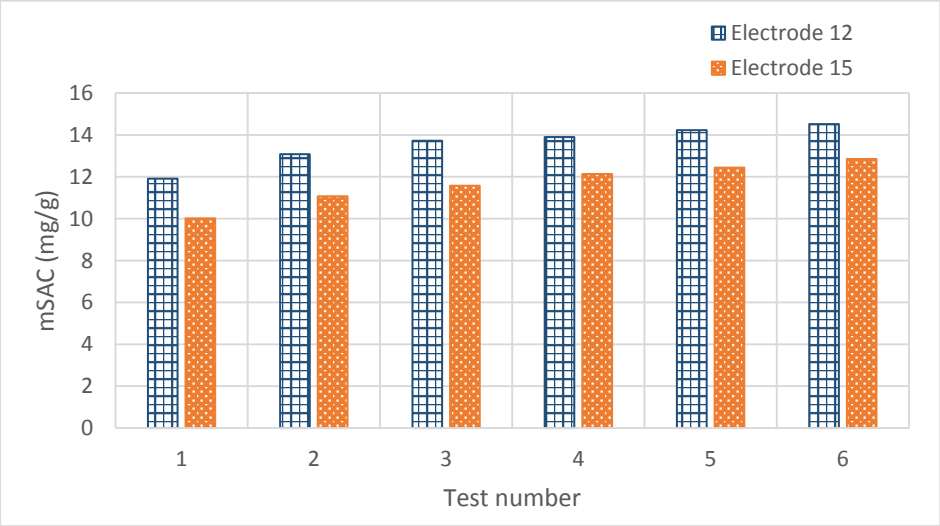

Figure 4.27 mSAC of electrode E12 and electrode E15 for each adsorption-desorption measurement.

On figure 4.26 adsorption-desorption measurement, electrode 12 showed higher adsorption than electrode 15. From the mSAC calculated E12 had the highest mSAC of 14.52 mg/g whereas E15 had a highest mSAC of 12.85 mg/g. A binder is required to maintain uniformity and mechanical stability in the electrode, using SEM analysis it was observed that the electrodes had a uniform surface and thickness (SEM images shown in Appendix B). The amount of the binder used affects the performance of the electrode therefore an optimum amount of binder has to be used for electrode production. Electrode E12 with 10% binder had higher micropore surface area and micropore volume compared to electrode E15 with 15% binder. Increasing the amount of binder by 5% reduced the total surface area, micropore area, external surface area and the micropore volume of the fabricated electrode. The use of excess

amount of binder reduced the adsorption capacity of electrodes. The binder added onto the ink solution for electrode production covers the surface area of the electrodes hence the decrease in the surface of the electrodes from that of the virgin activated carbon.

4.5.4.2 Comparison of electrode 13 and electrode 16

Two more electrodes with 10% and 15% binder ratios were fabricated to verify the effect of inflated amount of binder and optimize the amount of binder in the electrodes with YP80F as an activated carbon. E13 (80:10:10 YP80F: CB: PVDF) and E16 (75:5:15 YP80F: CB: PVDF) were fabricated, the BET analysis results obtained are shown in table 4.6. The summary of the BET results of electrodes E13 and E16 were recorded in table 4.12.

Table 4.12 Summary of the BET results of electrodes E13 and E16 and activated carbon YP80F.

Sample	**Normalized Surface Area (m^2/g)**				**MPV (cm^3/g)**
	Total	%	Micropore	External	
YP80F (SA: 2000-2500m^2/g)	2316		348	1969	0.16
E13-YP80-I13-JNT45 (10% Binder)	2010	87	386	1624	0.08
E16-YP80-I16-JNT45 (15% Binder)	1472	64	311	1161	0.20

The normalised surface area of electrode E13 was 87% that of virgin activated carbon YP80F, this slight decrease in the surface area was expected and is accounted for by the addition of the conductivity additive and binder into the ink solution. The normalised surface area of electrode E16 was found to be 64% relative to that of the virgin activated carbon YP80F. The surface area of the electrode E16 decreased greatly compared to that of electrode E13. The observed reduction in the available surface area of the active material in the electrode may be subscribed to the binder material that is blocking a portion of the highly developed surface of the activated carbon.

The adsorption-desorption measurement was performed in the MCDI cell, figure 4.28 shows the conductivity versus time plot. To determine the adsorption capacity, mSAC was calculated from the adsorption-desorption measurement data, figure 4.29 shows the mSAC obtained from each experiment for both electrode E13 and E16.

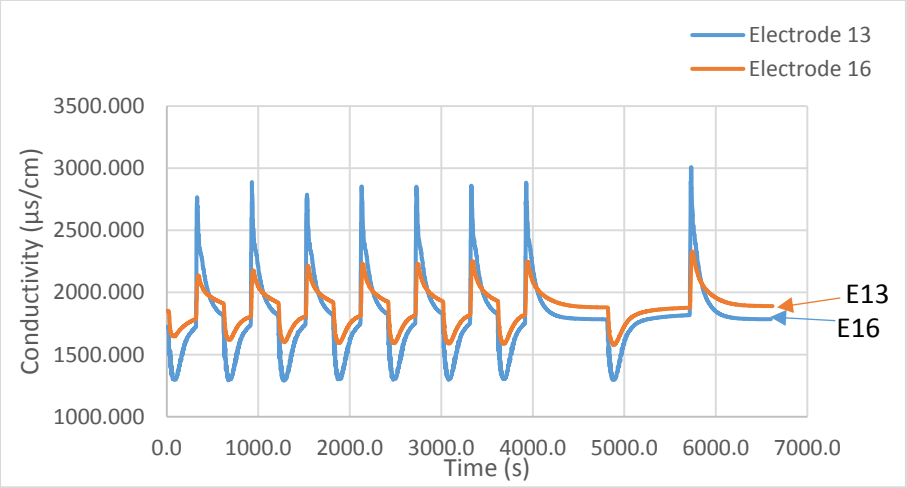

Figure 4.28 Adsorption-desorption measurement of electrode E13 and electrode E16.

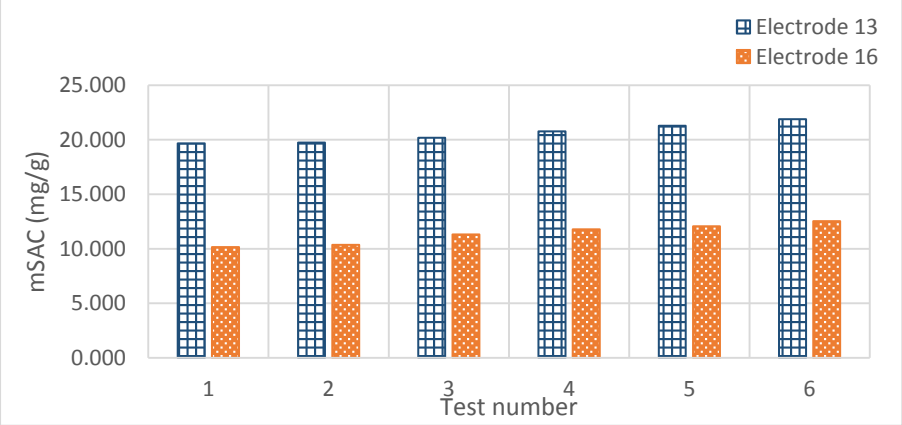

Figure 4.29 mSAC of electrode E13 and electrode E16 for each adsorption-desorption measurement.

A small analytical error in feed water preparation may have resulted in a slightly different feed water conductivity but other reasons to explain the rather significant difference should be investigated. A vast difference in the performance of electrode E13 and E16 was observed on the adsorption-desorption measurement plot. From the conductivity versus time plot in figure 4.28 electrode E13 showed higher adsorption than electrode E16. To determine the adsorption capacity of the electrodes, mSAC was calculated for both electrodes for each experiment. Electrode E13 had the highest mSAC of 21.88 mg/g whereas electrode E16 had the highest mSAC of 12.53 mg/g. An increase in the amount of binder in the electrode production reduced the surface area and pore size of electrode E16 thereby reducing the adsorption capacity of the electrode. The BET surface area, external surface area and pore size of electrode E16 were lower than that of electrode E13 due to the increase in the amount of binder. It can be can concluded that 10% binder is the desirable amount required for electrode production.

4.5.5 Effect of the Amount of Conductive Additive on Electrode Performance

CNTs were incorporated in the electrode materials to increase the conductivity of the electrodes. To study the effect of the CNTs on electrode performance three electrodes with 10%, 20% and 30% of the additive were produced; E17 (80:10:10 YP50F: CNT: PVDF), E23 (70:20:10 YP50F: CNT: PVDF) and E24 (60:30:10 YP50F: CNT: PVDF). BET analysis was conducted to determine the surface area and porosity of the activated carbon and the fabricated electrodes, the results were recorded in table 4.5. The summary of the BET results of the electrodes E17, E23 and E24 and their raw materials were recorded in table 4.13.

Table 4.13 Summary of BET results of the electrodes E17, E23 and E24 and their raw materials.

Sample	**Normalized Surface Area (m^2/g)**				**MPV (cm^3/g)**	**Pore Size (Å)**
	Total	%	Micropore	External		
YP50F (SA: 1500-1800m^2/g)	1680		1350	330	0.54	20
CNT (SA: 150-250m^2/g)	216		26	195	0.001	237
E17-YP50-I17-JNT45 (10 CNT)	1509	90	1204	305	0.20	22
E23-YP50-I23-JNT45 (20 CNT)	1187	71	923	264	0.14	27
E24-YP50-I24-JNT45 (30 CNT)	1036	62	776	257	0.097	35

The normalised surface area of electrode E17 with 10% CNTs had the highest surface area which was 90% that of the virgin activated carbon YP50F. The normalised surface area of electrode E23 with 20% CNTs was 71% that of the activated carbon YP50F. Electrode E24 had the least surface area of 62% that of the activated carbon YP50F. It was noted that the surface area and the micropore volume of the electrodes decreased when the amount of CNTs increased. However the pore size of the electrodes increased with increasing amount of CNTs which could be influenced by the high pore size of the CNTs. CNTs have a significantly lower surface area and micropore volume but high pore size compared to the activated carbon YP50F.

The adsorption-desorption measurement was performed in the MCDI cell, figure 4.30 shows the conductivity versus time plot. To determine the adsorption capacity, mSAC was calculated from the adsorption-desorption measurement data, figure 4.31 shows the mSAC obtained from each experiment for both electrode E13 and E16.

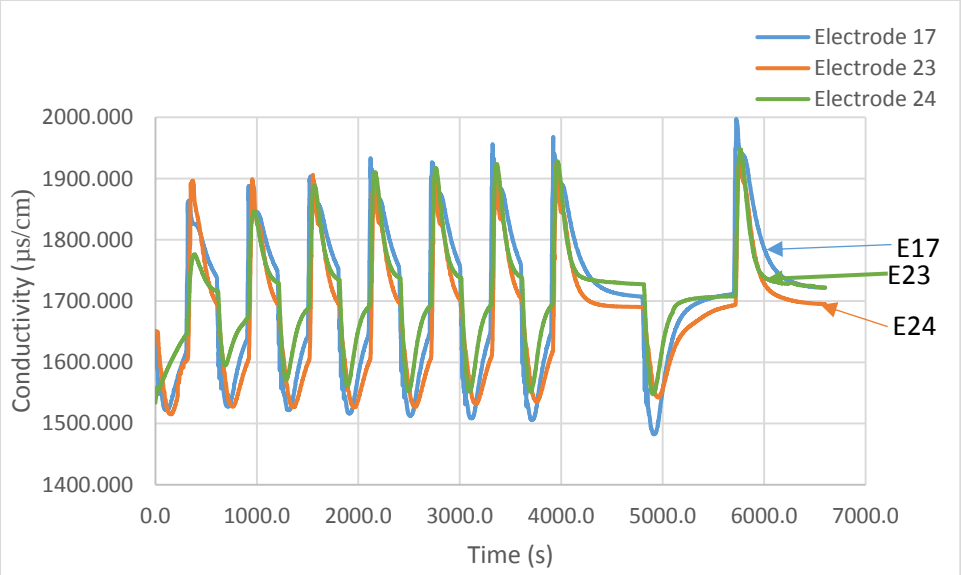

Figure 4.30 Adsorption-desorption measurement of electrodes E17, E23 and E24.

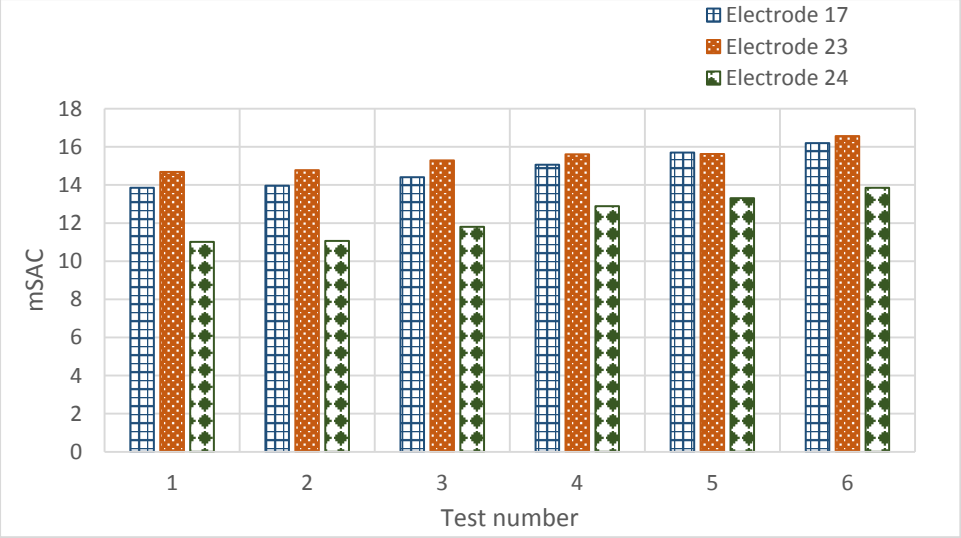

Figure 4.31 The calculated mSAC of electrode E17, E23 and E24 for each adsorption-desorption measurement.

CNTs had proved to be the preferred conductivity additive for electrodes with YP50F, to determine the optimum amount of CNTs required for electrode production electrodes E17, E23 and E24 were produced. Electrode E23 with 20% CNTs showed higher adsorption than electrode E17 and E24 with 10% and 30% CNTs respectively. However, there was only 4% difference in the adsorption capacity of electrodes E17 and E23. Electrode E17 had the highest mSAC of 16.19 mg/g, electrode E23 had the highest mSAC of 16.56 mg/g and electrode E24 had the highest mSAC of 13.85 mg/g.

The adsorption capacity of electrode E17 and E23 was almost the same however E23 had the highest capacity. This is in contrast with earlier observations as typically the highest surface area gave the highest capacity. Electrode E24 had very low surface area which resulted in the poor adsorption capacity. Porosity plays an important role in electrode adsorption capacity of the electrodes in the MCDI system. The optimum amount of CNTs to use for electrode fabrication would be 20% since electrode E23 showed superior adsorption. However for large scale electrode production the cost implications would have to be weighed against performance parameters to pick the preferred amount of the electrical conductive additive.

4.5.6 Effect of Ion Exchange Material on Electrode Performance

4.5.6.1 Comparison YP50F electrodes with IEM and binder

To optimize the electrodes for the MCDI cell ion exchange materials (IEM) was used to replace the binder solution in the electrodes. The IEM was incorporated in the electrode production method to increase the adsorption capacity of the electrodes. It was expected that the electrodes with IEM would have higher adsorption capacity. The IEM was expected to aid the efficient ion separation of the feed water ions. Electrodes E19 (80:10:10 YP50F: CB: CEM) and E20 (80:10:10 YP50F: CB: AEM) were produced using the casting method. BET analysis was performed for both electrodes and the results were shown in table 4.5. A summary of the BET results of electrodes E12, E19 and E20 and the activated carbon YP50F were recorded in table 4.14.

Table 4.14 Summary of the BET results of electrode E12, E19 and E20 and the activated carbon YP50F.

Sample	**Normalized Surface Area (m^2/g)**				**MPV (cm^3/g)**
	Total	%	Micropore	External	
YP50F (SA: 1500-1800m^2/g)	1680		1350	330	0.54
E12-YP50-I12-JNT45 (10% PVDF)	1437	86	1154	283	0.23
E19-YP50-I19-JNT45-Cathode (10% CEM)	1552	92	1238	317	0.21
E20-YP50-I20-JNT45-Anode (10% AEM)	1121	67	873	249	0.14

The normalised surface area of electrode E12 retained was 86% that of the virgin activated carbon YP50F. Electrode E19 with cathode exchange material retained a normalised surface area of 92% to that of the virgin activated carbon YP50F. Electrode E20 with anode exchange material retained a normalised surface area of 67% to that of the virgin activated carbon YP50F. The decrease in the surface area of electrode E12 with binder solution may be subscribed to the binder material that is blocking a portion of the highly developed surface of the activated carbon. The surface area of electrode E20 with AEM (anode) decreased greatly by 33%

compared to electrode E19 with CEM (cathode) which only decreased by 8% from that of the virgin activated carbon YP50F. The decrease in the surface area can be subscribed to the ion exchange polymers which served to maintain the mechanical stability and uniformity of the electrodes.

An adsorption-desorption measurement was performed in the MCDI cell to analyse the performance of the electrodes with IEM with E19 as the cathode and E20 as an anode. Figure 4.32 showed the conductivity versus time adsorption-desorption. Figure 4.33 showed the mSAC calculated from the data obtained from the adsorption-desorption measurements for each experiment performed.

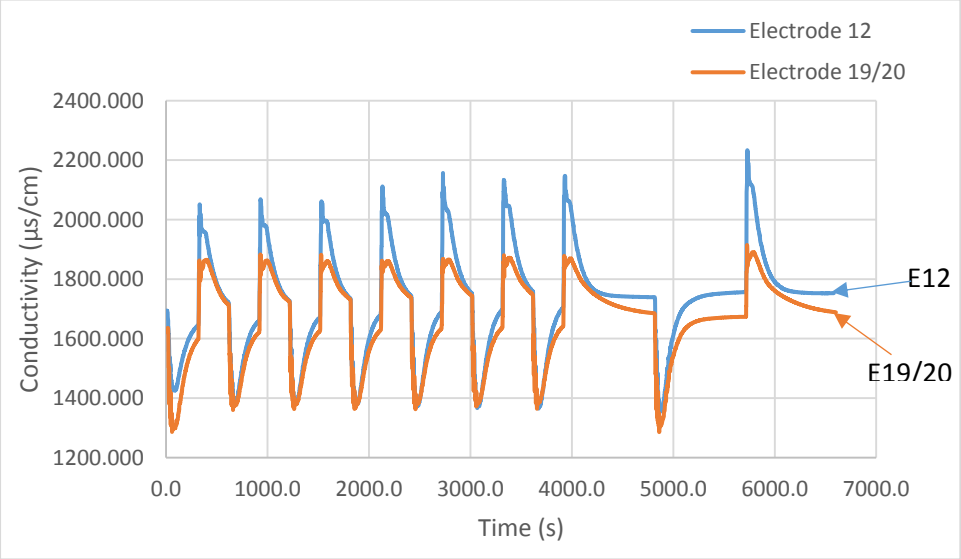

Figure 4.32 Adsorption-desorption measurement of electrode E12 and E19/20.

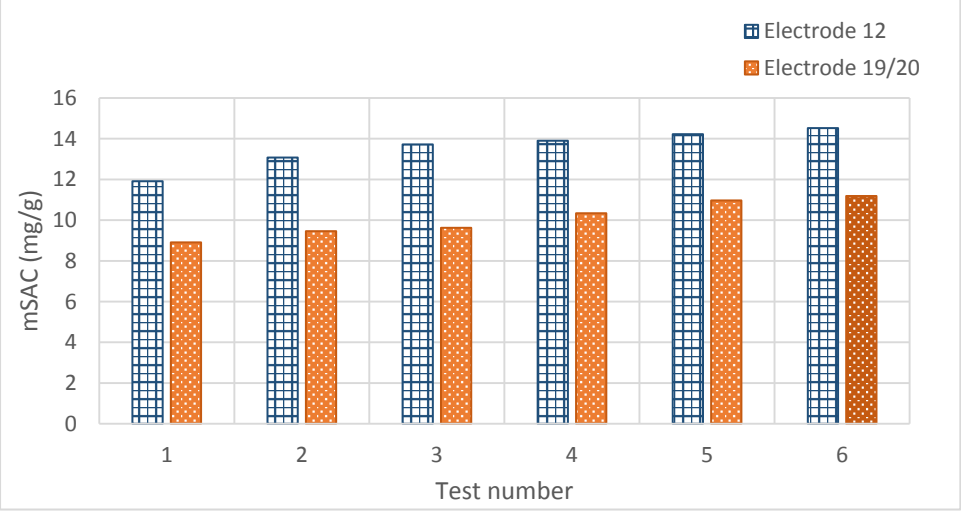

Figure 4.33 The mSAC calculated of electrode E12 and E19/20 for each experiment.

Electrodes with IEM showed lower adsorption than the electrode E12 with binder. Electrodes E19/20 had the highest mSAC of 11.19 mg/g whereas electrode E12 had the highest mSAC of 14.52 mg/g. It was expected that the IEM would enhance the adsorption capacity of the electrodes however that was proved to be untrue. The BET and adsorption-desorption results obtained are contrast to the earlier observations as typically the highest surface area gave the highest capacity. Electrode E12 had a lower surface area compared to the combined surface areas of electrode E19 and E20 but it had the highest adsorption capacity. It can be concluded that IEM aren't suitable for electrode production for the MCDI cell.

4.5.6.2 Comparison of YP80F electrodes with IEM and binder

The objective of the study was to optimize the fabrication method and composition of electrode for MCDI. IEM was introduced in the electrode material replacing the binder, in this section electrode E13 with binder is compared to cathode electrode E21 and anode electrode E22. Electrodes E13 (80:10:10 YP80F: CB: PVDF), E21 (80:10:10 YP80F: CB: CEM) and E22 (80:10:10 YP80F: CB: AEM) were fabricated using YP80F as the activated carbon. BET analysis was performed on the activated carbon and the fabricated electrodes, the results obtained were recorded in table 4.6 above. A summary of the BET results of electrodes E13, E21 and E22 and the activated carbon YP80F were recorded in table 4.15.

Table 4.15 Summary of the BET results of electrode E13, E20 and E22 and activated carbon YP80F.

Sample	**Normalized Surface Area (m^2/g)**				**MPV (cm^3/g)**
	Total	%	Micropore	External	
YP80F (SA: 2000-2500m^2/g)	2316		348	1969	0.16
E13-YP80-I13-JNT45	2010	86	386	1624	0.08
E21-YP80-I21-JNT45-Cathode	2039	87	388	1649	0.07
E22-YP80-I22-JNT45-Anode	2188	94	323	1798	0.06

Electrode E14 had a normalised surface area of 86% that of the virgin activated carbon YP80F, this slight decrease in the surface area was expected and is accounted for by the addition of the conductivity additive and binder into the ink solution. The normalised surface area of the cathode electrode E21 was 87% that of the activated carbon YP80F. For the anode electrode E22 the obtained normalised surface area was 94% that of the activated carbon YP80F. The electrodes with IEM had the highest surface area but lower micropore volume. The electrodes with PVDF binder had lower surface area but a higher micropore volume.

An adsorption-desorption measurement was performed in the MCDI cell to analyse the performance of the electrodes with IEM with E21 as the cathode and E22 as an anode. Figure

4.34 showed the conductivity versus time adsorption-desorption. Figure 4.35 showed the mSAC calculated from the data obtained from the adsorption-desorption measurements for each experiment performed.

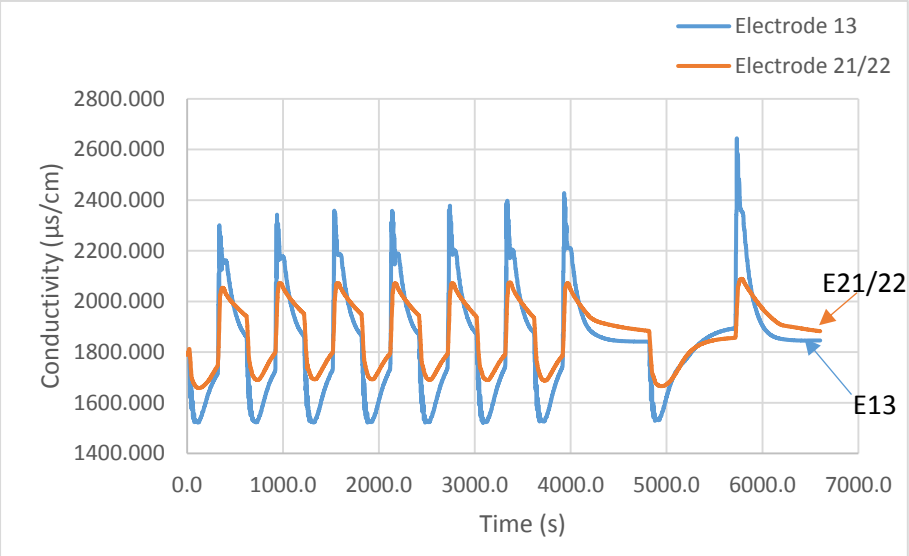

Figure 4.34Adsorption-desorption measurement of electrodes E13 and E21/22.

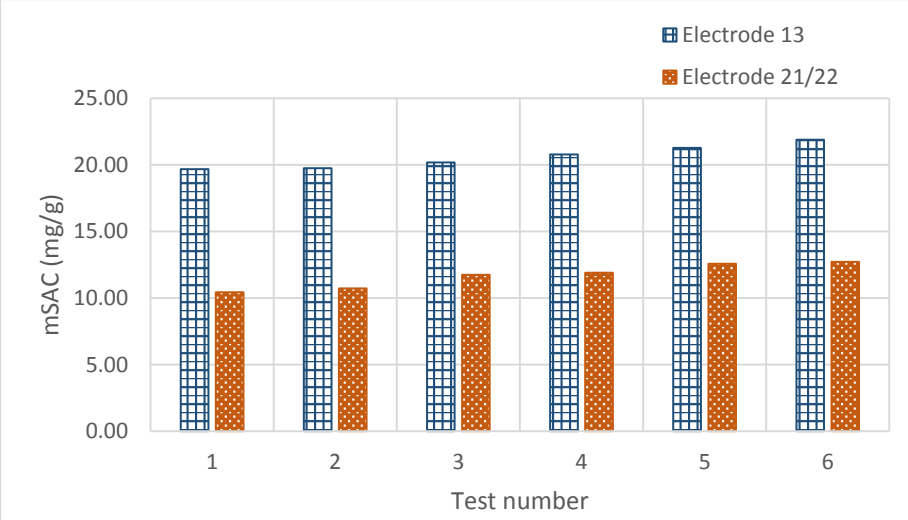

Figure 4.35 The mSAC of electrode E13 and E21/22 calculated for each experiment for both electrodes set.

The adsorption-desorption measurement of electrode E13 with PVDF showed higher adsorption than electrodes E21/22 with IEM. The adsorption capacity of electrode E13 was significantly higher than that of electrode E21/22. Electrode E13 had the highest mSAC of 21.88 mg/g whereas electrode E21/22 had the highest mSAC of 12.71 mg/g. Electrode E22 had highest surface area than electrode E13 whereas electrode E21 had lower surface area than electrode E13. The combined surface area of electrodes E21 and E22 was 87% of the virgin

activated carbon YP80F. The results obtained are in contrast to the earlier where typically the highest surface area gave the highest adsorption capacity. The adsorption capacity of the electrodes was not only affected by the surface area but by the porosity of the electrodes. When the electrodes containing IEM were immersed in a water a slight hydrophilicity was observed, the electrodes could not be properly wetted. The hydrophilicity detected in the electrodes could also result in the low adsorption of the electrodes with IEM therefore PVDF remains the preferable binder for MCDI electrode production.

4.5.6.3 Comparison of YP50F and YP80F Electrodes with Ion Exchange Material

Activated carbons YP50F and YP80F have different properties therefore are affected differently by the materials added in the ink solutions. Electrodes fabricated using both YP50F and YP80F were compared to determine an optimum electrode for MCDI. Electrodes E19 and E20, with electrode E19 as a cathode and electrode E20 as an anode were fabricated using YP50F. Electrodes E21 and E22, with electrode E21 as a cathode and electrode E22 as an anode were fabricated using YP80F. Tables 4.5 and 4.6 showed the results of the BET analysis of the activated carbons and fabricated electrodes.

Table 4.16 Summary of the BET results of the electrode pairs E19, E20, E21 and E22.

Sample	**Normalized Surface Area (m^2/g)**				**MPV (cm^3/g)**
	Total	%	Micropore	External	
E19-YP50-I19-JNT45-Cathode	1552	92	1238	317	0.21
E20-YP50-I20-JNT45-Anode	1121	67	873	249	0.14
E21-YP80-I21-JNT45-Cathode	2039	87	388	1649	0.07
E22-YP80-I22-JNT45-Anode	2188	94	323	1798	0.06

The normalised surface area electrode E19 cathode was found to be 92% of the virgin activated carbon YP50F whereas, electrode E20 anode had a normalised surface area of 67% of the activated carbon YP50F. Electrode E21 cathode had a normalised surface area 87% of the virgin activated carbon YP80F, and electrode E22 had a normalised surface area of 94% of the activated carbon YP80F. The surface area of YP80F electrode E21 and E22 was higher than that of YP50F electrode E19 and E20. The variation the surface area of these electrodes manufactured using the same composition and amounts of materials could be subscribed to the difference in the external surface area of the activated carbons (1969 m^2/g for YP80F and 330 m^2/g for YP50F).

The adsorption-desorption measurement was performed on YP50F and YP80F electrodes and the plot is shown in figure 4.36 below. The mSAC was calculated for both electrode pairs from

the adsorption-desorption results for each experiments, the results were plotted into a bar graph in figure 4.37.

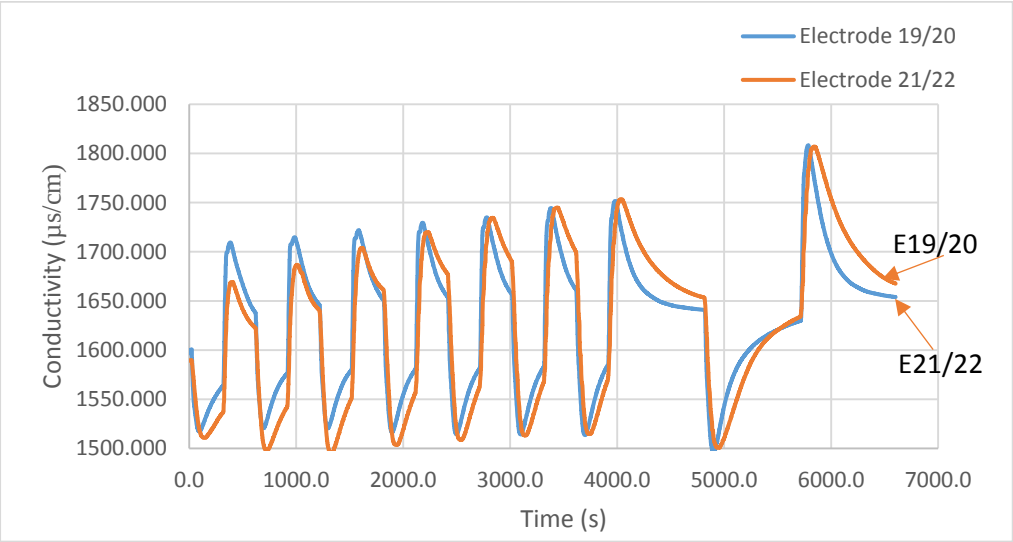

Figure 4.36 Adsorption-desorption measurement of electrode pair E19/20 and electrode pair E21/22.

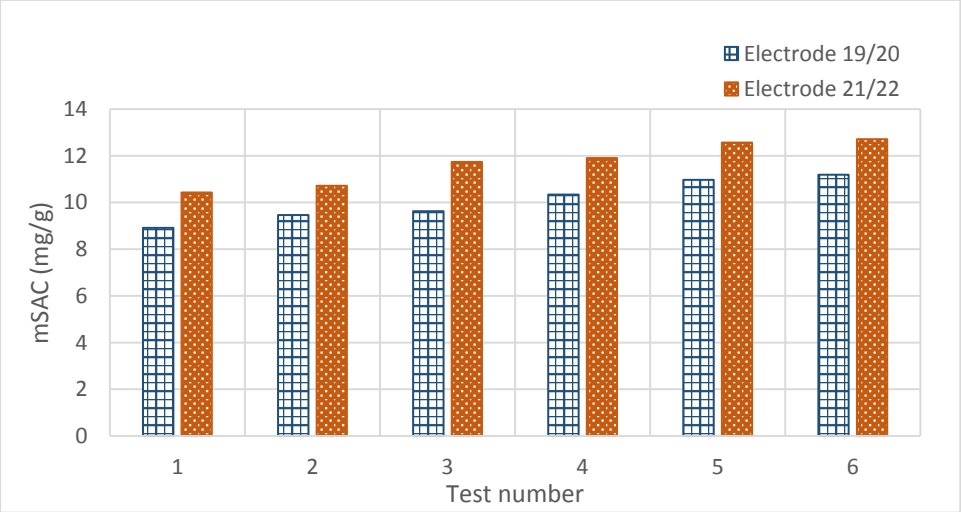

Figure 4.37 The mSAC of electrode pair E19/20 and electrode pair E21/22 calculated for 6 experiments series for both electrodes pairs.

Electrode pair E21/22 had a higher surface area than electrode pair E19/20, this contributed to the higher adsorption capacity of the electrodes. Electrode E21/22 had the highest mSAC of 12.71 mg/g whereas electrode E19/20 had the highest mSAC of 11.19 mg/g. There wasn't a significant variation in the adsorption capacities of electrode E19/20 and electrode E21/22 however electrodes fabricated with activated carbon YP80F remained superior to YP50F electrodes. Electrodes containing IEM showed low adsorption capacity compared to the electrodes with PVDF, the IEM did not enhance the adsorption capacity of the electrodes.

4.6 Kim-Yoon Diagram for Salt Adsorption Rate versus Capacity

Kim-Yoon diagram is a plot of Average Salt Adsorption Rate (ASAR) in mg/g/min against Salt Adsorption Capacity (SAC) in mg/g. The ASAR vs SAC plot known as the Kim-Yoon plot combines two key metrics in the MCDI system. SAC gives the salt adsorption capacity of a cell's adsorption-desorption cycle. SAC was calculated by dividing the mass of the salt removed from the feed water by the total mass of the electrode hence mg/g units. The SAC gives the amount of salt adsorption capabilities of the electrodes but not the rate at which the salt is removed from the solution. ASAR was calculated by dividing the salt adsorption capacity by the total cycle time. Several operational parameters can affect the ASAR such as the adsorption time, feed water concentration, cell architecture, cell resistance, electrode material and electrode thickness.

An adsorption-desorption measurement was performed on the MCDI cell with various half cycle times (HTC) at 1.2 V. The Kim-Yoon diagram was plotted from data of the following HTCs of 180, 120, 90, 60, and 30 seconds. Electrode E13-YP80-I13-JNT45 was used for the analysis. The Kim-Yoon diagram obtained was plotted in figure 4.38.

The Kim-Yoon plot allowed for the determination of the optimal cell operational conditions when both SAC and ASAR were close to their maximum attainable values. The plot made it possible to establish the operation conditions to achieve a high ASAR while ensuring an acceptable adsorption capacity. For MCDI applications in salt removal, finding the optimized operation condition that result in both a significant ASAR and SAC.

The blue line shows the expected pattern of the ASAR vs SAC values at 1.2 V whereas the orange squares represent the actual values derived from the ion adsorption experiment at various half cycle times. The highest ASAR obtained was 1.45 mg/g/min at 90 seconds HTC with a salt adsorption capacity of 7.0 mg/g. The highest SAC obtained was 9.4 mg/g with an ASAR of 0.98 mg/g/min. The optimal HTC for 1.2 V for salt removal for MCDI was found to be 120 seconds with the complete cycle being 240 seconds, the ASAR was found to be the highest with the SAC being the maximum achievable. The ASAR at the optimal HTC was 1.34 mg/g/min with a salt adsorption capacity of 8.6 mg/g.

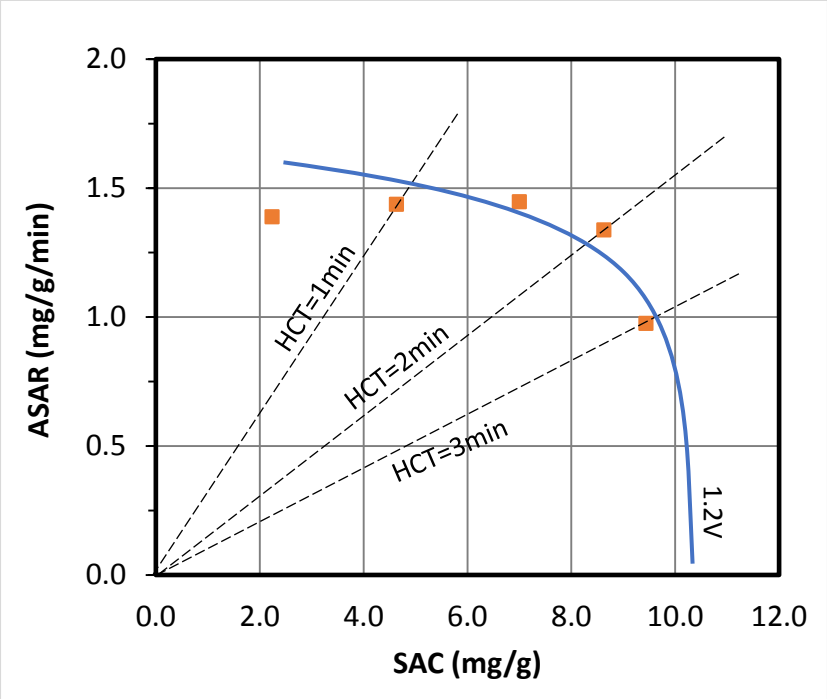

Figure 4.38 Kim-Yoon plot for average salt adsorption rate (ASAR) in a flow-by CDI cell with porous carbon electrode vs salt adsorption (SAC) at a charging voltage of 1.2 V.

4.7 Optimization of the MCDI operating parameters

For the MCDI system to operate optimally the effect of the spacer thickness on the adsorption capacity had to be determined and the flowrate optimized. In 4.7.1 results of how the spacer thickness affected the adsorption capacity were discussed and 4.7.2 the optimization of the flowrate was discussed.

4.7.1 The optimization of the MCDI Spacer

Two PVC/PET spacers of different size 0.30 mm and 0.50 mm were used in the MCDI system to determine the effect of spacer thickness on the adsorption capacity. Adsorption-desorption measurements were performed in the MCDI cell for both the 0.30 mm and 0.50 mm spacer. Electrode pair E18 was used for the adsorption-desorption experiments. The conductivity versus time adsorption-desorption measurement was plotted in figure 4.39. Figure 4.40 showed the mSAC calculated for both the 0.30 mm and 0.50 mm spacer adsorption-desorption measurement.

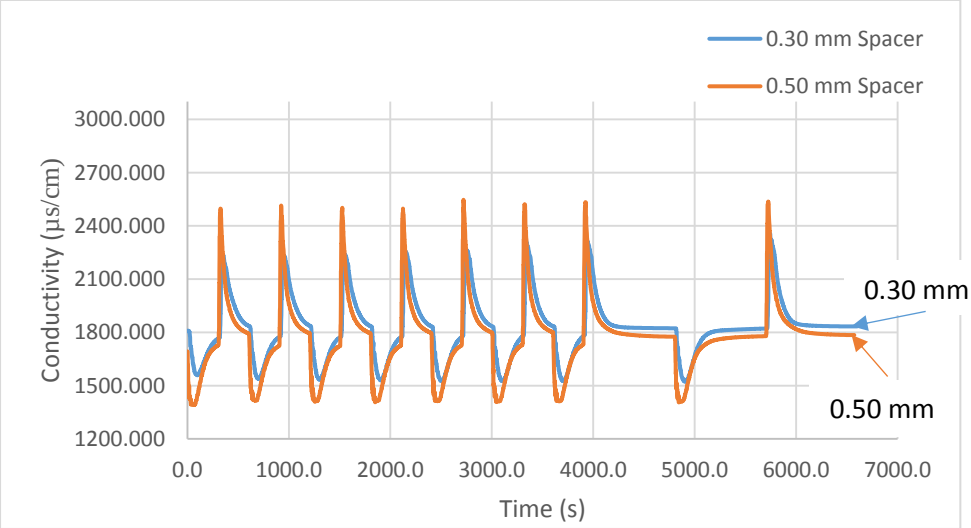

Figure 4.39 The adsorption-desorption measurements for the 0.30 mm and 0.50 mm spacer using electrode E18 electrode pair.

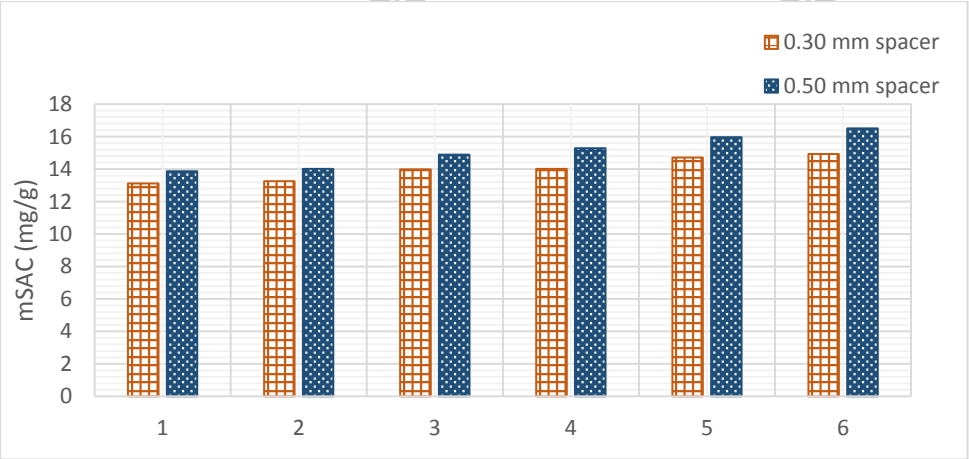

Figure 4.40 The mSAC calculated for the 0.30 mm and 0.50 mm spacer using electrode E18 electrode pair.

Based on the adsorption-desorption measurements the change in the spacer of the MCDI cell did not have a significant effect on the electrode's mSAC. The experiments performed with the 0.30 mm spacer showed a slightly lower mSAC (14.93 mg/g) compared to the results obtained with the 0.50 mm spacer (16.51 mg/g). However, a clear difference in the outlet concentration was noticed. The conductivity of the water exiting the cell during the adsorption cycle was lower for the cell setup with the larger spacer. Also, the conductivity of the water exiting the cell during desorption cycle was higher. This could be explained by the fact that the flowrate of the water between the membranes increased as the spacer thickness decreased. The treated water flows faster resulting in smaller concentration fluctuations during adsorption and desorption cycles.

4.7.2 Optimization of the Feed Flowrate

The feed flowrate in the MCDI system played a significant role in the adsorption, four flowrates 8 mL/min, 13 mL/min, 17 mL/min and 22 mL/min were used for the adsorption-desorption using electrode pair E11.

8 mL/min was the first flowrate to be used for the adsorption-desorption, however the electrodes did not adsorb any ions due to the flowrate being too low. 13 mL/min was then used for the adsorption-desorption, the conductivity versus time plot was shown in figure 4.41 and the mSAC calculated was shown in figure 4.42.

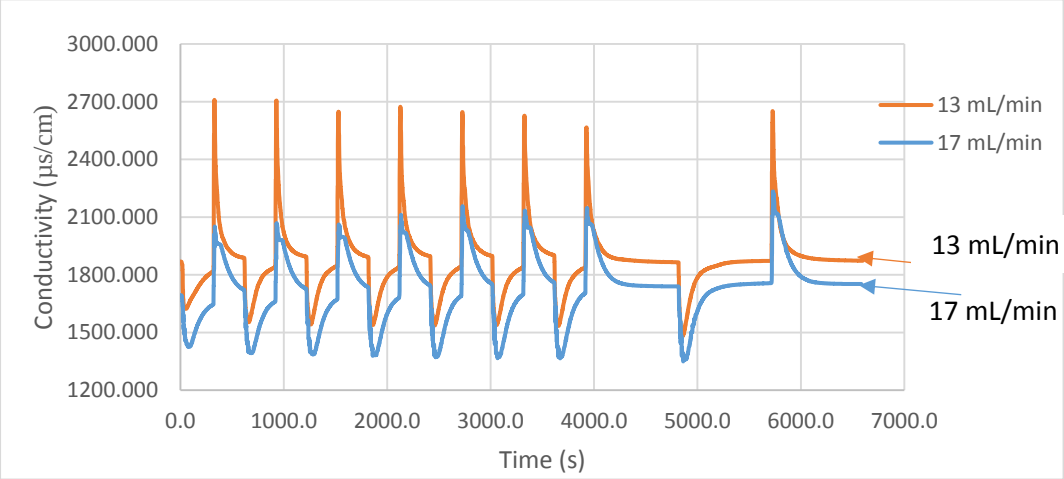

Figure 4.41 The adsorption-desorption measurements of the electrode pair E18 at flowrates 13 mL/min and 17 mL/min.

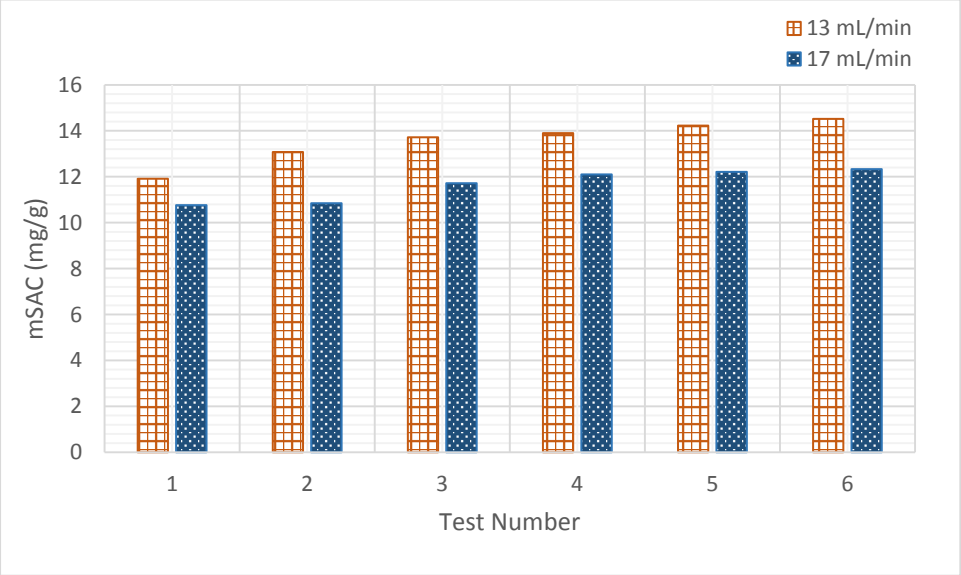

Figure 4.42 The mSAC obtained for the electrode pair E18 at flowrates 13 mL/min and 17 mL/min.

The adsorption-desorption measurement at flowrate of 17 mL/min was shown figure 4.41 and the mSAC calculated was shown in figure 4.42. At a flowrate of 22 mL/min the pressure in the MCDI cell was too high as such the feed inlet popped out after about 5 minutes.

According to the adsorption-desorption experimental results, electrode E18 showed a maximum adsorption capacity at a flowrate of 13 mL/min (14.52 mg/g). At a flowrate of 17 mL/min, the same electrode pair showed a maximum of 12.33 mg/g. It was concluded that as the flowrate increases, the electrode adsorption capacity decreases. The optimal flowrate for the MCDI system was found to be 13 mL/min.

Chapter 5 Conclusion

This chapter draws the conclusion of all the work that was done for this research study and future work that can be done.

5.1 Conclusion and Future Work

In summary a total of 15 electrodes were fabricated using two methods namely the spray coating and casting method. The compositions of the electrodes were varied in an attempt to optimize the fabrication methods and compositions of the electrodes. The research was taken a step further to optimize the ASAR, SAC, flowrate and the resistance in the MCDI system. Three activated carbons were utilized in this study, TOB, YP50F and YP80F, these activated carbons have different surface areas and porosity therefore were affected different by the materials added in the ink. Carbon black and carbon nanotubes were used as conductivity additives to enhance the conductivity of the electrodes. Lastly ion exchange materials were introduced in the electrodes fabrication in an attempt to optimize the electrodes. For the characterisation of the electrodes Cyclic Voltammetry, Scanning Electron Microscope, BET and MCDI cell were used. The objective of the study was to develop electrodes, optimize the fabrication methods and composition for MCDI.

To benchmark the MCDI system GDL electrodes were used, the results of the system obtained showed that the system was of the same standard as the results published in literature. It is of great significance to note that GDL electrodes are used in fuel cells and are not suitable for MCDI, GDL was only used due to lack of MCDI commercial electrodes.

Resistance of the MCDI cell was measured at different torque values (0.2, 0.4, 0.6, 0.8, 1.0 and 1.2 V) for both the sprayed and casted electrodes. When the torque was increased, the resistance in the cell decreased steadily. It can be concluded that a torque of 0.3 N.m was the optimum torque value for the adsorption-desorption in the MCDI system.

Reproducibility of the fabrication method was determined using cyclic voltammetry, three samples of ink I11 with the composition 80:10:10 YP50F: CB: PVDF were analysed. The voltammograms obtained for the samples overlapped and the standard deviation obtained showed that the ink fabrication method was reproducible. Electrode E11 used for the reproducibility experiments was fabricated using the spray coating method. The 3 electrode pairs of E11 had an even thickness, it could be deduced that the fabrication method was fairly reproducible. The reproducibility of the MCDI system performed using electrode E11 which

had 3 pairs was performed by a series of 6 adsorption-desorption measurements for each electrode pair. A difference of about 15% on the mSAC of the electrode pairs was observed, the results obtained from the MCDI system were reproducible.

SEM images showed uniformity in the fabricated electrodes in both the surface and the electrode thickness. The sprayed electrodes showed a thick layer of the ink on top of the substrate whereas casted electrodes showed a deep penetration of the ink onto the fibres of the substrate.

The surface area and porosity of the activated carbon utilized plays an important role in the electrode adsorption. To select a suitable activated carbon for the MCDI electrode production three activated carbons were utilized namely TOB, YP50F and YP80F. BET analysis was used to determine their surface areas and porosity, three electrodes were then fabricated using the spray coating method and an adsorption-desorption measurement was performed in the MCDI cell. YP80F had the highest surface area and pore size, TOB had higher surface area and micropore volume than YP50F however had a small pore size. The TOB had the least adsorption capacity, YP80F electrode had the highest adsorption capacity. TOB was eliminated as an activated carbon for electrode production, YP50F and YP80F were used for further electrode optimization.

To optimize the fabrication methods, spray coating method and casting method were utilized. The adsorption capacity of electrodes fabricated using the spray coating and casting methods were compared. It was determined the casted electrodes had superior adsorption capacity than the spray coated electrodes. The penetration of the ink onto the substrate pores enhanced the adsorption of the casted electrodes while the pores and surface area of the sprayed electrodes were significantly reduced.

A conductive additive was added into the electrode fabrication ink to enhance the conductivity of the electrodes. For all the surface particles of the electrodes to be charged with a voltage of ≤ 2 Volts the electrodes had to have a high conductivity. The activated carbon has low conductivity therefore required an additive. From the four electrodes fabricated using YP50F and YP80F with a composition of 80:10:10 using carbon black and carbon nanotubes as additives, it was found that for the YP50F electrodes carbon nanotubes were the preferred conductive additive. For YP80F electrodes, carbon black was found to be the preferred conductive additive. The two activated carbons have different properties in terms of surface

area and porosity and are affected differently by the additives. For large scale electrode production, the cost implications have to be weighed against performance parameters.

Two electrodes with an increased amount of CNTs was fabricated with YP50F having the following compositions 70:20:10 and 60:30:10 (YP50F: CB: PVDF). These electrodes were fabricated in an attempt to optimize the amount of conductive additive in the electrodes. It was found that the electrode with 20% CNTs had the highest adsorption capacity. For large scale production of electrodes, the cost implications would have to be weighed against the performance parameters of the electrodes.

A binder solution of PVDF was used in the electrode production to maintain the uniformity and mechanical stability of the fabricated electrodes. The binder also blocks the pores of the electrodes therefore an optimum amount of the binder used had to be determined. Four electrodes with these compositions were fabricated (80:10:10 and 75:15:10) using both YP50F and YP80F, carbon black was used as a conductive additive. For both YP50F and YP80F electrodes, the optimum amount of binder was found to be 10% in the electrode composition. The use of excess amount of binder resulted in a decrease in the surface area of the electrode. It could be concluded that 10% of the binder was the ideal amount required for electrode production.

Ion exchange polymers were used in the electrode production method to enhance the adsorption capacity of the electrodes. A total of four electrodes containing anion and cation polymers were fabricated using both YP50F and YP80F activated carbon. The composition of the electrodes was 80:10:10 with carbon black as the conductive additive. The electrodes containing IEM had higher surface area than the electrodes that had PVDF. The electrodes containing IEM showed some hydrophobicity when immersed in water. All the electrodes containing IEM had lower adsorption capacity. It was concluded that IEM could not maintain uniformity and mechanical stability in the electrodes and is not suitable for electrode production for the MCDI system.

The Kim-Yoon plot was drawn to determine the optimal ASAR and SAC using the casted electrode E13. The highest ASAR obtained was 1.45 mg/g/min at 90 seconds HTC with a salt adsorption capacity of 7.0 mg/g. The highest SAC obtained was 9.4 mg/g with an ASAR of 0.98 mg/g/min. The optimal HTC for 1.2 V for salt removal for MCDI was found to be 120 seconds with the complete cycle being 240 seconds, the ASAR was found to be the highest

with the SAC being the maximum achievable. The ASAR at the optimal HTC was 1.34 mg/g/min with a salt adsorption capacity of 8.6 mg/g.

The operational parameters of the cell setup were optimized by studying the effect of the spacer thickness on the adsorption capacity as well as the flowrate of the feed water. Two spacer thicknesses 0.30 and 0.50 mm were used for the adsorption-desorption measurements using electrode E18. The adsorption-desorption experiments performed showed that the mSAC for the 0.30 mm spacer was lower (14.93 mg/g) whereas the mSAC for 0.50 mm had a higher mSAC (16.51 mg/g). The PVC/PET spacer of 0.50 mm thickness was ideal for the MCDI cell setup as it allowed for higher adsorption capacity. The feed flowrate in the MCDI system played a significant role in the adsorption, four flowrates 8 mL/min, 13 mL/min, 17 mL/min and 22 mL/min were used for the adsorption-desorption using electrode pair E11. At 8 mL/min flowrate the electrodes did not adsorb any ions due to the flowrate being too low. At 13 mL/min flowrate the highest mSAC was found to be 14.52 mg/g. At 17 mL/min flowrate the highest mSAC was found to be 12.33 mg/g. At a flowrate of 22 mL/min the pressure in the MCDI cell was too high as such the feed inlet popped out after about 5 minutes. The optimal flowrate for the MCDI system was found to be 13 mL/min, it allowed for efficient adsorption-desorption of ions.

The objectives of this study were achieved, the fabrication methods were optimized with the casting method producing superior electrodes. The composition of the electrodes was also optimized with the 80:10:10 (activated carbon: conductive additive: binder) ratio being the optimum ratio. The casted electrode E13 was found to be the superior electrode from all the fabricated electrodes. It had the highest mSAC of 21.88 mg/g with a capacitance of 31.16 F/g which is the highest compared what has been published in literature. Based on the electrodes published in literature, researchers have been struggling to achieve a 100% efficiency and a high mSAC, with the highest recorded mSAC of 12.55 mg/g. For all the MCDI experiments performed, a charge efficiency of between 90-100% was achieved.

5.2 Future Work

Based on the analysis and conclusion of this study, a number of suggestions regarding priorities of future research directions and investigations are listed:

- The binder solution is used to maintain mechanical stability and uniformity in the electrodes however binders tend to be hydrophobic. For future studies contact angle analysis will be used to determine the hydrophilicity of the electrodes.
- The average salt adsorption (ASAR) is affected by several operational parameters can such as the adsorption time, feed water concentration, cell architecture, cell resistance, electrode material and thickness. For future studies, optimization of the ASAR at the various operational parameters is recommended.
- It was noted that the adsorption capacity of the electrodes increased with each adsorption-desorption experiment, it would be interesting to do BET analysis of the electrodes after the desalination of water to determine how the surface area and porosity of the electrodes were affected by the voltage applied.
- Optimization of the operational conditions such as constant current and flow modes.
- Activated carbon used for electrode production affects the electrodes therefore for future studies other activated carbon materials will be explored to further optimize the electrode compositions.
- The amount of binder utilized in the electrode production method was found to affect the electrode adsorption capacity. More electrodes with various compositions (different binder amounts) will be optimized to produce the optimum electrode.
- Currently there is a need for commercial CDI electrodes therefore a large scale electrode production cost study weighing the implications of the performance parameters would have to be done for commercialization of the electrodes.

References

1. O. N. Demirer, R. M. Naylor, C. A. Rios Perez, E. Wilkes and C. Hidrovo, *Energetic performance optimization of a capacitive deionization system operating with transient cycles and brackish water*, Desalination, 2013, 314, 130–138.
2. S. Porada, R. Zhao, A. Van Der Wal, V. Presser and P. M. Biesheuvel, *Review on the sciece and technology of water desalinationby capacitive deionization*, Progress in Materials Science, 2013, 58, 1388–1442.
3. M. Sadrzadeh and T. Mohammadi, *Sea water desalination using electrodialysis*, Desalination, 2008, 221, 440–447.
4. A. E. Anqi, N. Alkhamis and A. Oztekin, *Computational study of desalination by reverse osmsis-three-dimensional analyses*, Desalination, 2016, 388, 38–49.
5. Safe drinking water foundation, http://www.safewater.org/PDFS/resourcesknowthefacts/Ultrafiltration_Nano_ReverseOsm.pdf, (accessed on 04 February 2016).
6. Hydranautics, http://www.membranes.com/docs/trc/reverseo.pdf, (accessed on 04 February 2016).
7. D. Emadzadeh, W.J. Laua, M. Rahbari-Sisakht, A. Daneshfar , M. Ghanbari , A. Mayahi, T. Matsuura and A.F. Ismail, *A novel thin film nanocomposite reverse osmosis membrane with superior anti-organic fouling affinity for water desalination*, Desalination, 2015, 368, 106-113.
8. Fumatech, http://www.fumatech.com/EN/Membrane-processes/Process%2Bdescription/Reverse-osmosis/index.html, (Accessed on 10 October 2017).
9. H. K. Shon, S. Phuntsho, D. S. Chaudhary, S. Vigneswaran and J. Cho, *Nanofiltration for water and wastewater treatment- a mini* review, Drinking Water Engineering and Science, 2013, 6, 47–53.
10. K. D. Bhuyar, K. A. Loharkar and R. Solanki, *Design & fabrication of nanofiltration unit: A review*, International Journal of Innovations in Engineering and Technology, 2014, 4, 249–255.
11. H. Strathmann, *Assesment of electrodialysis water desalination process cost*, Proceedingsof the international conference on desalination costing, 2004, 32–54.
12. R. Semiat, *Multi-Effect Distillation (MED)*, Encyclopedia life support system, 2014, 13.

13. D.G. Daniels, Power magazine, http://www.powermag.com/water-and-power-will-your-next-power-plant-make-both/?pagenum=2, 9-01-2012.
14. R. Zhao, PhD thesis, *Theory and operation of capacitive deionization* systems, Wageningen University, 2013.
15. M. D. Víctor-ortega, J. M. Ochando-pulido, G. Hodaifa and A. Martínez-ferez, *Ion exchange as an efficient pretreatment system for reduction of membrane fouling in the purification of model OMW*, Desalination, 2014, 343, 198–207.
16. A. Bennett, *High purity: Advances in ion exchange* technology, Filtration + Separation, 2007, 5, 20-23.
17. P.-I. Liu, L.-C. Chung, C.-H. Ho, H. Shao, T.-M. Liang, M.-C. Chang, C.-C. M. Ma and R.-Y. Horng, *Comparitive insight into the capacitive deionization behaviour of the activated carbon electrodes by two electrochemical techniques*, Desalination, 2016, 379, 34–41.
18. R. Zhao, S. Porada, P.M Biesheuvel and A. Van der Wal, *Energy consumption in membrane capacitive deionization for different water recoveries and flow rates and comparison with reverse* osmosis, Desalination, 2013, 330, 35-41.
19. C. Huyskens, J. Helsen, W. J. Groot and A. B. De Haan, *Cost evaluation of large scale membrane capacitive deionization for biomass hydrolysate desalination*, Separation and Purification Technology, 2015, 146, 294–300.
20. P. Długołecki and A. Van Der Wal, *Energy recovery in membrane capacitive deionization*, Environmental Science and Technology, 2013, 47, 4904–4910.
21. P. M. Biesheuvel and A. van der Wal, *Membrane capacitive deionization*, Journal of Membrane Science, 2010, 346, 256–262.
22. P. M. Biesheuvel, R. Zhao, S. Porada and A. van der Wal, *Theory of membrane capacitive deionization including the effect of the electrode pore space*, Journal of Colloid and Interface Science, 2011, 360, 239–248.
23. H. Li and L. Zou, *Ion-exchange membrane capacitive deionization: A new strategy for brackish water desalination*, Desalination, 2011, 275, 62–66.
24. Puretecwater, http://puretecwater.com/resources/basics-of-reverse-osmosis.pdf, (Accessed on 05 February 2016).
25. T.J. Welgemoed, MSc thesis, *Capacitive deionization technology: development and evaluation of an industrial prototype* system, University of Pretoria, 2005.
26. L. Weinstein and R. Dash, *Capavitive deionization: challenges and opportunities*,

Desalination and water reuse, United states, 2013.

27. Electronic water purifier, http://aquaewp.com/wp-content/uploads/EWP-WH-2012-50-LPH-75-LPH-150-LPH-page-1.jpg, (Accessed on 5 February 2016).
28. J. Fajt, *Capacitive deionization (CDI)*, Miswaco, 2012.
29. Voltea, http://www.voltea.com.php56-33.ord1-1.websitetestlink.com/technology-4/, (Accessed on 04 April 2016).
30. P. Attard, *Electrolytes and the electric double layer*, Advances in Chemical Physics, 1996, 92, 1–159.
31. C. Lian, K. Liu, K. L. Van Aken, Y. Gogotsi, D. J. Wesolowski, H. L. Liu, D. E. Jiang and J. Z. Wu, *Enhancing the capacitive performance pf electric dounle-layer capacitors with ionic liquid* mixtures, ACS Energy Letters, 2016, 21–26.
32. D. A. B. Iozzo, M. Tong, G. Wu and E. P. Furlani, *Numerical analysis of electric double-layer capacitors with mesoporous electrodes: Effects of electrode and electrolyte properties*, Journal of Physical Chemistry, 2015, acs.jpcc.5b08409.
33. CDI-electrosorption, http://wwww.cdi-electrosorption.org/sample-page/, (Accessed on 10 February 2015).
34. Carbon nanomaterials, Editor Y. Gogotsi and V. Presser, CRC press, 2nd edition, Boca Raton, London, New york, 2014.
35. M.S. Alimoiqli, PhD Thesis, *Nanistructured ICP-CNT electrodes for capacitive deionisation and water clean up*, University of Wollongong, 2014.
36. F. A. AlMarzooqi, A. A. Al Ghaferi, I. Saadat and N. Hilal, *Application of capacitive deionisation in water desalination: A review*, Desalination, 2014, 342, 3-15.
37. J.-B. Lee, K.-K. Park, H.-M. Eum and C.-W. Lee, *Desalination of a thermal power plant wastewater by membrane capacitive deionization*, Desalination, 2006, 196, 125-134.
38. H. Li, Y. Gao, L. Pan, Y. Zhang, Y. Chen and Z. Sun, *Electrosorptive desalination by carbon nanotubes and nanofibreselectrodes and ion-exchange membranes*,Water reseach, 2008, 42, 4923-4928.
39. C.-H. Hou and C.-Y. Huang, *A comparitive study of electrosorption selectivity of ions by activated carbon electrodes in capacitive deionization*, Desalination, 2013, 314, 124-129.
40. G. Wang, Q. Dong, Z. Linq, C. Pan, C. Yu and J. Qlu, *Hierarchical activated carbon nanofibers webs with tuned structure fabricated by electrospinning for capacitive*

deionization, Journal of materials chemistry, 2012, 22, 21819-21823.

41. J.-B. Lee, K.-K. Park, S.-W. Yoon, P.-Y. Park, K.-I. Park and C.-W. Lee, *Desalination performance of a carbon-based composite electrode*, Desalination, 2009, 237, 155-161.
42. K.-K. Park, J.-B. Lee, P.-Y. Park, S.-W. Yoon, J.-S. Moon, H.-M. Eum and C.-W. Lee, *Development of a carbon sheet electrode for electrosorption desalination*, Desalination, 2007, 206, 86-91.
43. S. Porada, M. Bryjak, A. Van der Waal and P.M. Biesheuvel, *Effect of electrode thickness variation on operation of capacitive deionisation*, Electrochemica Acta, 2012, 75, 148-156.
44. Y. Zhan, C. Nie, H. Li, L. Pan and Z. Sun, *Enhancement of electrosorption capacity of activated carbon fibers by grafting with nanofibers*, Electrochemica Acta, 2011, 56, 3164-3169.
45. J.-H. Choi, *Fabrication of a carbon electrode using activated carbon powder and application of to the capacitive deionization process*, Separation and Purification Technology, 2010, 70, 362-366.
46. G. Wang, B. Qian, Q. Dong, J. Yang, Z. Zhao and J. Qiu, *Highly mesoporous activated carbon electrode for capacitive deionization*, Separation and Purification Technology, 2013, 103,216-221.
47. L. Zou, G. Morris and D. Qi, *Low cost activated carbon electrosorptive deionization of brackish water*, Desalination, 2008, 225, 329-340.
48. M.T.Z. Myint and J. Dutta, *Fabrication of Zinc oxide nanorods modified activated carbon cloth electrode for desalination of brackish water using capacitive deionization approach*, Desalination, 2012, 305, 24-30.
49. S. Porada, L. Weinstein, R. Dash, A. Van der Waal, M. Bryjak, Y. Gogotsi and P.M. Biesheuvel, *Water desalination using capacitive deionization with microporous carbon electrodes*, ACS Applied Materials and Interfaces, 2012, 4, 1194-1199.
50. L. Zhao, MSc thesis, University of Kentucky, 2014.
51. O.N. Demirer, MSc thesis, *Two different perspectives on capacitive deionization process: performance optimization and flow visualization*, University of Texas, 2013.
52. J.E. Dykstra, R. Zhao, P.M. Biesheuvel and A. Van der Wal, *Resistance identification and rational process design in capacitive deionization*, Water Research,2016, 13, 358-370.
53. I. Cohen, E. Avraham, Y. Bouhadana, A. Soffer and D. Aurbach, *Long term stability of*

capacitive de-ionization processes for water desalination: the challenge of positive electrodes corrosion, Electrochimica Acta, 2013, 106, 91–100.

54. P. Díaz, Z. González, M. Granda, R. Menéndez, R. Santamaría and C. Blanco, *Evaluating capacitive deionization for water desalination by direct determination of chloride ions*, Desalination, 2014, 344, 396–401.
55. B. Sai Shankar, K. P. Pranav and R. Kiran Raj, *Capacitive deionization based water desalination system using an MPPT based solar charge controller*, Power and engineering renewable energy conference, 2014, 277–282.
56. Y. Bian, P. Liang, X. Yang, Y. Jiang, C. Zhang and X. Huang, *Using activated carbon fiber separators to enhance the desalination rate of membrane capacitive deionization*, 2016, 381, 95–99.
57. C.J. Gabelich, T.I. Yun, C.R. Bartels, and J.F. Green, *Nonthermal technologies for salinity removal*, AWWA research foundation and the American Water Works Association, California, USA, 2001, 168-170.
58. H.K. Mutha, MSc thesis, *Carbon nanotubes electrodes for capacitive deionization*, Massachusetts institute of technology, 2013.
59. A.M. Johnson, A.W. Venolia, R.G. Wilbourne and J. Newman, *The electrosorb process for desaliting water*, U.S. Dept. of the Interior, Washngton, 1970.
60. A.M. Johnson and J. Newman, *Desalting by means of porous carbon electrodes*, Journal of the Electrochemical Society, 1971, 118(3), 510–517.
61. B. Jia and W. Zhang, *Preparation and application of electrodes in capacitive deionization (CDI): A state-of-the-art review*, Nanoscale Research Letter, 2016, 11, 64.
62. Y. Oren, *Capacitive deionization (CDI) for desalination and water treatment- past, present and future (review)*, Desalination, 2008, 10, 228-235.
63. M.-W. Ryoo and G. Seo, *Improvement in capacitive deionization function of activated carbon cloth by titania modification*, Water reseach, 2003, 37, 1527-1534.
64. X. Zhao, H. Tian, M. Zhu, K. Tian, J. J. Wang, F. Kang and R. A. Outlaw, *Carbon nanosheets as the electrode material in supercapacitor*, Journal of Power Sources, 2009, 194, 1208–1212.
65. R. V. VijayaDurga, C.; Srividya, A.; Ajitha, A. Umamaheswara, *An overview on cyclic voltammetry and its application in pharmaceutical analysis*, International Journal of Chemistry and Pharmaceutical Sciences, 2014, 5, 13–19.
66. E. Parameters, *A preview of techniques for electrochemical analysis*, Princeton Applied

Research, 1–15.

67. A. G. El-Deen, N. A. M. Barakat, K. A. Khalil, M. Motlak and H. Yong Kim, *Graphene/SnO_2 nanocomposite as an effective electrode material for saline water desalination uisng capacitive deionization*, Ceramics International, 2014, 40, 14627–14634.
68. G. Lu, G. Wang, P. H. Wang, Z. Yang, H. Yan, W. Ni, L. Zhang and Y. M. Yan, *Enhanced capacitive deionization with carbon electrodes prepared with a modified evaporation casting method*, Desalination, 2016, 386, 32–38.
69. X. Xu, Y. Liu, M. Wang, X. Yang, C. Zhu, T. Lu, R. Zhao and L. Pan, *Design and fabrication of mesoporous graphene via carbothermal reaction for highly efficient capacitive deionization*, Electrochimica Acta, 2016, 188, 406–413.
70. A. Bogner, P. H. Jouneau, G. Thollet, D. Basset and C. Gauthier, *A history of scanning electron microscopy developments: towards "wet-STEM" imaging*, Micron, 2007, 38, 390–401.
71. K. D. Vernon-Parry, *Scanning electron microscopy: an introduction*, III-Vs Review, 2000, 13, 40–44.
72. C. Stadtländer, *Scanning electron microscopy and transmission electron microscopy of mollicutes: challenges and opportunities*, Research and Educational Topics in Microscopy, 2007, 122–131
73. N. Hwang and A. R. Barron, *BET surface area analysis of nanoparticles*, Creative Commons Attribution License 3.0, 2010, 0.3, 1–11.
74. M. Thommes, *Textural characterization of zeoolites and orderd mesoporous materials by physical adsorption*, Quantachrome instruments, Springer Netherlands, Boynton beach USA, 2007, Chapter 5, pp 495-523.
75. S. Lowell, J.E. Shields, M.A. Thomas and M. Thommes, *Characterization of porous solids and powders: surface area, pore size and density*, Kluwer academic publishers, Netherlands, 1994, 1-154.

Appendix A

Excel sheet used for data analysis of the conductivity and current data obtained from Paraly and Nova software.

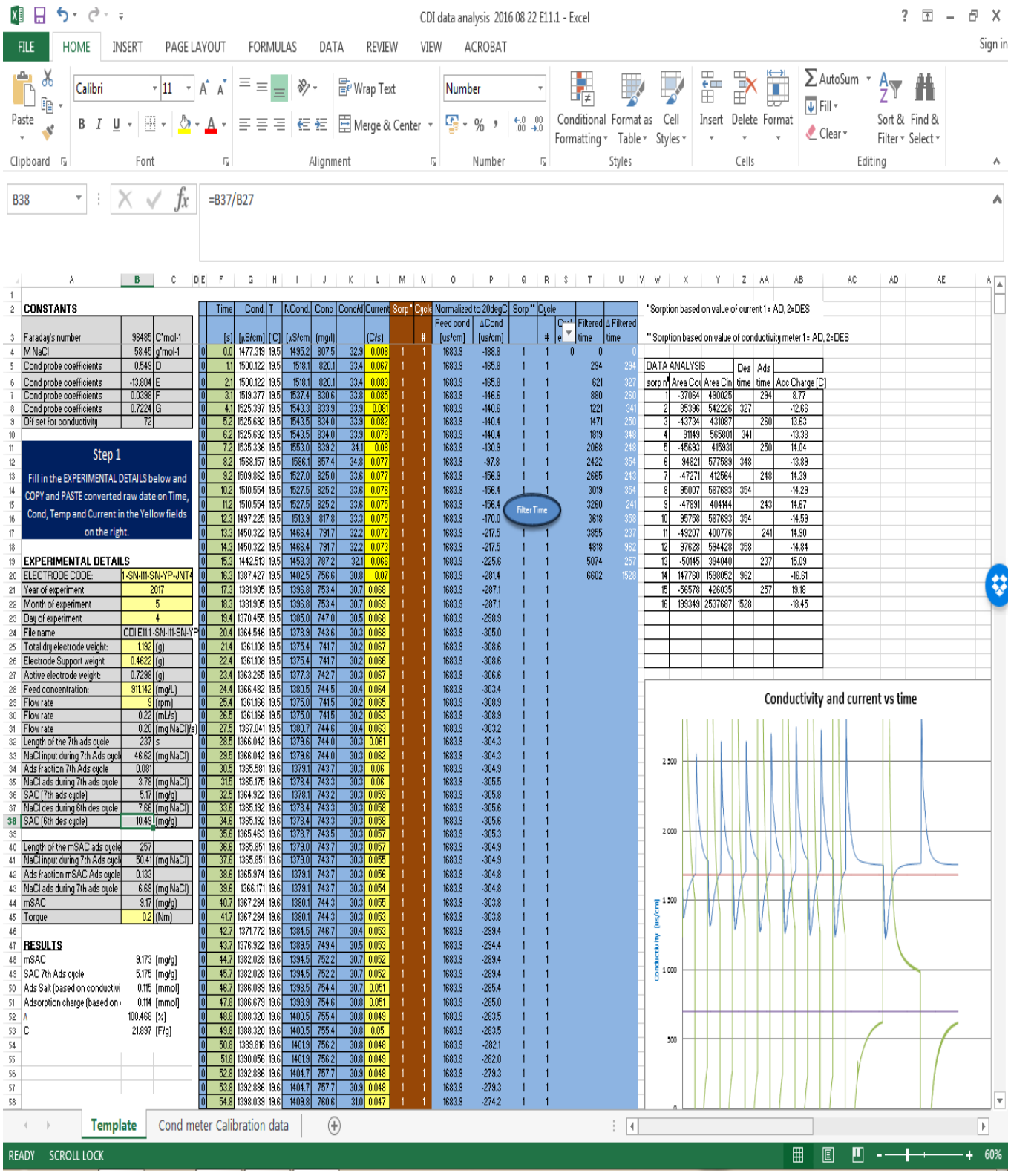

Appendix B

The excel sheet used for the calculation of the amount of activated carbon, conductive additive and binder required for a specific ink composition.

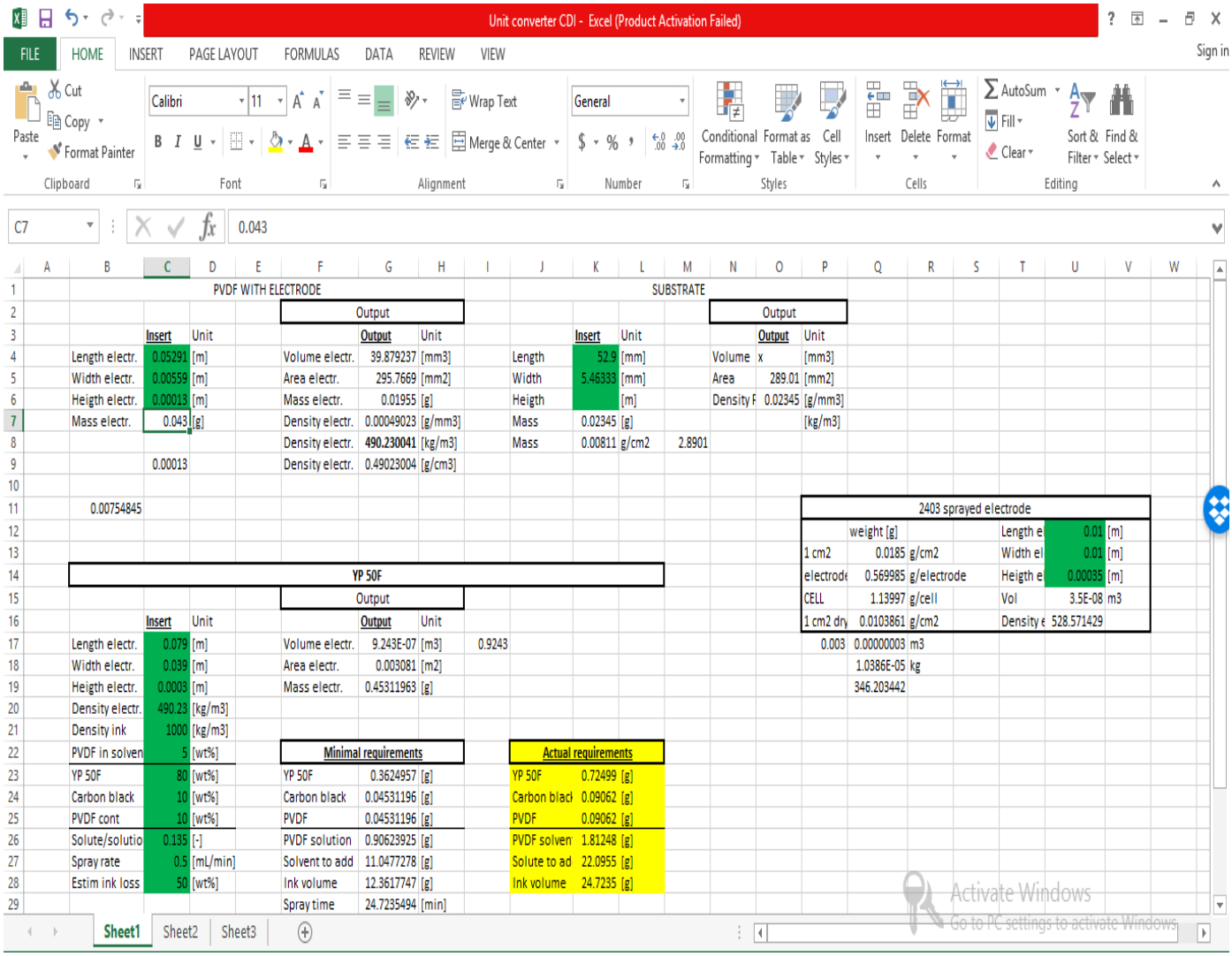

Unit converter CDI - Excel (Product Activation Failed)

		PVDF WITH ELECTRODE										SUBSTRATE												
					Output												Output							
		Insert	Unit		Output	Unit				Insert	Unit					Output	Unit							
	Length electr.	0.05291	[m]	Volume electr.	39.879237	[mm3]		Length	52.9	[mm]		Volume	x	[mm3]										
	Width electr.	0.00559	[m]	Area electr.	295.7669	[mm2]		Width	5.46333	[mm]		Area	289.01	[mm2]										
	Heigth electr.	0.00013	[m]	Mass electr.	0.01955	[g]		Heigth		[m]		Density F	0.02345	[g/mm3]										
	Mass electr.	0.043	[g]	Density electr.	0.00049023	[g/mm3]		Mass	0.02345	[g]				[kg/m3]										
				Density electr.	490.230041	[kg/m3]		Mass	0.00811	g/cm2	2.8901													
		0.00013		Density electr.	0.49023004	[g/cm3]																		
	0.00754845															2403 sprayed electrode								
																	weight [g]			Length e	0.01	[m]		
		YP 50F														1 cm2	0.0185	g/cm2		Width el	0.01	[m]		
				Output												electrode	0.569985	g/electrode		Heigth e	0.00035	[m]		
																CELL	1.13997	g/cell		Vol	3.5E-08	m3		
		Insert	Unit		Output	Unit										1 cm2 dry	0.0103861	g/cm2		Density e	528.571429			
	Length electr.	0.079	[m]	Volume electr.	9.243E-07	[m3]	0.9243										0.003	0.00000003	m3					
	Width electr.	0.039	[m]	Area electr.	0.003081	[m2]												1.0386E-05	kg					
	Heigth electr.	0.0003	[m]	Mass electr.	0.45311963	[g]												346.203442						
	Density electr.	490.23	[kg/m3]																					
	Density ink	1000	[kg/m3]																					
	PVDF in solven	5	[wt%]	Minimal requirements				Actual requirements																
	YP 50F	80	[wt%]	YP 50F	0.3624957	[g]		YP 50F	0.72499	[g]														
	Carbon black	10	[wt%]	Carbon black	0.04531196	[g]		Carbon blacl	0.09062	[g]														
	PVDF cont	10	[wt%]	PVDF	0.04531196	[g]		PVDF	0.09062	[g]														
	Solute/solutio	0.135	[-]	PVDF solution	0.90623925	[g]		PVDF solven	1.81248	[g]														
	Spray rate	0.5	[mL/min]	Solvent to add	11.0477278	[g]		Solute to ad	22.0955	[g]														
	Estim ink loss	50	[wt%]	Ink volume	12.3617747	[g]		Ink volume	24.7235	[g]														
				Spray time	24.7235494	[min]																		